(4)

AD-A211 785

GL-TR-89-0109

A SIMULATION STUDY OF THE OVERDETERMINED GEODETIC BOUNDARY VALUE PROBLEM USING COLLOCATION

Lucia Tsaoussi

DEPARTMENT OF GEODETIC SCIENCE AND SURVEYING
THE OHIO STATE UNIVERSITY
COLUMBUS, OHIO 43210

March 1989

SCIENTIFIC REPORT NO. 6

GEOPHYSICS LABORATORY
AIR FORCE SYSTEMS COMMAND
UNITED STATES AIR FORCE
HANSCOM AIR FORCE BASE, MASSACHUSETTS 01731-5000

Unclassified
SECURITY CLASSIFICATION OF THIS PAGE

REPORT DOCUMENTATION PAGE

Form Approved
OMB No. 0704-0188

1a REPORT SECURITY CLASSIFICATION Unclassified	1b RESTRICTIVE MARKINGS
2a SECURITY CLASSIFICATION AUTHORITY	3 DISTRIBUTION/AVAILABILITY OF REPORT Approved for public release; distribution Unlimited
2b DECLASSIFICATION/DOWNGRADING SCHEDULE	
4 PERFORMING ORGANIZATION REPORT NUMBER(S) OSU/DGSS Report No. 398	5. MONITORING ORGANIZATION REPORT NUMBER(S) GL-TR-89-0109
6a. NAME OF PERFORMING ORGANIZATION Department of Geodetic Science and Surveying 6b OFFICE SYMBOL (If applicable)	7a. NAME OF MONITORING ORGANIZATION Geophysics Laboratory
6c. ADDRESS (City, State, and ZIP Code) The Ohio State University Columbus, Ohio 43210	7b. ADDRESS (City, State, and ZIP Code) Hanscom AFB Massachusetts 01731-5000
8a. NAME OF FUNDING/SPONSORING ORGANIZATION 8b. OFFICE SYMBOL (If applicable)	9. PROCUREMENT INSTRUMENT IDENTIFICATION NUMBER F 19628-86-K-0016
8c. ADDRESS (City, State, and ZIP Code)	10. SOURCE OF FUNDING NUMBERS PROGRAM ELEMENT NO. 62101F; PROJECT NO. 7600; TASK NO. 03; WORK UNIT ACCESSION NO. AQ

11. TITLE (Include Security Classification)
A Simulation Study of the Overdetermined Geodetic Boundary Value Problem Using Collocation

12. PERSONAL AUTHOR(S)
Lucia Tsaoussi

13a. TYPE OF REPORT	13b. TIME COVERED	14. DATE OF REPORT (Year, Month, Day)	15. PAGE COUNT
Scientific No. 6	FROM _____ TO _____	1989 March	142

16. SUPPLEMENTARY NOTATION

17. COSATI CODES			18. SUBJECT TERMS (Continue on reverse if necessary and identify by block number)
FIELD	GROUP	SUB-GROUP	geodesy; geodetic boundary value problem; least-squares collocation

19. ABSTRACT (Continue on reverse if necessary and identify by block number)

The overdetermined geodetic boundary value problem is the object of this study. The problem is defined in general by the Laplacian and at least two different boundary conditions holding on a spherical boundary, or overlapping parts of it. The least-squares collocation method is applied to estimate spherical harmonic coefficients for the disturbing potential.

An algorithm was developed and the methodology was tested using simulated gravity anomaly and undulation signals. Point as well as mean boundary values were used, both with and without random noise added. The OSU86F spherical harmonic coefficient set was used to generate the simulated data and the required covariances. By computing statistics of the input field recovery, the applicability of the methodology is judged.

Several problems have been encountered while applying least-squares collocation to this problem. A theoretical singularity of the covariance matrix, caused by the truncation in the summation of the covariance function at a finite degree, is found to

20. DISTRIBUTION/AVAILABILITY OF ABSTRACT	21 ABSTRACT SECURITY CLASSIFICATION
☒ UNCLASSIFIED/UNLIMITED ☐ SAME AS RPT ☐ DTIC USERS	Unclassified

22a. NAME OF RESPONSIBLE INDIVIDUAL	22b TELEPHONE (Include Area Code)	22c. OFFICE SYMBOL
Christopher Jekeli		AFGL/LWG

DD Form 1473, JUN 86 Previous editions are obsolete. SECURITY CLASSIFICATION OF THIS PAGE

be eliminated numerically when summing to degree 180. Instability and singularity due to the data distribution are treated successfully by applying Tikhonov regularization. Inversion of a large covariance matrix resulting from global data coverage limits the feasibility of the solution. To make the computation manageable, the block-Toeplitz pattern of the auto-covariance matrices is exploited in forming and inverting them. A partitioned inversion procedure assists the assimilation of the influence of overlapping datasets into the inverse of the covariance matrix.

Numerical experiments were conducted using a global mean gravity anomaly dataset and four additional mean undulation datasets referring to 10° and 5° equiangular blocks. With errorless data and a regularized auto-covariance matrix, the error of the estimated solutions to degree 18 and 36 increases with degree, ranging from 0.5% to a maximum of 10% for the first half of the spectrum, and reaches 40% near the Nyquist frequency. The influence of the individual data types is investigated through several one-data-type solutions. Incorporating data error into the solutions estimated from mean gravity anomalies increased the average error of the estimated coefficients by 25% and 30% for expansions to degree 36 and 18, respectively. Corresponding figures for the undulation solutions were on the order of 3%. The discretization error is studied by estimating expansions to degrees 18, 36, 60 and 90 from mean data referring to 10°, 5°, 3° and 2° equiangular blocks. When using 2° instead of 10° block data, the average error of the estimated coefficients to degree 18 is reduced by 95% for the anomaly solutions and 80% for the undulation solutions. Errorless mean anomaly data, of all block sizes, were used to estimate coefficients with an error of less than 1% for the low degrees, approaching the value of 10% for coefficients half the Nyquist frequency and reaching 40% near the Nyquist frequency. On the other hand, the undulation data recover the low degree coefficients with an error of 10% to 20%, increasing with degree, reaching 90% near the Nyquist frequency.

FOREWORD

This report was prepared by Lucia S. Tsaoussi, Graduate Research Associate, Department of Geodetic Science and Surveying, under the supervision of Professor Richard H. Rapp. This study was supported by Air Force Geophysics Laboratory Contract No. F19628-86-K-0016, The Ohio State University Research Foundation Project No. 718188. This contract was administered by the Air Force Geophysics Laboratory, Hanscom Air Force Base, Massachusetts, with Dr. Christopher Jekeli, Scientific Program Officer.

Substantial computer funding was provided by the Instruction and Research Computer Center of The Ohio State University as well as the Pittsburgh Supercomputing Center through Grant PSCA17.

This report was also submitted to the Graduate School of The Ohio State University in partial fulfillment of the requirements of the degree Doctor of Philosophy.

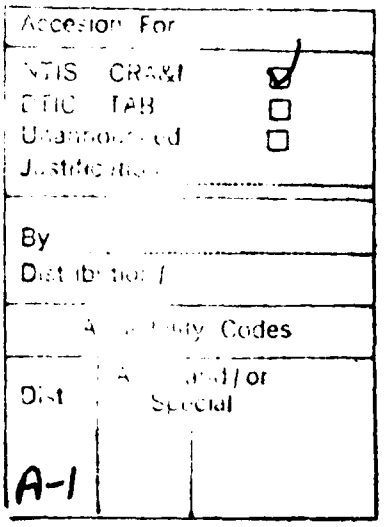

TABLE OF CONTENTS

FOREWORD iii

TABLE OF CONTENTS iv

LIST OF TABLES vi

LIST OF FIGURES ix

CHAPTER PAGE

I. GENERAL BACKGROUND AND SCOPE 1

1.1 Introductory overview of the geodetic boundary value problems 1
1.2 Theory of the overdetermined geodetic boundary value problems and existing solutions 5
1.3 Perspective and general methodology of a collocation approach 13

II. FORMULATION OF A COLLOCATION SOLUTION OF THE OVERDETERMINED BOUNDARY VALUE PROBLEM 16

2.1 Fundamental principles of collocation 16
2.2 Estimation of spherical harmonic coefficients for the disturbing potential 23
2.3 Toeplitz pattern and inversion algorthms 38

III. IMPLEMENTATION OF THE COLLOCATION PREDICTION FORMULAE 47

3.1 The auto-covariance matrix of the observed signals 47
3.2 On the regularization of the covariance matrix 62
3.3 Computational algorithm and software development 67

IV. NUMERICAL RESULTS AND ANALYSIS 75

4.1 General experiment strategy 75
4.2 Specifications for the data simulation 79
4.3 The effect of the covariance functions on the potential coefficient recovery 82
4.4 Data error consideration and regularization effects 87
4.5 Recovery in relation to the grid size 96
4.6 Solutions combining data types 114

V. CONCLUSIONS 123

REFERENCES 128

LIST OF TABLES

TABLE PAGE

1. Condition numbers of covariance matrices for 10° regular grid..... 61
2. Condition numbers of covariance matrices for 5° regular grid..... 61
3. Supercomputer upgrading at PSC..... 68
4. Time consumed in forming and inverting Toeplitz covariance matrices . 72
5. Recovery for 10° $\overline{\Delta g}$ data, with mean cross-covariance matrices and point and mean auto-covariance matrices, with Nmax = 180..... 84
6. Recovery for 10° $\bar{N}$ data, with mean cross-covariance matrices and point and mean auto-covariance matrices, with Nmax = 180..... 84
7. Mean auto-covariance comparison of 5° $\overline{\Delta g}$ data, reported by Colombo (1981) and present calculations, Nmax = 180, latitudinal row between 0° and 5° N..... 86
8. Mean auto-covariance comparison of 5° $\overline{\Delta g}$ data, reported by Colombo (1981) and present calculations, Nmax = 180, latitudinal row between 80° and 85° N..... 86
9. Recovery for 10° $\bar{N}$ data, mean covariance matrices and truncation at Nmax = 360 and 3000..... 87
10. Anomaly and undulation standard deviations to degree Nmax, derived from the estimated accuracy of the OSU86D..... 88
11. Recovery for 10° $\overline{\Delta g}$ data with error, mean covariance matrices and Nmax = 180..... 90
12. Recovery for 10° $\bar{N}$ data with error, mean covariance matrices and Nmax = 180..... 90
13. Recovery for 10° $\bar{N}$ data with error, mean covariance matrices with Nmax = 180 and regularization of $\alpha \approx 23$..... 91
14. Recovery for 10° $\bar{N}$ errorless data, mean covariance matrices with Nmax = 180 and variance $\alpha\tilde{\sigma}^2_{\bar{N}} = 9\ m^2$..... 92

15. Recovery for 5° $\overline{\Delta g}$ data with error, mean covariance matrices and Nmax = 180 and variance $\alpha\tilde{\sigma}^2_{\Delta g}$ = 3 mgals^2 93

16. Recovery for 5° $\overline{\Delta g}$ errorless data, mean covariance matrices with Nmax = 180 and variance $\alpha\tilde{\sigma}^2_{\Delta g}$ = 3 mgals^2 93

17. Recovery for 5° $\bar{N}$ data with error, mean covariance matrices with Nmax = 180 and variance $\alpha\tilde{\sigma}^2_{\bar{N}}$ = 9 m^2 94

18. Recovery for 5° $\bar{N}$ errorless data, mean covariance matrices with Nmax = 180 and variance $\alpha\tilde{\sigma}^2_{\bar{N}}$ = 9 m^2 94

19. RMS undulation differences (in meters) for 10° $\bar{N}$ errorless data and mean covariance matrices (Nmax = 360) from various regularized solutions. Variance = $\alpha\ \tilde{\sigma}^2_{\bar{N}}$ 95

20. RMS anomaly differences (in mgals) for 10° $\bar{N}$ errorless data and mean covariance matrices (Nmax = 360) from various regularized solutions. Variance = $\alpha\ \tilde{\sigma}^2_{\bar{N}}$ 95

21. Average correlation to various degrees, Nmax, between the input coefficients and the coefficients recovered from $\overline{\Delta g}$ errorless data given on various grids 105

22. Average percent difference to various degrees, Nmax, between the input coefficients and the coefficients recovered from $\overline{\Delta g}$ errorless data given on various grids 105

23. RMS undulation difference (in meters) to various degrees, Nmax, between the input coefficients and the coefficients recovered from $\overline{\Delta g}$ errorless data on various grids 106

24. RMS anomaly difference (in mgals) to various degrees, Nmax, between the input coefficients and the coefficients recovered from $\overline{\Delta g}$ errorless data on various grids 106

25. Average correlation to various degrees, Nmax, between the input coefficients and the coefficients recovered from $\bar{N}$ errorless data given on various grids 106

26. Average percent difference to various degrees, Nmax, between the input coefficients and the coefficients recovered from $\bar{N}$ errorless data given on various grids 107

27. RMS undulation difference (in meters) to various degrees, Nmax, between the input coefficients and the coefficients recovered from $\bar{N}$ errorless data on various grids 107

28. RMS anomaly difference (in mgals) to various degrees, Nmax, between the input coefficients and the coefficients recovered from $\bar{N}$ errorless data on various grids 107

29. Extreme values of negative variances and all related coefficients, derived from 10° $\bar{N}$ errorless data 109

30. Extreme values of negative variances and all related coefficients, derived from 5° $\bar{N}$ errorless data 109

31. Recovery statistics for 10° $\overline{\Delta g}$ and $\bar{N}$ combined errorless data 119

32. Recovery statistics for 5° $\overline{\Delta g}$ and $\bar{N}$ combined errorless data 119

33. Overall recovery to degree Nmax obtained from $\overline{\Delta g}$ and $\bar{N}$ combined errorless data given on 10° and 5° regular grids 120

34. Extreme values of negative variances and all related coefficients derived from 10° $\overline{\Delta g}$ and $\bar{N}$ combined errorless data 120

LIST OF FIGURES

FIGURE PAGE

1. Data arrangement for the block-Toeplitz structure..... 40

2. Gravity anomaly point covariance function, computed from eq. (2.2-26) for Nmax = 180 and degree variances implied by the OSU86F field.... 52

3. Undulation point covariance function, computed from eq. (2.2-33) for Nmax = 180 and degree variances implied by the OSU86F field 53

4. Point and mean anomaly covariance functions, for polar and equatorial blocks for 10° regular grid, computed with Nmax = 180 and degree variances implied by the OSU86F field..... 54

5. Point and mean anomaly covariance functions, for polar and equatorial blocks for 5° regular grid, computed with Nmax = 180 and degree variances implied by the OSU86F field..... 55

6. Point and mean anomaly covariance functions, for polar and equatorial blocks for 3° regular grid, computed with Nmax = 180 and degree variances implied by the OSU86F field..... 56

7. Point and mean undulation covariance functions for polar and equatorial blocks for 10° regular grid, computed with Nmax = 180 and degree variances implied by the OSU86F field..... 57

8. Point and mean undulation covariance functions for polar and equatorial blocks for 5° regular grid, computed with Nmax = 180 and degree variances implied by the OSU86F field..... 58

9. Point and mean undulation covariance functions for polar and equatorial blocks for 3° regular grid, computed with Nmax = 180 and degree variances implied by the OSU86F field..... 59

10. Sequence of computations..... 69

11. Sufficient elements for the auto-covariance matrix in a single data group..... 70

12. Sufficient elements for the data cross-covariance matrices..... 71

13. The configuration of the partitioned inversion 72

14. Percent difference per degree between the input coefficients and the coefficients recovered from 10° $\overline{\Delta g}$ errorless data to degree 18 97

15. Percent difference per degree between the input coefficients and the coefficients recovered from 5° $\overline{\Delta g}$ errorless data to degree 36 97

16. Percent difference per degree between the input coefficients and the coefficients recovered from 3° $\overline{\Delta g}$ errorless data to degree 60 98

17. Percent difference per degree between the input coefficients and the coefficients recovered from 2° $\overline{\Delta g}$ errorless data to degree 90 98

18. Correlation per degree between the input coefficients and the coefficients recovered from 10° $\overline{\Delta g}$ errorless data to degree 18 99

19. Correlation per degree between the input coefficients and the coefficients recovered from 5° $\overline{\Delta g}$ errorless data to degree 36..... 99

20. Correlation per degree between the input coefficients and the coefficients recovered from 3° $\overline{\Delta g}$ errorless data to degree 60..... 100

21. Correlation per degree between the input coefficients and the coefficients recovered from 2° $\overline{\Delta g}$ errorless data to degree 90..... 100

22. Percent difference per degree between the input coefficients and the coefficients recovered from 10° $\overline{N}$ errorless data to degree 18 101

23. Percent difference per degree between the input coefficients and the coefficients recovered from 5° $\overline{N}$ errorless data to degree 36..... 101

24. Percent difference per degree between the input coefficients and the coefficients recovered from 3° $\overline{N}$ errorless data to degree 60..... 102

25. Percent difference per degree between the input coefficients and the coefficients recovered from 2° $\overline{N}$ errorless data to degree 90..... 102

26. Correlation per degree between the input coefficients and the coefficients recovered from 10° $\overline{N}$ errorless data to degree 18 103

27. Correlation per degree between the input coefficients and the coefficients recovered from 5° $\overline{N}$ errorless data to degree 36..... 103

28. Correlation per degree between the input coefficients and tne coefficients recovered from 3° $\overline{N}$ errorless data to degree 60..... 104

29. Correlation per degree between the input coefficients and the coefficients recovered from 2° $\overline{N}$ errorless data to degree 90..... 104

30. RMS and extreme absolute values of the normalized differences between the input and the recovered coefficients from 10° $\overline{\Delta g}$ errorle s data 110

31. RMS and extreme absolute values of the normalized differences between the input and the recovered coefficients from 5° $\overline{\Delta g}$ errorless data 111

32. RMS and extreme absolute values of the normalized differences between the input and the recovered coefficients from 10° $\overline{N}$ errorless data 111

33. RMS and extreme absolute values of the normalized differences between the input and the recovered coefficients from 5° $\overline{N}$ errorless data 112

34. RMS and extreme absolute values of the normalized differences between the inpu' and the recovered coeffecients from 5° $\overline{\Delta g}$ with noise 113

35. RMS and extreme absolute values of the normalized differences between the input and the recovered coeffecients from 5° $\overline{N}$ with noise 114

36. Undulation data coverage for the combination solutions 116

37. Percent difference per degree between the input coefficients and the coefficients recovered from 10° $\overline{\Delta g}$ and $\overline{N}$ combined errorless data to degree 18 117

38. Percent difference per degree between the input coefficients and the coefficients recovered from 5° $\overline{\Delta g}$ and $\overline{N}$ combined errorless data to degree 36 117

39. Correlation per degree between the input coefficients and the coefficients recovered from 10° $\overline{\Delta g}$ and $\overline{N}$ combined errorless data to degree 18 118

40. Correlation per degree between the input coefficients and the coefficients recovered from 5° $\overline{\Delta g}$ and $\overline{N}$ combined errorless data to degree 36 118

41. RMS and extreme absolute values of the normalized differences between the input and the recovered coefficients from 10° $\overline{\Delta g}$ and $\overline{N}$ combined errorless data 121

42. RMS and extreme absolute values of the normalized differences between the input and the recovered coefficients from 5° $\overline{\Delta g}$ and $\overline{N}$ combined errorless data 121

CHAPTER I

GENERAL BACKGROUND AND SCOPE

1.1 Introductory overview of the geodetic boundary value problems

When studying the geodetic boundary value problems it is necessary to consider theoretical as well as numerical aspects and limitations. Historically, however, the availability and nature of the measurements have been the driving forces for further theoretical considerations and development. It is thus appropriate not to separate theory and practice, but rather, study them as a whole in a particular solution of the geodetic boundary value problem. The evolution of geodetic boundary value problems represents the effort to reconcile theoretical and practical issues, either by making approximations, or by varying the problem to one with fewer approximations, leading to a progression of problems of increasing complexity.

The classical geodetic boundary value problem solution is the implementation of fundamental potential theory concepts; namely Dirichlet's principle, which states that there always exists a harmonic function (inside or outside a boundary surface) that takes an arbitrarily prescribed set of values on the given boundary. Furthermore Stokes' theorem proves the uniqueness of such a harmonic function for a particular set of boundary values. The problem of determining a harmonic function outside a boundary from its values at the boundary is called Dirichlet's problem, or first boundary value problem of potential theory. Poisson's integral is an explicit solution of this problem for a spherical boundary by means of spherical harmonics (Heiskanen and Moritz, 1967).

The third or mixed boundary value problem of potential theory is the determination of the harmonic function assuming boundary values which are a linear combination of the function and its derivative. Stokes' formula provides the solution to this problem in physical geodesy where the "fundamental equation of physical geodesy" is used as boundary condition. It relates the gravity anomalies (Δg) and the disturbing potential (T)

at the ellipsoid, but its spherical approximation is used in Stokes' formulation by neglecting the flattening of the ellipsoid, a sufficiently accurate approximation for many applications. Still the boundary values must be given on the ellipsoid which approximates the geoid. Since the gravity measurements are actually made at the topographic surface of the earth, they must be appropriately reduced to the geoid. This becomes a serious shortcoming of this solution due to the density assumptions required in the various gravity reduction methods, together with the necessity of eliminating the masses exterior to the ellipsoid, (Heiskanen and Moritz, 1967; Moritz, 1980).

In this manner the anomalous potential for a "regularized" earth is determined. The determination of the geoid as a level surface inside the masses, that is, without a regularization process, is made possible by using two known functions at the boundary (Molodenskii et al., 1962). For example, Molodenskii's formula makes use of the gravitational potential of the external masses and gravity anomalies similar to free-air anomalies. Still, the mass distribution assumptions do not allow for a rigorous solution and the determination of the geoid in this case involves in addition an inverse problem of potential theory.

In order to avoid the inverse problem and inherent mass distribution assumptions, Molodenskii reformulated the problem into a free boundary value problem; namely the determination of the earth's physical surface and the external gravitational field using two functions on the surface: the acceleration of gravity ($\vec{g}$) and the geopotential (W) (Molodenskii et al., 1962). The resulting non-linear integral equation is linearized and is expanded in powers of a small parameter (k), taking the telluroid as a first approximation of the unknown physical surface (ibid, pp. 120-123). The solution of the linearized integral equation is obtained through an infinite system of integral equations which is solved step by step by means of Stokes' function. The first equation gives a first approximation which corresponds to Stokes' formula for the surface of the earth, while in further approximations the topography is considered.

Thus, the ellipsoidal heights of the points on the surface are computed from the sum of the height anomalies (ζ), determined from the disturbing potential on the surface, and the normal heights (H), determined from the values of the geopotential on the surface. The existence as well as the uniqueness of the solution were examined, and although the existence can be guaranteed for exact and physically meaningful data, the uniqueness cannot be guaranteed, given gravimetric data alone (ibid.). Four additional parameters must be determined by astronomical and geodetic measurements.

An alternative linearized solution to Molodenskii's problem was derived by Brovar (Moritz, 1980) by introducing a different harmonic function in the expression of the potential of a surface layer and thus arriving at a different and somewhat simpler integral equation.

Molodenskii's problem, which is a third type free boundary value problem involving an oblique derivative has been called the "modern" geodetic boundary value problem, in contrast to Stokes' classical problem. Certain simplifications are still present in the modern theory. The earth is considered rigid and uniformly rotating around a fixed axis passing through the center of mass. Also, only the masses interior to the earth are considered and tidal effects are neglected. Despite these simplifications the problem has not been solved in general and recently there have been important theoretical advances of considerable mathematical complexity. In view of the new developments, Molodenskii's problem as outlined briefly above is referred to as "the classical modern geodetic boundary value problem" (Sansò, 1984).

A non-linear solution for Molodenskii's problem was obtained by Hörmander using Nash's iteration method to develop the inverse function theorem (Moritz, 1980).

Since most of the difficulty is due to the unknown boundary, the "gravity space" approach developed by Sansò constitutes a significant contribution, by transforming the free boundary to a fixed one. This is done by describing the problem in gravity coordinates, that is using the three Cartesian components of actual gravity $\vec{g} = (g_{x_1}, g_{x_2}, g_{x_3})$ as the coordinates of the point where they are computed. Since $\vec{g}$ and $W = W(\vec{g})$

are known on the boundary, then the boundary is known in the new coordinate system. The serious disadvantage of this approach is the limitation to a non-rotating earth, because the centripetal acceleration does not allow for a one-to-one mapping between the ordinary Euclidean space $\mathbb{R}^3$ (x) and the gravity space $\mathbb{R}^3$ (g). This problem is handled by considering only the gravitational potential and a new function called the adjoint potential is introduced. Detailed reviews of the recent theoretical developments have been given by Sansò (1984) and Sacerdote and Sansò (1987).

A common point between the classical and the modern theory is the requirement of continuous gravimetric data coverage, although such situation is far from being realized. On the other hand large amounts of altimetric data have been available since the last decade. This prompted the formulation and study of new geodetic boundary value problems of great practical importance, the so-called altimetry-gravimetry problems.

A most distinguishing new element of the altimetry-gravimetry problems is the partitioning of the boundary in two parts where different boundary conditions hold. Two types of altimetry-gravimetry problems have been proposed. The first one, presented by Sansò (1984), is a boundary value problem for the Laplace equation with a Dirichlet condition over the sea surface (S_S: fixed) and the geopotential and gravity vector given over the land surface (S_L: free). The second one, presented by Holota (1980), is a boundary value problem for the Laplace equation with a Neumann condition over the sea surface (S_S: fixed) and the geopotential and gravity vector given over the land (S_L: free). Only the linearized versions of these problems have been studied following Molodenskii's classical treatment, except from adopting a different telluroid definition to fit the known S_S. The relevant existence and uniqueness theorems have been studied under a spherical boundary approximation (Sansò, 1983).

While the above outlined problems have practical applications, it is currently the case, and even more so the future situation, that different types of data exist in overlapping parts of the boundary. The corresponding boundary value problems are called overdetermined. A fundamental distinction from the altimetry-gravimetry problems, where the different observables cover disjoint parts of the boundary surface, is that the redundant observations must be attached a meaning of statistical nature.

Obviously, if the observations were exact there would be no reason for retaining overlapping ones. Hence, the solution of overdetermined boundary value problems must implement procedures capable of handling erroneous data in contrast to the deterministic solutions of the classical and Molodenskii's problems. A stochastic approach to the altimetry-gravimetry problem has been proposed by Bjerhammar (1983) utilizing the Gauss-Markov model and the MINQUE method to estimate variance components, and from them, the weight matrix to be used.

To conclude this conceptual overview, the principle of Integrated Geodesy is mentioned as the "philosophy" to use all available geodetic (and other pertinent) observations in a unified procedure for three-dimensional or four-dimensional geodesy (Hein, 1986). In support of the attainability of integrated data processing is the tremendous advance in the technology of the supercomputers for handling large amounts of data and for achieving high speed computations.

1.2 Theory of the overdetermined geodetic boundary value problems and existing solutions

It is a decisive characteristic of the overdetermined boundary value problem theory that the estimation and not the determination of the gravity field is sought. A rigorous mathematical framework has been laid by Sacerdote and Sansò (1985) for the solution of overdetermined boundary value problems in general, together with the particular formulation of geodetically meaningful cases, namely the overdetermined altimetry-gravimetry and the gravimetry-gradiometry problems. The essential ideas of this work are presented briefly in the following, starting from the definition of the problem.

For the unknown function T, the following conditions must be fulfilled

$$\begin{aligned} & \nabla^2 T = 0 && \text{in } \Omega : \mathbb{R}^3 \supset \Omega, \\ (1)\quad & B_1\, T = f_1 \\ (2)\quad & B_2\, T = f_2 && \text{on } \partial\Omega, \end{aligned} \tag{1.2-1}$$

where Ω is the domain where the Laplacian (∇^2) holds and $\partial\Omega$ its boundary; that is, a closed surface where the boundary conditions (1) and (2) are given. B_1 and B_2 are assumed to be linear operators, and f_1 and f_2 the boundary data which are functions defined on $\partial\Omega$.

If the problem defined by the Laplacian and boundary condition (1) only is considered and assumed to have a unique solution then the function T is completely determined and so is f_2. However, this is not the case in reality since f_1 and f_2 are imperfect measurements and therefore the problem as defined has no solution. A problem stated as such is called overdetermined and a solution can be obtained under a chosen error minimization principle. In this sense a best linear estimate: $\hat{f} = (\hat{f}_1, \hat{f}_2)$ is found from the data: $f^{(0)} = (f_1^{(0)}, f_2^{(0)})$ by means of the linear operator $\mathfrak{T}$, so that the functions $\hat{f}_1$ and $\hat{f}_2$ are consistent, and a unique solution of (1.2-1) is obtained from:

$$\hat{f} = B\,\hat{T} \tag{1.2-2}$$

where $B \equiv (B_1, B_2)$ and $\hat{f} = \mathfrak{T}\, f^{(0)}$.

Following these ideas one may view the solution to the overdetermined boundary value problem as the infinite dimensional generalization of the least-squares estimation of parameters from redundant data.

Let y_0 be a set of measurements of a random variable with covariance matrix C and x be the parameters in the linear model y=Bx. Then an unbiased estimate $\hat{y}$ is obtained using the least-squares principle:

$$(\hat{y} - y_0)^T C^{-1} (\hat{y} - y_0) = \min_{y=Bx} (y - y_0)^T C^{-1} (y - y_0), \tag{1.2-3}$$

where

$$\hat{y} = B\hat{x} = B(B^T C^{-1} B)^{-1} B^T C^{-1} y_0. \tag{1.2-4}$$

The equivalent minimum principle for the linear model (1.2-2) is the infinite dimensional generalization of the principle (1.2-3), where the vectors y and y_0 are replaced by the functions f and $f^{(0)}$ and the covariance matrix C becomes an operator C. Then the variational principle may be expressed in general as:

$$\langle C^{-1}(\hat{f}-f^{(0)}), (\hat{f}-f^{(0)})\rangle = \min_{f=BT} \langle C^{-1}(f-f^{(0)}), (f-f^{(0)})\rangle. \tag{1.2-5}$$

The operator C is symmetric and invertible, defined from:

$$(Cv)_i(X_1) = \int_{\partial\Omega} \sum_{j=1}^{2} C_{ij}(X_1, X_2)\, v_j(X_2)\, d\sigma x_2 \ , \quad i = 1, 2 \tag{1.2-6}$$

where the kernel function C_{ij} is the covariance function:

$$C_{ij}(X_1, X_2) = E\left\{\left[f_i(X_1) - \bar{f}_i(X_1)\right]\left[f_j(X_2) - \bar{f}_j(X_2)\right]\right\}. \tag{1.2-7}$$

Finally, the equation corresponding to equation (1.2-4) is given as:

$$\hat{f} = B\,(B^{+}C^{-1}\,B)^{-1}\,B^{+}\,C^{-1}\,f^{(0)}, \tag{1.2-8}$$

where B^{+} is the adjoint of B. However this formula is not accepted since the operator C^{-1} cannot, in general, be proved to be bounded. It is only proved adequate in a simple case where the boundary $\partial\Omega$ is a sphere and the Dirichlet and Neumann boundary conditions are given for the data f_1 and f_2 which, in this case, can be expressed in spherical harmonic series.

In order to obtain an acceptable estimator in all cases Sacerdote and Sansò (ibid.) proceed by employing another minimizing principle. The mean square error principle, which is proved equivalent to least-squares, is written as:

$$E\left\{\left\|\hat{y}-\bar{y}\right\|^2\right\} = \min_{y=Bx} E\left\{\left\|y-\bar{y}\right\|^2\right\} \tag{1.2-9}$$

where $\bar{y} = E\{y\}$. Imposing the condition of obtaining an unbiased linear estimator the above principle becomes:

$$E\left\{\left\|\hat{y}-\bar{y}\right\|^2\right\} = tr\, L^T B^T Q^{-1} BLC \tag{1.2-10}$$

where L is the unknown matrix introduced in the unbiasedness condition BLB = B, and Q^{-1} is any positive definite matrix used in the norm definition in $\mathbb{R}^n$:

$$\|y\|^2 = y^T Q^{-1} y \tag{1.2-11}$$

The estimator finally obtained from the minimization of (1.2-10) is independent of the choice of the norm, i.e. the matrix Q^{-1}.

The above formulation is generalized to the infinite dimensional case, where the result corresponding to (1.2-10) is:

$$E\left\{\left\|BL\left(f^{(0)}-\bar{f}\right)\right\|^2\right\} = \sum_{n=1}^{\infty} \langle L^+ B^+ Q^{-1} BLCe_n, e_n\rangle$$
$$\equiv tr\, L^+ B^+ Q^{-1} BLC, \tag{1.2-12}$$

where $\{e_n\}$ is an orthonormal basis in the Hilbert space where the norm is defined.

The convergence of the series in equation (1.2-12) is required and can be secured by choosing an appropriate covariance operator C. In order to assure a solution, the minimizing principle is regularized and further modified to lead to linear equations. However the unbiasedness condition must be released and the new minimizing principle is:

$$tr\, \hat{L}^+ B^+ Q^{-1} B\hat{L}C + \alpha tr\, \hat{L}^+ B^+ Q^{-1} B\hat{L}Q =$$

$$\min\left(\mathrm{tr}\, L^{+} B^{+} Q^{-1} BLC + \alpha \mathrm{tr}\, L^{+} B^{+} Q^{-1} BLQ\right) \tag{1.2-13}$$

where α is the scalar regularization parameter. The estimator derived by utilizing equation (1.2-13) is biased, but it is proved that a sequence of biased estimates converges to the unbiased one:

$$\hat{T} = \left(B^{+} D_{\alpha}^{-1} B\right)^{-1} B^{+} D_{\alpha}^{-1} f^{\{0\}} \tag{1.2-14}$$

where $D_\alpha = C + \alpha Q$ is proved in general to be a bounded operator, except when $\alpha \to 0$. Comparing to equation (1.2-8) the above result may be viewed as a regularized least-squares estimator, since the presence of the term αQ in the definition of the covariance operator is the only difference. For the actual computation of the estimate $\hat{T}$, it is suggested that a basis $\{n_k\}$ is introduced so that:

$$\hat{T} = \sum_{k=1}^{\infty} T_k n_k . \tag{1.2-15}$$

Obviously the resulting system of an infinite number of equations, involving the sum of an infinite series, is solved by truncating the series at N_{max} and considering only as many equations. In conclusion, the computational procedure is further illustrated in the overdetermined altimetry-gravimetry problem:

$$BT = \begin{bmatrix} \Delta g_{|\mathrm{land}} \\ T_{|\mathrm{sea}} \\ \delta g_{|\mathrm{sea}} \end{bmatrix}, \tag{1.2-16}$$

where the solid spherical harmonics are used as basis functions in the T parameterization. Heavy computation burden is required for the formation of the system and also the solution of the system depending on the choice of the N_{max}.

Because of the extensive computational requirements of the global solution, Sansò (1986) favors a local solution, based on regionally defined functions. A basis of finite element shape functions, for instance, would lead to a patterned normal matrix which could be exploited with sufficient gain to make the solution plausible.

Other than the computational difficulties there still remains a drawback in the solution described above: the dependence of the solution on an arbitrary regularization parameter. To avoid this Sansò (1988) proposed another approach, which utilizes a suitable generalization of Wiener's process and Wiener's integral over a manifold. On this basis, the white noise process is defined on the boundary, together with its relation to the measurement noise. Then, by defining the solution of Laplace's equation given white noise as boundary values, a stochastic solution of a boundary value problem is reached and the minimum mean square error principle is imposed to handle the overdetermination. The stochastic model adopted in this development allows for a constant and independent white noise in each boundary condition. As a next step a constant correlation is admitted between different measurements referring to the same location. Further generalizations need to be made by considering variable variances and correlations.

Despite the theoretical limitations that Sansò has proved for a least-squares adjustment solution to the overdetermined boundary value problems, actual computations have shown a rather successful practical result. In particular, high degree global geopotential models (GPM1 and GPM2) were derived by Wenzel (1985), who adjusted together mean gravity anomalies, mean altimetric geoid heights and satellite derived geopotential models. This procedure involves the solution of a large system of equations (of about 40,000 unknowns) and a large number of observations (about 100,000). In return, different types of observations can be included, without transforming from one type to another, while the observation equations can be as exact as possible. Also, the accuracy of the adjusted parameters is estimated and the residuals serve as good indicators of the measurement errors. Due to the large number of observations the weight matrix (P) is assumed to be diagonal and the elements of the normal matrix (N) are computed by means of analytical expressions, since matrix operations cannot be afforded.

Considering the estimation of the spherical harmonic coefficients of a geopotential model to degree and order 200, the normal matrix to be dealt with has 8×10^8 elements in symmetric storage. However, it is a diagonally dominant matrix with small off-diagonal elements. In an attempt to bring matrix N to a banded form, the normal equations are scaled:

$$N' = SNS \tag{1.2-17}$$

so that all diagonal elements of N' are set to 1. Then the matrix S is a diagonal matrix such that:

$$[Sii] = \frac{1}{\sqrt{|Nii|}} . \tag{1.2-18}$$

All off-diagonal elements $[N_{ij}] < \epsilon$, where ϵ is a chosen limit size, are ignored and only the ones $[N_{ij}] \geq \epsilon$ are taken into account. Since the exact location of the very small $[N_{ij}]$'s depends on the data coverage and the weight distribution, it cannot be predicted à priori. Thus, to obtain a minimum bandwidth of the matrix an appropriate ordering of the unknowns is necessary. As a last step an iterative solution is employed by using the banded part of the normal matrix

$$N' = B + R \tag{1.2-19}$$

where B is the banded part and R the remaining part of N'. Then the iteration procedure is given by the following equations:

$$l_i = L - AX_{i-1} \tag{1.2-20}$$

$$X_i = X_{i-1} + B^{-1} (A^T P l_i) .$$

Convergence is expected and reached when:

$$X_i - X_{i-1} = B^{-1} (A^T P l_i) \rightarrow 0 . \tag{1.2-21}$$

For the computation of GPM1 and GPM2 models, Wenzel (ibid) used only the diagonal terms of the normal matrix in B. Specifically, for the derivation of GPM2 complete to degree 200, 55,454 observations of mean gravity anomalies, 62,003 observations of mean altimetric geoid heights and 570 potential coefficients of the GEM L2 model were used, a total of 118,027 observations and 40,401 unknowns.

The problems that are associated with this approach are addressed by Wenzel (ibid), and they are mainly the two following: a) the spectral resolution of the data (especially mean values) and b) the data gaps, which generate strong, short periodic variations in the estimated model, unless a suitable stabilization is used. From the experience of the GPM1 and GPM2 computations, particular problem areas are reported, which should be handled to avoid unstable iterations in the adjustment: systematic differences among various data sets should be known à priori and any existing data blunders should not be included.

In addition to these two models, there exist a group of high degree geopotential models which are widely used and can be considered solutions to the overdetermined problem, although they do not follow the typical definition presented here. On the other hand, these models are the result of the combination of all available data, and, in that sense, represent a non-rigorous but practically accessible solution. Among them there has been continuing refinement in the procedure as well as the input data sets used. For example, the RAPP81 field, computed by Rapp (1981) to degree and order 180 is based on three data sources: a 1° x 1° mean gravity anomaly data set derived from Seasat altimetric data, combined with a 1° x 1° updated terrestrial data set, yielding one set of 56,761 values; also an à priori satellite derived potential coefficient set (GEM 9) complete to degree 20 with additional terms up to (30, 28). The combined anomaly set reached complete global coverage by filling in the missing data with values computed from the à priori coefficient set. Overlapping boundary values in the two gravity anomaly sets were empirically merged to choose the most accurate values and eliminate inconsistencies. Then, the à priori coefficients and the global gravity anomaly data set were used together in a least-squares adjustment, and the potential coefficients (other than the adjusted ones) were computed from the adjusted data through an optimum quadrature procedure. The

accuracy of the coefficients was estimated by error propagation considering measurement and sampling error.

As the databases improved with time, more rigorous procedures were employed to estimate even more detailed fields. Rapp and Cruz (1986a) discuss the computation of two potential coefficient sets, OSU86C and OSU86D, the only difference between them being that 5,547 geophysically predicted gravity anomalies were included in the derivation of the latter. The procedure followed was essentially similar to the one described above: a low degree satellite derived set of coefficients was combined with a global set of 1° x 1° mean gravity anomalies in a least-squares adjustment. A special version of GEML2 was used together with six additional coefficient pairs, after an ellipsoidal correction was applied. The anomaly data set was developed from the merging of the June 1986 terrestrial set, after applying downward continuation, and the Geos 3/Seasat altimeter data using empirical criteria. The adjusted data were then used in a least-squares collocation solution to compute the remaining potential coefficients complete to degree 250, together with the associated accuracy estimates. Since test runs of replacing the collocation estimation with the integration formula procedure showed good agreement, the latter procedure was used in deriving the next two fields, OSU86E and OSU86F (Rapp and Cruz, 1986 b). The adjusted potential coefficients of the previous fields were adopted. For the computation of the remaining ones to degree and order 360, a 30′ x 30′ gravity anomaly data set of 149,670 values was used in an optimum quadrature procedure. Accuracy estimates could not be easily obtained in this methodology and it is suggested to follow the values computed in OSU86C/D models up to degree 175 and assign 100% uncertainty for higher degree coefficients.

Comparison of these potential coefficient sets with GPM1 and GPM2 and other existing global models with regard to their theoretical basis, problems and advantages is given by Rapp (1986). Further comparative analysis concerning applications as well as the usefulness and future needs of high degree models is presented by Rapp (1987).

1.3 Perspective and general methodology of a collocation approach

A solution to the overdetermined geodetic boundary value problem, as defined in the previous section, is the objective of this study. Considering the established theory, the achieved practical solutions and the data situation, a collocation approach is implemented in a simulation analysis.

This attempt is primarily intended to provide the methodology for the computation of a global gravity field model. The à priori goals were the development of a procedure as general as possible to handle all possible types of existing information and data types, rigorous with regard to the solution of the system and one-step, i.e. avoiding data pre-processing and transformation to other types. Finally and most importantly, the computational feasibility of such a procedure is sought.

In general, an operational approach is followed here, as opposed to a model approach, eg. the classical boundary value problem solution (Moritz, 1980, p. 221). In essence, operational is considered the approach of solving a problem by finding the best possible solution in the presence of all relevant information, instead of deriving a model and acquiring the appropriate data to obtain its parameters.

A widely familiar method from "operational geodesy" and "integrated geodesy", the least-squares collocation, is implemented here. Although collocation is mostly viewed with a statistical interpretation, it possesses the analytical structure of approximation methods. The particular properties of the gravity field enter in a basic covariance function from which all other necessary covariance functions are derived via propagation.

The choice of the method of collocation is advantageous for the following reasons: a) it provides the best linear unbiased estimate of the predicted signal (and parameters when applicable) b) heterogeneous and noisy data can be handled and heterogeneous signals can be predicted provided all the necessary covariance functions are known, c) in cases of data gaps the prediction reflects the corresponding covariance functions, d) provides accuracy measures of the estimated quantities.

The most important disadvantage of the method is the required computational effort, which makes it impossible to use in many cases. This is because the inverse of the covariance matrix of the observed quantities or the solution of the equivalent system of equations must be computed, the former being more time consuming than the latter.

Despite the large amounts of data involved in the problem at hand, the implementation of collocation is undertaken in this work in light of the following: a) the block-Toeplitz structure of the covariance matrix of the observations under certain covariance function assumptions, which is exploited in generating and inverting the matrix, b) the sequential algorithm of incorporating additional data groups based on a partitioned inversion, and c) the recent advances in the supercomputer technology and already achieved substantial improvement over the CRAY X-MP/48 which was used in this work.

CHAPTER II

FORMULATION OF A COLLOCATION SOLUTION OF THE OVERDETERMINED BOUNDARY VALUE PROBLEM

2.1 Fundamental principles of collocation

The method of collocation was introduced in geodesy through Moritz' work of gravity anomaly interpolation. Furthermore, Bjerhammar presented the idea of approximating the potential at the points where gravity anomalies are measured, using collocation and a set of potentials that are regular down to a sphere imbedded within the earth. It was the valuable work of Krarup (1969) which provided the foundation for the application of the general collocation model in physical geodesy. His studies originated from the instability suspected in Molodenskii's boundary value problem. Also, the reality of finite measurements gave the motivation to look at the determination of the gravity field as a problem of interpolation, or approximation. Along these lines it is natural to formulate the boundary value problem as an adjustment problem, where an improvement of the boundary value, made minimum in some least-squares sense, would provide a unique solution. Krarup generalized Moritz' interpolation formulation to find directly the potential, instead of using the predicted gravity anomalies in Stokes' formula. In addition, his generalization included other types of measurements, including satellite-related and deflections of the vertical, as well as a treatment of data error, in what he called a smoothing procedure.

Collocation, in applied mathematics, is called the determination of a function by fitting an analytical approximation to a set of given linear functionals (Moritz, 1980, p. 85). This definition is consistent with two aspects of collocation: the prediction aspect where discrete values of the function are predicted, and the one of finding the interpolating continuous function as an entity. In other words, there is a finite and an infinite dimensional aspect of collocation (Krarup, 1969, p. 29), which are both applicable in physical geodesy. The first one when a certain number of values of linear functionals of the gravity field are predicted at discrete points, and the second one when

the gravity potential is determined as a function in space.

Consider a function T in a Hilbert space H, and the given linear functionals L_k of T,

$$L_k T = l_k \ , \qquad k = 1, 2, ..., q \tag{2.1-1}$$

where $l_k \in \mathbb{R}^q$. By defining the linear operator $B = [L_k]$, the above equation becomes:

$$BT = l \tag{2.1-2}$$

with the transformation $B: H \rightarrow \mathbb{R}^q$.

Assuming that a reproducing kernel function K (P, Q) exists in H, then it is unique and satisfies two fundamental properties:

$$K (P, Q) \in H \text{ for Q fixed,} \tag{2.1-3}$$

$$f (Q) = \langle f (P), K (P, Q) \rangle_p \text{ for all } f \in H. \tag{2.1-4}$$

From the above it follows that the kernel function is symmetric and positive definite, which is expressed by the following relations:

$$K (P, Q) = K (Q, P) \tag{2.1-5}$$

$$\sum_{i=0}^{n} \sum_{k=0}^{n} x_i x_k K (P_i, P_k) > 0, \tag{2.1-6}$$

for all sets of n points P_i and n corresponding numbers $x_i \neq 0$, where i = 1, 2, ... , n for all natural numbers n.

The kernel function may be expressed in terms of the basis functions φ_i (P), which form a complete orthonormal base in H:

$$K(P, Q) = \sum_{i=1}^{\infty} \varphi_i(P)\, \varphi_i(Q). \tag{2.1-7}$$

It also holds that:

$$\varphi_i(P) = L_i^Q K(P, Q) \tag{2.1-8}$$

and since $T \in H$, it can be approximated by:

$$\hat{T}(P) = \sum_{i=1}^{n} b_i\, \varphi_i(P), \tag{2.1-9}$$

where b_i are unknown coefficients, which are determined by substituting (2.1-9) into (2.1-1):

$$L_k \hat{T} = L_k \hat{T}(P_k) = \sum_{i=1}^{n} b_i\, L_k^P L_i^Q K(P_k, Q_i) = l_k. \tag{2.1-10}$$

Following the notation introduced in (2.1-2), the base functions are written as:

$$[\varphi_i] = BK, \tag{2.1-11}$$

and the equations (2.1-9) and (2.1-10) are written as:

$$\hat{T} = (BK)^T b \qquad \text{and} \tag{2.1-12}$$

$$B(BK)^T b = l. \tag{2.1-13}$$

Solving (2.1-13) for b and substituting into (2.1-12) the function T is determined from:

$$\hat{T} = (BK)^T \left[B(BK)^T\right]^{-1} l . \qquad (2.1\text{-}14)$$

It can be proved that the solution given from (2.1-14) minimizes the norm of T (i.e. $||\hat{T}||^2 \leq ||T||^2$) in the Hilbert space H. In particular this norm has the value (Moritz, 1980, p. 214):

$$\left\|\hat{T}\right\|^2 = \langle \tilde{T}, \hat{T} \rangle = \sum_i \sum_j b_i b_j L_i^Q L_j^P K(P,Q) . \qquad (2.1\text{-}15)$$

The above equation may be expressed in the notation of equations (2.1-11) to (2.1-14) as:

$$\left\|\hat{T}\right\|^2 = b^T B (BK)^T b , \qquad (2.1\text{-}16)$$

and after substituting b from (2.1-13) the norm is given as function of the data:

$$\left\|\hat{T}\right\|^2 = l^T \left(BKB^T\right)^{-1} l . \qquad (2.1\text{-}17)$$

It is seen that the determination of the function $\hat{T}$ depends on the choice of the norm in Hilbert space H, and subsequently the kernel function K (P, Q). The particular choice of the reproducing kernel defines the metric in the Hilbert space, which allows for a geometric interpretation of collocation.

The geometry of collocation seen as a least-squares adjustment problem is shown by (Krarup, 1967, pp. 34-38), in connection with the classical least-squares adjustment. Two finite or infinite dimensional spaces are considered H_1 and H_2. Given a bounded operator A: $H_1 \rightarrow H_2$ and an element $\alpha \in H_2$, find $x \in H_1$: $||z||_2$ = minimum, where:

$$z = Ax - \alpha . \qquad (2.1\text{-}18)$$

If the operator A^TA is invertible, the unique solution of this problem is the commonly used least-squares adjustment (observation equations) formula:

$$x = (A^TA)^{-1} A^T \alpha . \qquad (2.1\text{-}19)$$

Given a bounded operator B: $H_2 \rightarrow H_1$ and an element $b \in H_1$, find $x \in H_2$:

$$Bx = b \qquad (2.1\text{-}20)$$

and $|| x ||_2 =$ minimum. The solution in this case is a least-squares collocation solution:

$$x = B^T (BB^T)^{-1} b. \qquad (2.1\text{-}21)$$

The geometry of other least-squares adjustment problems, a generalized adjustment model and the collocation model is illustrated by Dermanis (1976). Most importantly, the duality in interpretation of these models is elaborated and the relation between the least-squares adjustment and collocation is shown.

In the derivations presented to this point, the definition of the metric in Hilbert space is arbitrary, so that there is an infinite number of functions $\hat{T}$ determined from equation (2.1-14) which fit the given data l, depending on the choice of the kernel function K (P, Q). In order to obtain a unique and meaningful solution, a statistical interpretation is attached to the function K (P, Q): it is identified with the covariance function of T. This is possible since both functions share the properties of symmetry and positive definiteness. Also, all the other relevant covariance functions are derived using the propagation law of the kernel (or covariance propagation law) and the appropriate linear operators. Thus, equations (2.1-14) and (2.1-17) are written as:

$$\hat{T} = C_{Tl}\, C_{ll}^{-1}\, l \quad \text{and} \qquad (2.1\text{-}22)$$

$$\left\|\hat{T}\right\|^2 = l^T C_{ll}^{-1}\, l, \qquad (2.1\text{-}23)$$

where

$$C_{ll} = \text{cov}(l,l) \text{ and} \tag{2.1-24}$$

$$C_{Tl} = \text{cov}(T,l)\,. \tag{2.1-25}$$

Under the statistical interpretation this solution can be derived by minimizing the variance of the predicted quantities i.e.:

$$\sigma_k^2 = E\left\{\varepsilon_k^2\right\} = E\left\{\left(\hat{T}_k - T_k\right)^2\right\} = \text{minimum}, \tag{2.1-26}$$

which corresponds to the minimum error norm approximation:

$$\left\|\hat{T} - T\right\|^2 = \text{minimum}. \tag{2.1-27}$$

An additional equation in this case is the covariance of the predicted quantities:

$$C_{\varepsilon\varepsilon} = C_{TT} - C_{Tl} C_{ll}^{-1} C_{Tl}^{T}\,. \tag{2.1-28}$$

The least-squares collocation prediction method maintains the same analytical structure and properties with the analytical collocation, while providing the best linear estimates, in the sense of minimum variance of the predicted signal.

An extensive treatment of the least-squares collocation model, from the stochastic view point is given by Moritz (1980). For the sake of completeness the general least-squares collocation model with parameters is briefly described here in matrix notation and compared to the observation equation model of least-squares adjustment.

Consider the linear model:

$$l = AX + BT + n = AX + t + n, \tag{2.1-29}$$

where the data l are represented by a systematic part AX, a random signal part BT, and random noise n. This model reduces to least-squares prediction with noise for A=0; for B=0, it reduces to ordinary least-squares adjustment. The estimation includes the non-random parameters X and the random parameters $s = [t : u]^T$. The minimum principle satisfied is:

$$s^T C_{ss}^{-1} s + n^T C_{nn}^{-1} n = \text{minimum}, \tag{2.1-30}$$

and the final estimates are given from:

$$\hat{x} = \left(A^T \bar{C}^{-1} A\right)^{-1} A^T \bar{C}^{-1} l \tag{2.1-31}$$

$$\hat{s} = C_{st} \bar{C}^{-1} \left(l - A\hat{X}\right) \tag{2.1-32}$$

where $\bar{C} = C_{tt} + C_{nn}$. In contrast, the minimum principle involved in least-squares adjustment is:

$$n^T C_{nn}^{-1} n = \text{minimum}, \tag{2.1-33}$$

where n is the only random quantity. In the case of prediction and filtering (or smoothing), equation (2.1-32) becomes:

$$\hat{s} = C_{st} \left(C_{tt} + C_{nn}\right)^{-1} l. \tag{2.1-34}$$

The above estimates are optimal in the minimum variance sense, provided the covariances involved are known. When $C_{nn}=0$, equation (2.1-34) reduces to equation $\hat{s} = C_{st} C_{tt}^{-1} l$, known as Wiener-Kolmogorov formula (ibid., p. 211).

Other than the derivations outlined above, these formulae can be obtained in a deterministic way, by adopting quadratic norms and solving the corresponding variational problems.

2.2 Estimation of spherical harmonic coefficients for the disturbing potential.

The aim of this work being to find the function of the anomalous gravity potential T of the earth, a set of basis functions is needed so T can be expressed as their linear combination. Then the unknown coefficients are to be calculated as shown in equations (2.1-9) and (2.1-10). The foundation study of Krarup (1969) has discussed the usefulness of spherical harmonics as such a base from the practical point of view, beyond the fact that they represent a solution to Laplace's equation. These concepts will be briefly exposed in the following.

Let Σ be the space outside a sphere with radius R and surface σ ($\sigma \notin \Sigma$) and sets of potentials φ which are regular in Σ and at infinity so that:

$$\lim_{P \to \infty} \varphi(P) = 0. \qquad (2.2\text{-}1)$$

A set S of these potentials which are continuous in Σ and σ have continuous boundary values on the surface σ of the sphere. It is proved that if the boundary values are known, then φ can be found by means of Poisson's integral and that Poisson's kernel can be expressed in spherical harmonics. From that, a symmetric kernel function K (P, Q) can be defined as:

$$K(P, Q) = \sum_{n=0}^{\infty} (2n + 1) \left(\frac{R^2}{r_P r_Q} \right)^{n+1} P_n(\cos \psi). \qquad (2.2\text{-}2)$$

It is shown (ibid. p. 44) that K (P, Q) is the reproducing kernel for a Hilbert space H, which can be proved to consist of potentials regular in Σ, with square integrable boundary values on the sphere. After defining the functions $\{\varphi_n^m(P)\}$ by:

$$\varphi_n^m(P) = \begin{cases} \left(\frac{R}{r_P}\right)^{n+1} \bar{R}_{nm}(Q_P, \lambda_P), & m \geq 0 \\ \left(\frac{R}{r_P}\right)^{n+1} \bar{S}_{nm}(Q_P, \lambda_P), & m < 0 \end{cases} \tag{2.2-3}$$

where $\bar{R}_{nm}$ and $\bar{S}_{nm}$ are fully normalized surface spherical harmonics, then (2.2-2) is written:

$$K(P, Q) = \sum_{n=0}^{\infty} \sum_{m=-n}^{n} \varphi_n^m(P)\, \varphi_n^m(Q), \tag{2.2-4}$$

which means that the spherical harmonics $\{\varphi_n^m\}$ form a complete orthonormal system for the Hilbert space H. Then for every potential $\varphi \in H$ a series expansion may be written:

$$\varphi(P) = \sum_{n=0}^{\infty} \sum_{m=-n}^{n} \alpha_n^m\, \varphi_n^m(P), \quad \text{for } P \in \Sigma. \tag{2.2-5}$$

There exists a sphere of radius R_1, for which the above series converges uniformly on the surface and outside of any concentric sphere R, such that $R > R_1$. Additionally, there are regions of convergence within the limit sphere R_1. In this sense the series provides an analytical continuation of the exterior potential within the body. The potential of a homogeneous sphere for example, can be analytically continued into the whole space except the center. In the current application it is of interest to know whether the limit sphere for the disturbing potential would be located below the earth's surface. It can be proved that even if that were true, the addition of some mass at a location above the surface will result in a potential with singularity at this particular location. Thus, it is not practically meaningful to speak of convergence of the series near the surface, since it is a very unstable condition. As it is stated in the literature (ibid. p. 51, Moritz, 1980, p. 64):

"if the series were convergent at the surface of the earth, a displacement of a single grain of sand would spoil the convergence". The remedy to this problem is supplied by Runge's theorem, which states (Krarup, 1969, p. 54): "Given any potential regular outside the surface of the earth and any sphere in the interior of the earth. For every closed surface surrounding the earth, there exists a sequence of potentials regular in the whole space outside the given sphere and uniformly converging to the given potential on and outside the given surface". Hence, the potential can be approximated arbitrarily well by polynomials of spherical harmonics down to the surface of a sphere interior to the earth.

In order to proceed with finding the spherical harmonic coefficients of the approximation of the disturbing potential using collocation, a choice of the reproducing kernel function K (P, Q) is necessary to obtain a unique solution. This is accomplished by introducing a stochastic interpretation of the kernel as the covariance function of T. This is, however, faced with both conceptual and practical problems.

First, the covariance function cannot be found from formal stochastic theory directly, since this would require a population of earths and the corresponding number of realizations of T measured at all points. Considering T as a stochastic process on the sphere, an empirical covariance function may be computed from only one realization of the process by replacing the expectation operator E (i.e. phase average) by a suitable space average M, and assuming that the process is an ergodic process on the sphere (Moritz, 1980, p. 285).

A second problem is that T is not directly measured. This is handled with the propagation law of covariances which allows for the covariance K (P, Q) to be computed from the covariances of its functionals (e.g. C (P, Q) of gravity anomalies).

Despite these problems, a positive consideration is that certain properties of K (P, Q) are known, namely its symmetry, positive definiteness and harmonicity, as discussed in Section 2.1.

Finally, another assumption is made considering T to be a rotation invariant stochastic process. This results in a covariance function which depends on the spherical distance ψ between the points P and Q. Such a function is called homogeneous (origin independent) and isotropic (azimuth independent) (ibid. p. 283). Since the earth is not a sphere, such assumption may be questionable. It is nevertheless considered a feasible approximation of the statistical model (Krarup, 1969, p. 22).

In the following the formulae for the least-squares collocation prediction of the spherical harmonic coefficients are presented. The procedure is essentially the one outlined by Moritz (1980, sec. 21). Certain other equations are derived by Sjoberg (1978).

By eliminating the systematic part from equation (2.1-29) the measurements are modelled as:

$$l = t + n, \tag{2.2-6}$$

where l are the measurements, consisting, for this study, of gravity anomaly (Δg) and undulation (N) data. The signal part of l is t and n is the measurement noise. Since the disturbing potential function $T \in H$ is expanded into an infinite series, the spherical harmonic coefficients comprise an infinite dimensional vector,

$$s = [s_1\ s_2\ s_3\ \ldots\ ]^T, \tag{2.2-7}$$

of the Hilbert space l_2. The equivalence between T and s defines an isomorphism (Moritz, 1980, p. 213) between the corresponding spaces:

$$T \rightarrow s\ :\ H \rightarrow l_2, \tag{2.2-8}$$

which is also shown to be isometric:

$$\|T\|^2 = \|s\|^2. \tag{2.2-9}$$

Thus, equation (2.2-6) is written:

$$l = Bs + n, \tag{2.2-10}$$

where the operator B is expressed as a q x ∞ matrix (where q is the dimension of the vector l). The kernel K is a symmetric infinite matrix, and the formulae of the finite dimensional case may be applied:

$$\hat{s} = C_{st}(C_{tt} + C_{nn})^{-1} l, \tag{2.2-11}$$

under the condition:

$$s^T K^{-1} s + n^T D^{-1} n = \text{minimum} \tag{2.2-12}$$

where:

$$\left.\begin{aligned} C_{st} &= \text{cov}(s, t) = KB^T \\ C_{tt} &= \text{cov}(t, t) = BKB^T \\ C_{nn} &= \text{cov}(n, n) = D \\ C_{ss} &= \text{cov}(s, s) = K \end{aligned}\right\} \tag{2.2-13}$$

The accuracy estimate of the predicted signal is given by:

$$E_{ss} = C_{ss} - C_{st} (C_{tt} + C_{nn})^{-1} C_{st}^T . \tag{2.2-14}$$

Next, the formulae for the computation of the covariances in (2.2-13) are given, starting from the basic covariance function K (P, Q). A detailed derivation is given by Rapp (1988).

$$K(P, Q) = M\{T(P)\, T(Q)\} = K(\psi_{PQ})$$

$$= \frac{1}{8\pi^2} \int_{\lambda=0}^{2\pi} \int_{\theta=0}^{\pi} \int_{\alpha=0}^{2\pi} T(\theta,\lambda)\, T(\theta',\lambda') \sin\theta \, d\theta \, d\lambda \, d\alpha \tag{2.2-15}$$

where

$$\cos\psi = \cos\theta \cos\theta' + \sin\theta \sin\theta' \cos(\lambda'-\lambda) \tag{2.2-16}$$

$$T(\theta, \lambda) = \frac{kM}{R} \sum_{n=2}^{\infty} \sum_{m=0}^{n} \left[\bar{C}_{nm} \cos m\lambda + \bar{S}_{nm} \sin m\lambda \right] \bar{P}_{nm}(\cos\theta). \tag{2.2-17}$$

In the above expression $\bar{C}_{nm}$ and $\bar{S}_{nm}$ are the conventional fully normalized spherical harmonic coefficients of the disturbing potential, where R is the associated scaling parameter. Also $\bar{P}_{nm}$ are the fully normalized associated Legendre functions.

After performing the integration in equation (2.2-15) (Heiskanen and Moritz, 1967, pp. 257-258) and considering no zero and first degree harmonics:

$$K(P, Q) = \sum_{n=2}^{\infty} k_n P_n(\cos\psi) \tag{2.2-18}$$

where k_n are the potential degree variances given by

$$k_n = \left(\frac{kM}{R}\right)^2 \sum_{m=0}^{n} \left(\bar{C}_{nm}^{\,2} + \bar{S}_{nm}^{\,2} \right). \tag{2.2-19}$$

$\bar{C}_{nm}$ and $\bar{S}_{nm}$ are fully normalized spherical harmonic coefficients. The extension of K(P,Q) in three dimensions is done through:

$$K(P, Q) = \sum_{n=2}^{\infty} k_n \left(\frac{R^2}{r_p r_Q} \right)^{n+1} P_n(\cos\psi). \tag{2.2-20}$$

Now, the potential is expressed in terms of Laplace surface harmonics $T_n(\theta, \lambda)$:

$$T(P) = \sum_{n=2}^{\infty} \left(\frac{R}{r_p}\right)^{n+1} T_n(\theta,\lambda), \tag{2.2-21}$$

and the radial component of the gravity anomaly at a point is also expressed in terms of $T_n(\theta, \lambda)$ as:

$$\Delta g(P) = \frac{1}{r_p} \sum_{n=2}^{\infty} (n-1) \left(\frac{R}{r_p}\right)^{n+1} T_n(\theta,\lambda). \tag{2.2-22}$$

Proceeding with the same argument as the one used for the derivation of K (P, Q), the covariance function for the gravity anomalies is obtained:

$$\mathrm{cov}\left(\Delta g_p, \Delta g_Q\right) = C(P, Q) = \sum_{n=2}^{\infty} c_n \left(\frac{R^2}{r_p r_Q}\right)^{n+2} P_n(\cos\psi), \tag{2.2-23}$$

where c_n are the gravity anomaly degree variances given by (Rapp, 1988, p.18)

$$c_n = \left(\frac{n-1}{R}\right)^2 k_n. \tag{2.2-24}$$

By substituting equation (2.2-19) in the above and making a spherical approximation for γ evaluated at a sphere of radius R, (i.e. $\gamma = kM/R^2$) the above equation becomes:

$$c_n = \gamma^2 (n-1)^2 \sum_{m=0}^{n} \left(\bar{C}_{nm}^2 + \bar{S}_{nm}^2\right). \tag{2.2-25}$$

Note that the anomaly degree variances evaluated from the above equation refer to a sphere of radius R (Rapp, 1988, eq. (101)). If used for the computation of covariance

between data points on the surface of a sphere with radius R_E, the equation (2.2-23) is usually written as:

$$C(\psi) = \sum_{n=2}^{\infty} c_n s^{n+2} P_n(\cos\psi), \tag{2.2-26}$$

where

$$s = \left(\frac{R}{R_E}\right)^2 .$$

The same result for $C(\psi)$ is reached by using the covariance propagation formula, as is illustrated in the derivation of the covariance function between the anomaly and undulation signals. In general it holds:

$$\mathrm{cov}(\Delta g_P, N_Q) = L_i^P L_j^Q K(P,Q) . \tag{2.2-27}$$

Since, without loss of generality the radial component of the gravity anomaly can be expressed in a spherical approximation as:

$$\Delta g_p = -\left.\frac{\partial T}{\partial r}\right|_p - \frac{2}{r_p} T_p$$

the operator L_i is defined as

$$L_i^p = \left[-\frac{\partial}{\partial r} - \frac{2}{r}\right]_p , \tag{2.2-28}$$

and from $N_Q = T_Q/\gamma$, the other operator involved is

$$L_j^Q = \left.\frac{1}{\gamma}\right|_Q . \tag{2.2-29}$$

By applying the above operators to K(P, Q), using a constant γ, and further manipulation:

$$\operatorname{cov}\left(\Delta g_P, N_Q\right) = \frac{1}{\gamma}\left[- \left.\frac{\partial K(P,Q)}{\partial r}\right|_P - \frac{2}{r_P} K(P,Q)\right]$$

$$= \frac{R^2}{\gamma r_P} \sum_{n=2}^{\infty} \frac{c_n}{n-1} \left(\frac{R^2}{r_P r_Q}\right)^{n+1} P_n(\cos\psi). \qquad (2.2\text{-}30)$$

For computations of covariance between points on the sphere of radius R_E, the above formula yields:

$$\operatorname{cov}\left(\Delta g_P, N_Q\right) = \frac{R^2}{\gamma R_E} \sum_{n=2}^{\infty} \frac{c_n}{n-1} s^{n+1} P_n(\cos\psi). \qquad (2.2\text{-}31)$$

Similarly, the autocovariance function for the undulation measurements is obtained as:

$$\operatorname{cov}\left(N_P, N_Q\right) = \frac{1}{\gamma^2} \sum_{n=2}^{\infty} k_n \left(\frac{R^2}{r_P r_Q}\right)^{n+1} P_n(\cos\psi), \qquad (2.2\text{-}32)$$

and for computations on the sphere R_E:

$$\operatorname{cov}\left(N_P, N_Q\right) = \frac{R^2}{\gamma^2} \sum_{n=2}^{\infty} \frac{c_n}{(n-1)^2} s^{n+1} P_n(\cos\psi). \qquad (2.2\text{-}33)$$

When including data which are area means of point data values the need for mean covariance functions arises. For a less time-consuming computation of such covariances for signals on the sphere, the equations (2.2-26), (2.2-31) and (2.2-33) are modified by introducing a smoothing operator, called the Pellinen operator (Sjoberg, 1978) β_n. The corresponding equations are:

$$\overline{C}(P,Q) = \sum_{n=2}^{\infty} \beta_n^P \beta_n^Q c_n s^{n+2} P_n(\cos\psi), \tag{2.2-34}$$

$$\mathrm{cov}\left(\overline{\Delta g}_P, \overline{N}_Q\right) = \frac{R^2}{\gamma R_E} \sum_{n=2}^{\infty} \beta_n^P \beta_n^Q \frac{c_n}{n-1} s^{n+1} P_n(\cos\psi), \tag{2.2-35}$$

$$\mathrm{cov}\left(\overline{N}_P, \overline{N}_Q\right) = \frac{R^2}{\gamma^2} \sum_{n=2}^{\infty} \beta_n^P \beta_n^Q \frac{c_n}{(n-1)^2} s^{n+1} P_n(\cos\psi), \tag{2.2-36}$$

where,

$$\beta_n = \frac{1}{1-\cos\psi_0} \frac{1}{2n+1} \left[P_{n-1}(\cos\psi_0) - P_{n+1}(\cos\psi_0)\right],$$

and ψ_0 is the equivalent spherical cap radius for the block. When equal area means are used, as given by Sjoberg (1978), the value of ψ_0 is constant, and for blocks at the equator is given from the equation:

$$\sin\left(\frac{\psi_0}{2}\right) = \left(\frac{\theta \sin\theta}{4\pi}\right)^{1/2}, \quad \theta = \Delta\lambda \tag{2.2-37}$$

and in equations (2.2-34 to 36) it holds $\beta_n^P = \beta_n^Q$. For area means referring to an equiangular grid the value of ψ_0 is computed as shown by Katsambalos (1979),

$$\cos\psi_0 = 1 - \frac{\theta\left(\sin\varphi_N - \sin\varphi_S\right)}{2\pi}. \tag{2.2-38}$$

For efficient computation of the β_n factors the following recursive formula is used:

$$\beta_n = \frac{2n-1}{n+1}\cos\psi_0\,\beta_{n-1} - \frac{n-2}{n+1}\beta_{n-2} \tag{2.2-39}$$

where the starter values are $\beta_0 = 1$ and $\beta_1 = (1 + \cos\psi_0)/2$.

A second group of required covariances pertains to the cross-covariances (C_{st}) between the observed signal and the predicted spherical harmonic coefficients, defined by the relations (2.2-13). The matrix K, which defines the metric in the space l_2, may be derived from the function K (P, Q) by propagation. Starting from the representation of the anomalous potential on the sphere R_E:

$$T(R_E,\theta,\lambda) = \sum_{n=2}^{\infty}\sum_{m=0}^{n}\left(\frac{R}{R_E}\right)^{n+1}\left[\bar{a}_{nm}\,\bar{R}_{nm}(\theta,\lambda) + \bar{b}_{nm}\,\bar{S}_{nm}(\theta,\lambda)\right], \tag{2.2-40}$$

the coefficients are found from,

$$\left.\begin{aligned}\bar{a}_{nm} &= \frac{1}{4\pi}\int_{\sigma} T(\theta,\lambda)\,\bar{R}_{nm}(\theta,\lambda)\,d\sigma, \quad \text{and}\\ \bar{b}_{nm} &= \frac{1}{4\pi}\int_{\sigma} T(\theta,\lambda)\,\bar{S}_{nm}(\theta,\lambda)\,d\sigma.\end{aligned}\right\} \tag{2.2-41}$$

Applying covariance propagation to K (P, Q) and using the operators defined in (2.2-41)

$$\mathrm{cov}\left(\bar{a}_{nm}, \bar{a}_{pq}\right) = \frac{1}{16\pi^2}\int_{\sigma}\int_{\sigma'} K(P,Q)\,\bar{R}_{nm}(\theta,\lambda)\,\bar{R}_{pq}(\theta,\lambda)\,d\sigma\,d\sigma' \tag{2.2-42}$$

where $d\sigma$ and $d\sigma'$ are differential surface elements on the sphere. Next, the function K (P, Q) is substituted from equation (2.2-17) where $P_n(\cos\psi)$ is expressed by the decomposition formula. After the interchange of summation and integration and applying the orthogonality properties, the result is (Moritz, 1980, p. 160)

$$\left.\begin{aligned} &\operatorname{cov}\left(\bar{a}_{nm}, \bar{a}_{nm}\right) = \frac{k_n}{2n+1} \quad \text{and} \\ &\operatorname{cov}\left(\bar{a}_{nm}, \bar{a}_{pq}\right) = 0, \text{ for } n \neq p \text{ or } m \neq q \text{ or both.} \end{aligned}\right\} \tag{2.2-43}$$

Similarly:

$$\left.\begin{aligned} &\operatorname{cov}\left(\bar{b}_{nm}, \bar{b}_{nm}\right) = \frac{k_n}{2n+1} \quad \text{and} \\ &\operatorname{cov}\left(\bar{b}_{nm}, \bar{b}_{pq}\right) = 0, \text{ for } n \neq p \text{ or } m \neq q \text{ or both.} \end{aligned}\right\} \tag{2.2-44}$$

$$\operatorname{cov}\left(\bar{a}_{nm}, \bar{b}_{pq}\right) = 0, \text{ always.} \tag{2.2-45}$$

For the usual representation of T,

$$T(r,\theta,\lambda) = \frac{kM}{r} \sum_{n=2}^{\infty} \left(\frac{R}{r}\right)^n \sum_{m=0}^{n} \left[\bar{C}_{nm} \cos m\lambda + \bar{S}_{nm} \sin m\lambda\right] \bar{P}_{nm}(\cos\theta), \tag{2.2-46}$$

the corresponding covariance among the coefficients $\bar{C}_{nm}$ and $\bar{S}_{nm}$ is easily found as:

$$\operatorname{cov}\left(\bar{C}_{nm}, \bar{C}_{nm}\right) = \operatorname{cov}\left(\bar{S}_{nm}, \bar{S}_{nm}\right) = \left(\frac{R}{kM}\right)^2 \frac{k_n}{2n+1}, \tag{2.2-47}$$

and zero in any other coefficient combination. Then the matrix K is a diagonal matrix of infinite dimension:

$$C_{ss} = K = \begin{bmatrix} k_{11} & & & 0 \\ & k_{22} & & \\ & & k_{33} & \\ 0 & & & \ddots \end{bmatrix}, \tag{2.2-48}$$

where the value of k_{ii} is the same for all coefficients of a particular degree n and

$$k_{nn} = \frac{c_n}{\gamma^2 (n-1)^2 (2n+1)} = [C_{ss}]. \tag{2.2-49}$$

In order to derive the matrix B defined in (2.2-10), the gravity anomaly and the undulation are written in terms of spherical harmonics:

$$\Delta g(r,\theta,\lambda) = \gamma \sum_{n=2}^{\infty} (n-1) \left(\frac{R}{r}\right)^{n+2} \sum_{m=0}^{n} \left[\bar{C}_{nm} \cos m\lambda + \bar{S}_{nm} \sin m\lambda\right] \bar{P}_{nm}(\cos\theta), \tag{2.2-50}$$

and

$$N(r,\theta,\lambda) = R \sum_{n=2}^{\infty} \left(\frac{R}{r}\right)^{n+1} \sum_{m=0}^{n} \left[\bar{C}_{nm} \cos m\lambda + \bar{S}_{nm} \sin m\lambda\right] \bar{P}_{nm}(\cos\theta). \tag{2.2-51}$$

Hence the element of the B matrix relating the spherical harmonic coefficients of degree and order (n, m) to the anomaly measured at point P is:

$$\left[B_p^{C_{nm}}\right] = \gamma (n-1) \left(\frac{R}{r_p}\right)^{n+2} \cos m\lambda_p \bar{P}_{nm}(\cos\theta_p) \tag{2.2-52}$$

$$\left[B_p^{S_{nm}}\right] = \gamma (n-1) \left(\frac{R}{r_p}\right)^{n+2} \sin m\lambda_p \bar{P}_{nm}(\cos\theta_p). \tag{2.2-53}$$

Equations corresponding to (2.2-50) and (2.2-51) for mean data are:

$$\bar{\Delta g}(r,\theta,\lambda) = \frac{\gamma}{\sigma} \sum_{n=2}^{\infty} (n-1) \left(\frac{R}{r}\right)^{n+2} \sum_{m=0}^{n} \left[\bar{C}_{nm} \int_{\sigma} \bar{P}_{nm}(\cos\theta) \cos m\lambda \, d\sigma\right.$$

$$+\bar{S}_{nm}\int_{\sigma}\bar{P}_{nm}(\cos\theta)\sin m\lambda\, d\sigma\Big], \tag{2.2-54}$$

$$\bar{N}(r,\theta,\lambda)=\frac{R}{\sigma}\sum_{n=2}^{\infty}\left(\frac{R}{r}\right)^{n+1}\sum_{m=0}^{n}\Big[\bar{C}_{nm}\int_{\sigma}\bar{P}_{nm}(\cos\theta)\cos m\lambda\, d\sigma +$$

$$+\bar{S}_{nm}\int_{\sigma}\bar{P}_{nm}(\cos\theta)\sin m\lambda\, d\sigma\Big], \tag{2.2-55}$$

where σ is the area of the block on the unit sphere, with block boundaries the parallels φ_N, φ_S and the meridians λ_E, λ_W, given by:

$$\sigma=(\lambda_E-\lambda_W)(\sin\varphi_N-\sin\varphi_S). \tag{2.2-56}$$

Note that R in the above equations is the scaling parameter associated with the coefficients $\bar{C}_{nm}$ and $\bar{S}_{nm}$. The integrals are computed analytically on the unit sphere, where $d\sigma = \sin\theta\, d\theta\, d\lambda$, and using the notation PI_{nm} for the integrated Legendre functions:

$$PI_{nm}=\int_{\theta=\theta_1}^{\theta_2}\bar{P}_{nm}(\cos\theta)\sin\theta\, d\theta, \tag{2.2-57}$$

the integrals are as follows:

$$\text{integral term of } \bar{C}_{nm}=\frac{PI_{nm}}{m}\Big[\sin m\lambda_E-\sin m\lambda_W\Big],\ m\neq 0 \tag{2.2-58}$$

$$\text{integral term of } \bar{C}_{no}=PI_{nm}\Big[\lambda_E-\lambda_W\Big] \tag{2.2-59}$$

$$\text{integral term of } \bar{S}_{nm}=\frac{PI_{nm}}{m}\Big[\cos m\lambda_W-\cos m\lambda_E\Big],\ m\neq 0 \tag{2.2-60}$$

$$\text{integral term of } \bar{S}_{no}=0. \tag{2.2-61}$$

After further manipulation the above equations give the elements of the C_{st} matrix, which are also derived by Sjoberg (1978, p. 8), although following a different argument.

A comparison between the practical application of the collocation formulation presented here and the least-squares adjustment is made by Moritz (1980, pp. 166-167). By estimating a finite number of coefficients $s = [s_1\ s_2\ \dots\ s_N]^T$, the infinite matrix B reduces to dimension q x N; for N<q an overdetermined system of equations is to be solved. The solution equation (2.2-11) is written:

$$\hat{s} = KB^T\left(BKB^T + D^{-1}\right)^{-1} l \tag{2.2-62}$$

and, by applying a matrix identity:

$$\hat{s} = \left(B^T D^{-1} B + K^{-1}\right)^{-1} B^T D^{-1}\, l. \tag{2.2-63}$$

Since the matrices K and D are diagonal, the difference between the implementation of equations (2.2-62) and (2.2-63) is that the first requires the inversion of a q x q matrix, whereas the second of an N x N matrix. If the matrix K has the form:

$$K = \lambda I \tag{2.2-64}$$

where I is the unit matrix and λ a scalar, the equation (2.2-63) becomes:

$$\hat{s} = \left(B^T D^{-1} B + \frac{1}{\lambda} I\right)^{-1} B^T D^{-1} l. \tag{2.2-65}$$

and for $\lambda \rightarrow \infty$

$$\hat{s} = \left(B^T D^{-1} B\right)^{-1} B^T D^{-1}\, l. \tag{2.2-66}$$

which is the least-squares adjustment solution of the observation equation model (2.2-10) under the condition $n^T D^{-1} n$ = minimum and treating the coefficients s as non-random parameters.

2.3 Toeplitz pattern and inversion algorithms

Practical applications of collocation are often limited due to the tedious computations required. Most of the effort is spent in formulating and inverting the covariance matrix of the observations, which makes the method prohibitive to use in applications where a very large amount of measurements is involved. In order to work around this problem, studies have been made in various cases to identify special properties of the covariance functions and the underlying process, that result in patterned matrices consuming less computational time for their formation or inversion or both.

In geodetic applications a certain pattern develops from data regularly sampled on a sphere (Colombo, 1979). For data given on an equiangular grid under the assumptions of complete coverage of the sphere, excluding the poles, and the covariance function dependent only on the longitude separation between two points, the corresponding covariance matrix is a block matrix of Toeplitz circulant blocks (ibid. pp. 4-5). Such structure is exploited to enable a very efficient inversion of the covariance matrix as demonstrated by Colombo (1981) in harmonic analysis of data on the sphere.

A Toeplitz matrix of dimension (N+1) x (N+1), is a matrix $T_N = [t_{kj}]$, where for each element t_{kj} it holds that:

$$t_{k,j} = t_{k-j}\ , \qquad k, j = 0, 1, \ldots , N. \tag{2.3-1}$$

Then the matrix may be presented in the form:

$$T_N = \begin{bmatrix} t_0 & t_{-1} & t_{-2} \ldots\ldots & t_{-N} \\ t_1 & t_0 & t_{-1} \ldots\ldots & t_{-(N-1)} \\ t_2 & t_1 & t_0 \ldots\ldots & t_{-(N-2)} \\ \cdot & \cdot & \cdot & \\ t_N & t_{N-1} & t_{N-2} & t_0 \end{bmatrix} . \qquad (2.3\text{-}2)$$

The matrix T_N is a persymmetric matrix, that is, it has a symmetry with respect to the secondary diagonal. There exists a general class of integral equations which reduce to linear systems with Toeplitz type matrices (Tyrtyshnikov, 1980). The solutions of this class have the following characteristic properties: a) the kernel is invariant under some transformations, and b) the region of integration is obtained from parts of it by applying transformations under which the kernel is invariant. These invariance properties correspond to the stationarity property of the stochastic processes and the associated covariance function. In addition to the Toeplitz structure, the covariance matrices are symmetric and positive definite.

A special case of a Toeplitz matrix is a circulant Toeplitz defined by the condition:

$$t_{-k} = t_{N+1-k}\,, \qquad k = 1, 2, \ldots., N. \qquad (2.3\text{-}3)$$

For example, such matrix is the covariance matrix of data equally spaced over a complete circle, when the data belong to a stationary process. Also, the Toeplitz circulant pattern appears for data regularly sampled completely over a sphere, as shown by Colombo (1979). The advantage in inversion of such matrices is also explained by Eren (1980), by demonstrating their diagonalization in the frequency domain.

Of particular interest in this study are block-Toeplitz matrices. Such structure is completely equivalent to block matrices with Toeplitz blocks, which is the one followed by Colombo (1979). It can be proved that a block Toeplitz matrix is transformed to a

block matrix with Toeplitz blocks, and vice versa, by reordering of the data (Tyrtyshnikov, 1980).

Consider the data arrangement, as shown in the figure 1, of equally spaced observations along four parallels and three meridians:

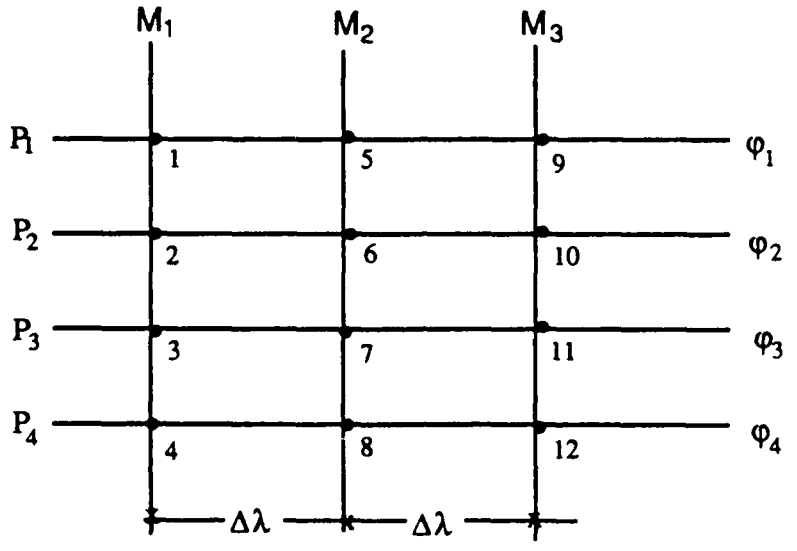

Figure 1. Data arrangement for the block-Toeplitz structure.

The covariance matrix of the observations arranged along the meridians (i.e. M_1, M_2, M_3) may be written in terms of block matrices (i.e. M_1 M_1, M_1 M_2, ... etc), which are teh covariance matrices between the observations on the corresponding meridians (i.e. M_1 and M_1, M_1 and M_2, ... etc).

$$C = \begin{bmatrix} M_1M_1 & M_1M_2 & M_1M_3 \\ & M_2M_2 & M_2M_3 \\ \text{symmetric} & & M_3M_3 \end{bmatrix} \qquad (2.3\text{-}4)$$

Then the matrices M_1M_1, M_2M_2, ... etc, according to equations (2.2-34 to 36) are as follows:

$$M_1M_1 = \begin{bmatrix} f(\varphi_1) & f(\varphi_1,\varphi_2) & f(\varphi_1,\varphi_3) & f(\varphi_1,\varphi_4) \\ & f(\varphi_2) & f(\varphi_2,\varphi_3) & f(\varphi_2,\varphi_4) \\ \text{symmetric} & & f(\varphi_3) & f(\varphi_3,\varphi_4) \\ & & & f(\varphi_4) \end{bmatrix} \tag{2.3-5}$$

The notation f (φ_1, φ_2) stands for "function of φ_1 and φ_2" and so on. It is easily seen that the covariances among the data within the meridians M_2 and M_3 are the same as for the meridian M_1, i.e:

$$M_1M_1 = M_2M_2 = M_3M_3. \tag{2.3-6}$$

Now consider the covariances among meridians separated by $\Delta\lambda$.

$$M_1M_2 = \begin{bmatrix} f(\varphi_1,\Delta\lambda) & f(\varphi_1,\varphi_2,\Delta\lambda) & f(\varphi_1,\varphi_3,\Delta\lambda) & f(\varphi_1,\varphi_4,\Delta\lambda) \\ & f(\varphi_2,\Delta\lambda) & f(\varphi_2,\varphi_3,\Delta\lambda) & f(\varphi_2,\varphi_4,\Delta\lambda) \\ \text{symmetric} & & f(\varphi_3,\Delta\lambda) & f(\varphi_3,\varphi_4,\Delta\lambda) \\ & & & f(\varphi_4,\Delta\lambda) \end{bmatrix}. \tag{2.3-7}$$

It is also obvious that the matrices reflecting the covariances between any two meridians separated by $\Delta\lambda$ are the same:

$$M_1M_2 = M_2M_3. \tag{2.3-8}$$

As already stated above the matrix C in equation (2.3-4) is a block Toeplitz matrix, where the blocks are general symmetric matrices. Had the observations been ordered along the parallels, instead of along the meridians, the matrix C would have been a general block matrix, where the individual blocks are Toeplitz matrices. Note, that it is not necessary for the parallels to be equally spaced, but only for the meridians, so that the resultant matrix C is of the form described above.

It follows from the Toeplitz structure and the symmetry of the matrix C that the top row of blocks completely defines the matrix. In addition, the blocks are themselves symmetric matrices, which substantially reduces the computations of forming the matrix, as well as the storage requirement. Furthermore, the pattern of the inverse of Toeplitz and block-Toeplitz matrices is such that the matrix is defined by one row, while the rest of the rows are easily computed by recurrence relationships (Kutikov, 1967). The algorithm developed by Kutikov for the case of block Toplitz matrices is presented next.

Consider the block matrix of order (N+1) x (q+1) defined as:

$$R_N = \begin{bmatrix} \Gamma_{00}\,\Gamma_{01}\cdots\Gamma_{0N} \\ \Gamma_{10}\,\Gamma_{11} \\ \vdots \\ \Gamma_{N0} \qquad\qquad \Gamma_{NN} \end{bmatrix}. \tag{2.3-9}$$

The algorithm has been derived under the following conditions:

a) R_N is non-singular,

b) Γ_{ks} (for k, s = 0, 1, ..., N) are square matrices of order (q+1), such that $\Gamma_{ks} = \Gamma_{sk}^T$, and

c) $\sum_{k,s=0}^{n} C_k \Gamma_{ks} C_s^T > 0, \quad (n = 0, 1, \ldots, N)$,

i.e. the blocks are positive definite, and thus R_N is positive definite.

In order to describe the structure of R_N^{-1} the block matrices A and B are introduced, defined from the relation:

$$R_N^{-1} = B^T A\, B, \tag{2.3-10}$$

which is valid for:

$$A = \begin{bmatrix} A_{00}^{2} & & & \\ & A_{11}^{2} & 0 & \\ 0 & . & . & \\ & & & A_{NN}^{2} \end{bmatrix} \quad \text{and} \quad B = \begin{bmatrix} I & & & \\ B_{10} & I & & 0 \\ & . & . & \\ B_{N0} & B_{N1} & & I \end{bmatrix} \tag{2.3-11}$$

where A_{nn}^{2} and B_{nk} (n, k = 0, 1, ... , N) are square matrices of order (q+1). Considering block-Toeplitz matrices, the matrix R_N of equation (2.3-9) is written in the form:

$$R_N = \begin{bmatrix} \Gamma_0 & \Gamma_{-1} & \cdots & \Gamma_{-N} \\ \Gamma_1 & \Gamma_0 & & \\ . & . & & \\ \Gamma_N & \Gamma_{N-1} & \cdots & \Gamma_0 \end{bmatrix}. \tag{2.3-12}$$

Associated with the matrix R_N^{T} are the matrices Δ_{nk} and Ω_{nn}^{2}, introduced as the B_{nk} and A_{nn}^{2} in equations (2.3-11). Then the following recurrence relations hold (ibid):

$$B_{nn} = \Delta_{nn} = I, \qquad n = 0, 1, ..., N \tag{2.3-13}$$

$$B_{n+1,k} = B_{n,k-1} + B_{n+1,0}\,\Delta_{n,n-k}, \qquad k = 1, ..., n \text{ and } n = 1, ..., N-1 \tag{2.3-14}$$

$$\Delta_{n+1,k} = \Delta_{n,k-1} + \Delta_{n+1,0}\,B_{n,n-k}, \qquad k = 1, ..., n \text{ and } n = 1, ..., N-1 \tag{2.3-15}$$

$$B_{n+1,0} = -E_n \Omega_{nn}^{2}, \qquad n = 0, ..., N-1 \tag{2.3-16}$$

$$\Delta_{n+1,0} = -H_n A_{nn}^{2}, \qquad n = 0, ..., N-1 \tag{2.3-17}$$

$$A_{nn}^{2} = \sum_{k=0}^{n} B_{nk}\,\Gamma_{n-k}^{T}, \qquad n = 0, \ldots, N \tag{2.3-18}$$

$$\Omega_{nn}^{2} = \sum_{k=0}^{n} \Delta_{nk}\,\Gamma_{n-k}^{T}, \qquad n = 0, \ldots, N \tag{2.3-19}$$

$$E_n = \sum_{k=0}^{n} B_{nk} \Gamma_{k+1}, \qquad n = 0, \ldots, N-1 \tag{2.3-20}$$

$$H_n = \sum_{k=0}^{n} \Delta_{nk} \Gamma_{k+1}^{T}, \qquad n = 0, \ldots, N-1 \tag{2.3-21}$$

Now, let the inverse of R_N be represented in terms of square blocks of order (q+1), then:

$$R_N^{-1} = \begin{bmatrix} Z_{00}^N \cdots Z_{0N}^N \\ . \\ Z_{N0}^N \cdots Z_{NN}^N \end{bmatrix}. \tag{2.3-22}$$

Then they can be computed from the following equations:

$$Z_{Nt}^N = \left[Z_{tN}^N\right]^T = A_{NN}^2 B_{Nt}, \qquad t = 0, 1, \ldots, N. \tag{2.3-23}$$

$$Z_{s-1,t-1}^N = \left[Z_{t-1,s-1}^N\right]^T = Z_{st}^N - \left[\Delta_{N,N-s}\right]^T \Omega_{NN}^2 \Delta_{N,N-t} + \left[B_{N,s-1}\right]^T A_{NN}^2 B_{N,t-1}, \tag{2.3-24}$$

$$s, t = 1, 2, \ldots, N \text{ and } s \geq t.$$

For the implementation of the above algorithm, the matrices B_{Nk}, A_{NN}^2, Δ_{Nk} and Ω_{NN}^2 are computed using the recursive relationships (2.3-13) to (2.3-21). Then equation (2.3-23) is used to compute the blocks of the bottom row of R_N^{-1}. Then all other block rows are computed by means of equation (2.3-24). This algorithm is simplified for the case of symmetric blocks Γ_n (n = 0, 1, ..., N). Thus, the formulae implemented in this work are as described above, but with

$$A_{nn}^2 = \Omega_{nn}^2, \qquad n = 0, 1, \ldots, N \tag{2.3-25}$$

$$B_{nk} = \Delta_{nk}, \qquad k = 0, 1, \ldots, n-1 \text{ and } n = 1, 2, \ldots, N. \tag{2.3-26}$$

In addition to the Toeplitz inversion, a partitioned inversion algorithm has also been implemented in this work. Let

$$T = \begin{bmatrix} A & B \\ C & D \end{bmatrix} \tag{2.3-27}$$

Where A, D and T are square matrices. Then the inverse of T is given (Faddeeva, 1959)

$$T^{-1} = \begin{bmatrix} P & Q \\ R & S \end{bmatrix} \tag{2.3-28}$$

where:

$$\left.\begin{aligned} S &= \left(D - CA^{-1}B\right)^{-1} \\ Q &= -A^{-1}BS \\ R &= -SCA^{-1} \\ P &= A^{-1} - A^{-1}BR \end{aligned}\right\}. \tag{2.3-29}$$

For a symmetric matrix T the above equations become:

$$T = \begin{bmatrix} A & B \\ B^T & D \end{bmatrix} \quad \text{and} \quad T^{-1} = \begin{bmatrix} P & Q \\ Q^T & S \end{bmatrix} \tag{2.3-30}$$

where:

$$\left.\begin{aligned} S &= \left(D - B^T A^{-1} B\right)^{-1} \\ Q &= - A^{-1} B S \\ P &= A^{-1} - A^{-1} B Q^T \end{aligned}\right\}. \qquad (2.3\text{-}31)$$

This partitioning is applied several times for the inversion of the covariance matrix and it essentially results in a form of stepwise or sequential collocation (Moritz, 1980, sec. 19). However, in that case, a new term which reflects the influence of new measurements is added directly to the predicted signal and the associated covariance matrix.

CHAPTER III

IMPLEMENTATION OF THE COLLOCATION PREDICTION FORMULAE.

3.1 The auto-covariance matrix of the observed signals

In implementing the matrix formulation (2.2-11) for the predicted potential harmonic coefficients and (2.2-14) for their error covariance matrix, one is faced with the theoretical requirement of positive definiteness for the covariance matrices. Additionally, the covariance matrix of the observed signal, C_{tt}, must be numerically non-singular to enable the computation of predicted signals for the case of errorless observations. Since the theoretical and numerical properties of this matrix are determined completely by the covariance function and the particular data sampling employed, both of these factors will be examined below with regard to the positive definiteness and the singularity or numerical instability of the matrix C_{tt}.

At first, the positive definiteness of the signal auto-covariance matrix is examined, which is equivalent to the positive definiteness of the covariance function in the case of a continuous signal (Moritz, 1976). This property is expressed by equation (2.1-6) for the covariance function K (P,Q). Considering the form of the fundamental covariance function implemented here, as given by (2.2-20), this condition is subsequently transferred to the degree variances k_n. By means of the correspondence of the covariance function and the power spectrum of the disturbing potential, the set of all degree variances k_n constitutes the power spectrum (Colombo, 1981, p. 5). Then, a necessary and sufficient condition for the covariance function to be positive definite is the condition for the power spectrum to be positive (Moritz, 1976, p. 14), i.e.

$$k_n > 0 , \quad \text{for all n.} \tag{3.1-1}$$

The above is also seen from a different viewpoint by considering an equivalent to the spectral decomposition of the matrix C_{tt}, namely the eigenvector and eigenvalue decomposition (Colombo, 1979, p. 14); the matrix of dimension q is given in terms of

the eigenvalues λ_i and eigenvectors μ_i

$$C_{tt} = \sum_{i=1}^{q} \lambda_i \mu_i \mu_i^T . \tag{3.1-2}$$

Then the positive definiteness of C_{tt} is assured for positive eigenvalues, and the matrix is invertible only for

$$\lambda_i > \varepsilon > 0 , \text{ for } i = 1, ..., q \tag{3.1-3}$$

where ε is a sufficiently large number to avoid numerical problems. Should the equality be allowed in equations (3.1-1) and (3.1-3), the covariance function will be positive semi-definite and the matrix C_{tt} will be singular, as footnoted by Moritz (1980, p. 93). From the preceding arguments one can conclude that, when using the series covariance function expressions, the summation should theoretically be carried out to infinity in order to avoid singularity of the covariance matrix.

This fact is also evident by examining the matrix formulation of the collocation prediction. In particular, equation (2.2-13) where the matrix C_{tt} is given from:

$$C_{tt} = BKB^T. \tag{3.1-4}$$

As shown in equation (2.2-48), K is a diagonal matrix. If the values of k_n are set to zero for $n > Nmax$, then

$$\text{Rank } (K) = (Nmax + 1)^2 , \tag{3.1-5}$$

which is the number of coefficients of the spherical harmonic expansion to degree Nmax. Then, assuming that B has full column rank,

$$\text{Rank } (C_{tt}) = \text{Rank } (BKB^T) = \text{Rank } (K) = (Nmax + 1)^2 , \tag{3.1-6}$$

while the dimension of C_{tt} is the number of observed signals. Finally, it may be stated that the disturbing potential function belongs to an infinite dimensional space, thus involving an infinite number of frequencies, or equivalently, infinite spherical harmonics. This fact is also inherent the definition of the geodetic boundary value problem describing the unknown potential function to be regular outside the attracting masses including infinity, which, in turn, is by definition expandable to a converging infinite Taylor series.

So far, the covariance function analyzed relates to point data, as expressed by the equations (2.2-20), (2.2-26) and (2.2-33). When the observed signals are area mean values, the corresponding covariance function for the gravity anomaly, for example, is given by (Sjoberg, 1978, p. 4).

$$\operatorname{cov}\left(\bar{\Delta}g_P, \bar{\Delta}g_Q\right) = \frac{1}{\sigma_P \sigma_Q} \int_{\sigma_P} \int_{\sigma_Q} C(P, Q)\, d\sigma_P\, d\sigma_Q \tag{3.1-7}$$

where σ_P and σ_Q are the areas on the sphere that the values of $\bar{\Delta}g_P$ and $\bar{\Delta}g_Q$, respectively, represent. To lessen the computations involved with the above formula, an approximation is implemented in this study as given by equations (2.2-34) to (2.2-36). These formulae approximate the mean covariance functions by smoothing the respective point covariance functions by means of the Pellinen smoothing operators β_n (equation 2.2-39)). These operators, derived by Meissl (1971, p. 23), are called smoothing operators in the narrow sense, since the properties $\beta_n \underset{n\to\infty}{\to} 0$ and $\beta_0 = 1$ hold, thus reproducing the constant part and damping the irregularities of the function they are applied to. This approximation of the mean covariance function has been adopted by Sjoberg (1979) for 10° equal area means successfully, but it is rejected by Colombo (1979, p. 13) as too crude of an approximation, except for the case of a very fine grid. The dependence of the approximation on the area block size is expected, since the operators are derived over a circular area with angular radius $\tilde{\psi}_0$, which is here approximated by the block area on the sphere (σ) and the equivalent spherical cap radius ψ_0, given by (2.2-38).

The possibility of utilizing the approximation of the mean covariance function with the point covariance computed at the appropriate altitude as suggested by Tscherning and Rapp (1974), has been examined by Sjoberg (1978) and abandoned by him due to the poor results obtained in his computations.

Clearly the discussion pertaining to the relation between the point covariance function and the singularity of the covariance matrix is valid for the mean covariance functions implemented in this work. They have the same analytical form, but with a smoothed set of degree variances instead of k_n.

Regarding the actual computations, the truncation of the series is necessary, and therefore a choice on the maximum degree included in the summation must be made. Sjoberg (ibid.) found Nmax = 200 acceptable for his application. Later on, Colombo (1981) analyzed thoroughly the truncation effect by comparing his mean covariance function approximation (ibid., p. 84) and formula (2.2-34) with the rigorous covariance function in equation (3.1-7), computed by numerical quadratures. His experiments included values of Nmax = 180, 300 and 400, for 5° and 1° block mean gravity anomalies. The reported discrepancies in covariance vary among different cases considered. In the case of 5° blocks the discrepancy reaches the maximum of 8% for blocks near the pole and Nmax = 180, whereas for 1° blocks the difference is at most 5% near the poles, for Nmax = 180.

In this study the values of Nmax = 180 and 360 were used, but the value of Nmax = 3000 was only used in a single experiment. The sufficient Nmax value was judged on the basis of the final results, namely the recovery of the input potential coefficients, which will be discussed in detail in the next chapter.

In the following, figures 2 and 3 show the point covariance functions for Δg and N respectively, computed from equations (2.2-26) and (2.2-33), at 1° intervals, where the summation is carried out to Nmax = 180. The anomaly degree variances c_n have been computed by means of equation (2.2-25) using the spherical harmonic potential coefficient set OSU86F.HARMIN.TO360, described by Rapp and Cruz (1986b). In

order to show the covariances for the mean gravity anomaly signal, figures 4, 5 and 6 have been created by plotting the point covariance function (as in figure 2) and the mean covariance functions, at 0°.05 intervals, for polar and equatorial blocks, for equiangular grids of 10°, 5° and 3° respectively. The mean covariances were computed from equation (2.2-34) with the same parameters (c_n and Nmax) used in the point covariance computation. It may be seen that there is a larger effect of the smoothing operators on the equatorial block mean function, these blocks being larger in area, while the polar block mean function rapidly approaches the point function. This is more prominent when decreasing the grid size; in particular for 3° grid the difference between the point covariance and the polar block mean covariance is at most 17 mgals^2. Similarly, figures 7, 8 and 9 show the point and mean covariance functions, computed at 0°.05 intervals, for the undulation signal. The differences among the three curves in each figure are much smaller and the effect of the smoothing is not as prominent, due to the undulation being a low frequency signal. In particular, even for the 5° grid, the polar block mean covariance function almost coincides with the point covariance, with maximum difference of 0.8 m^2.

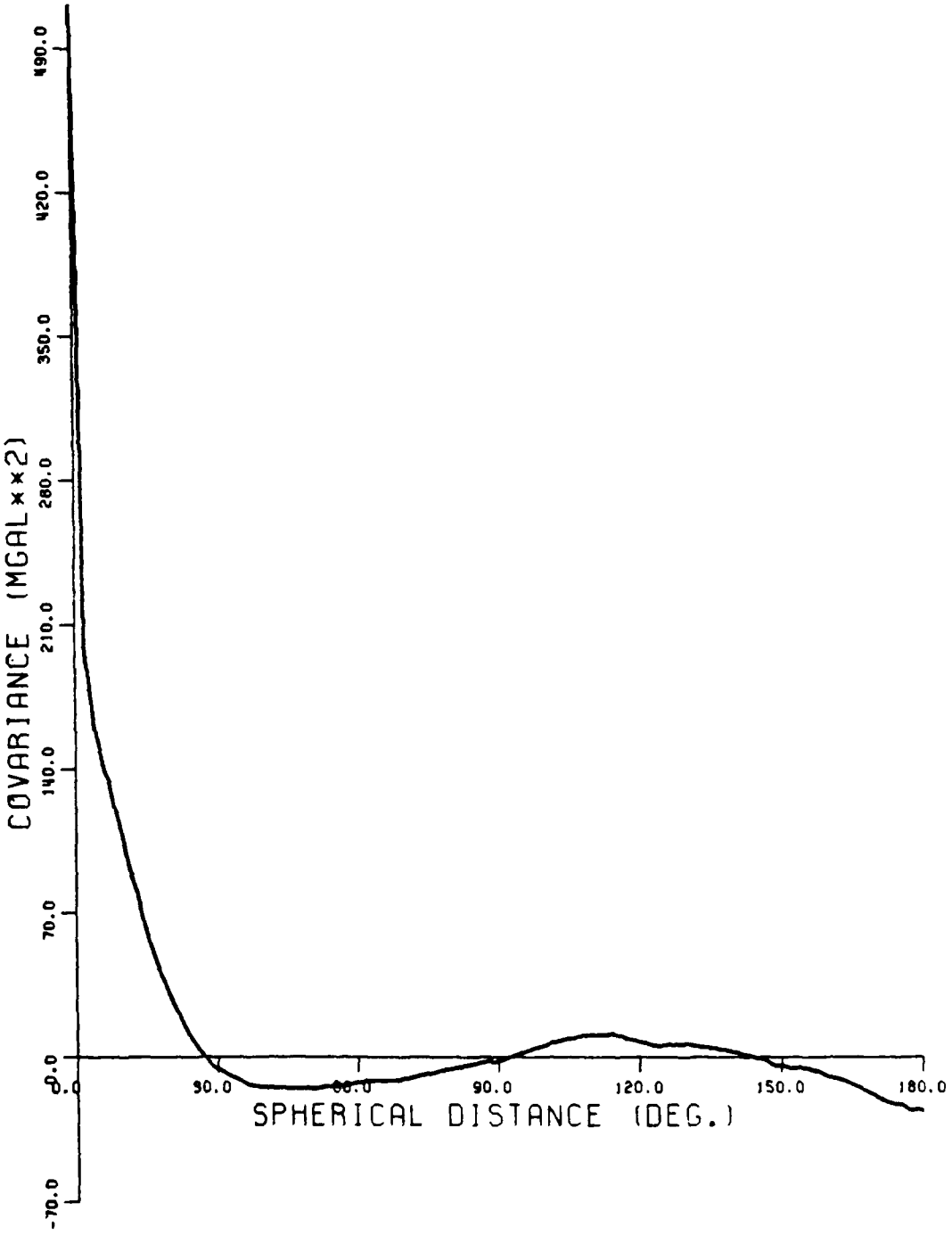

Figure 2. Gravity anomaly point covariance function computed from eq (2.2-26) for Nmax = 180 and degree variances implied by the OSU86F field.

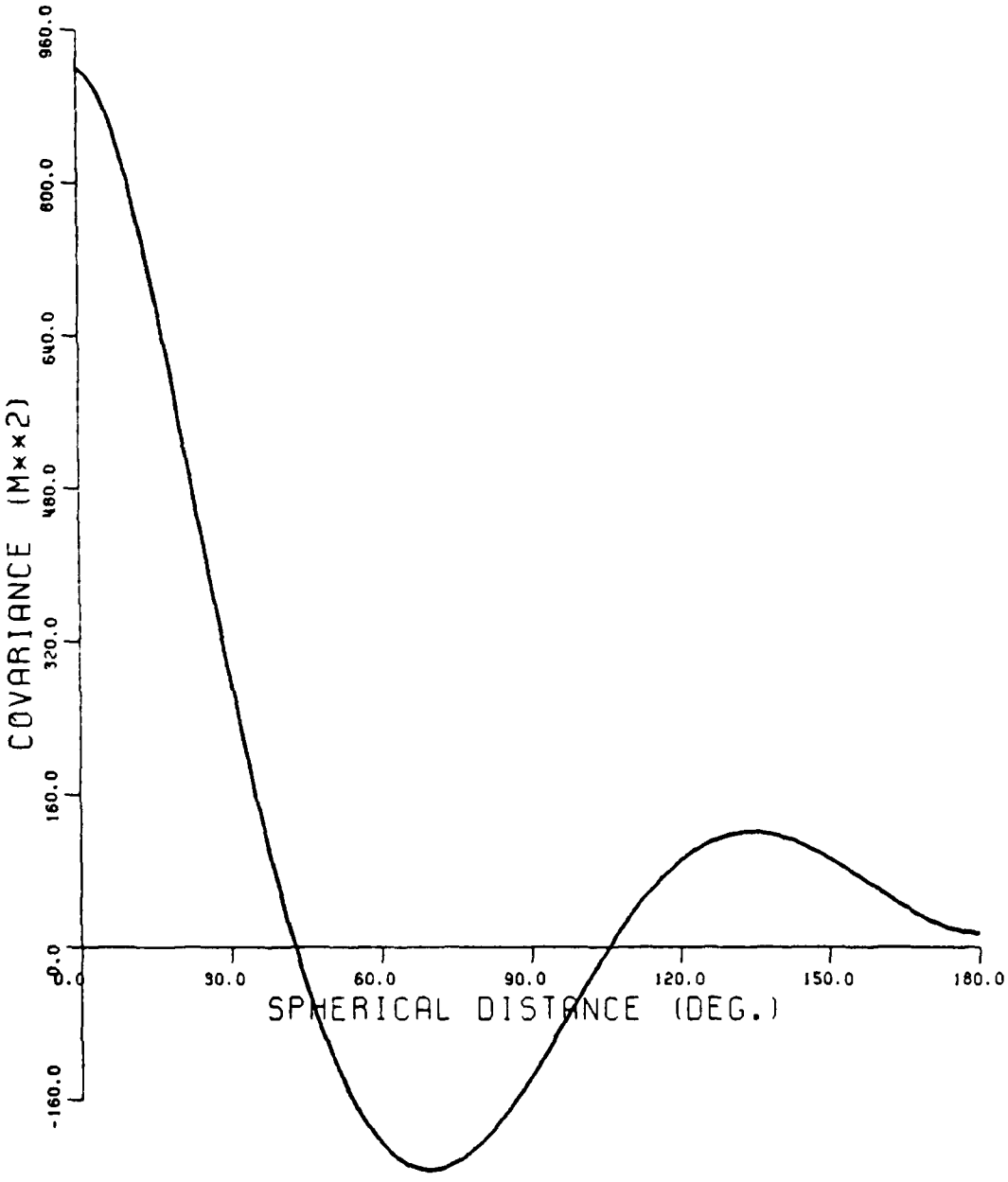

Figure 3. Undulation point covariance function, computed from eq. (2.2-33) for Nmax=180 and degree variances implied by the OSU86F field.

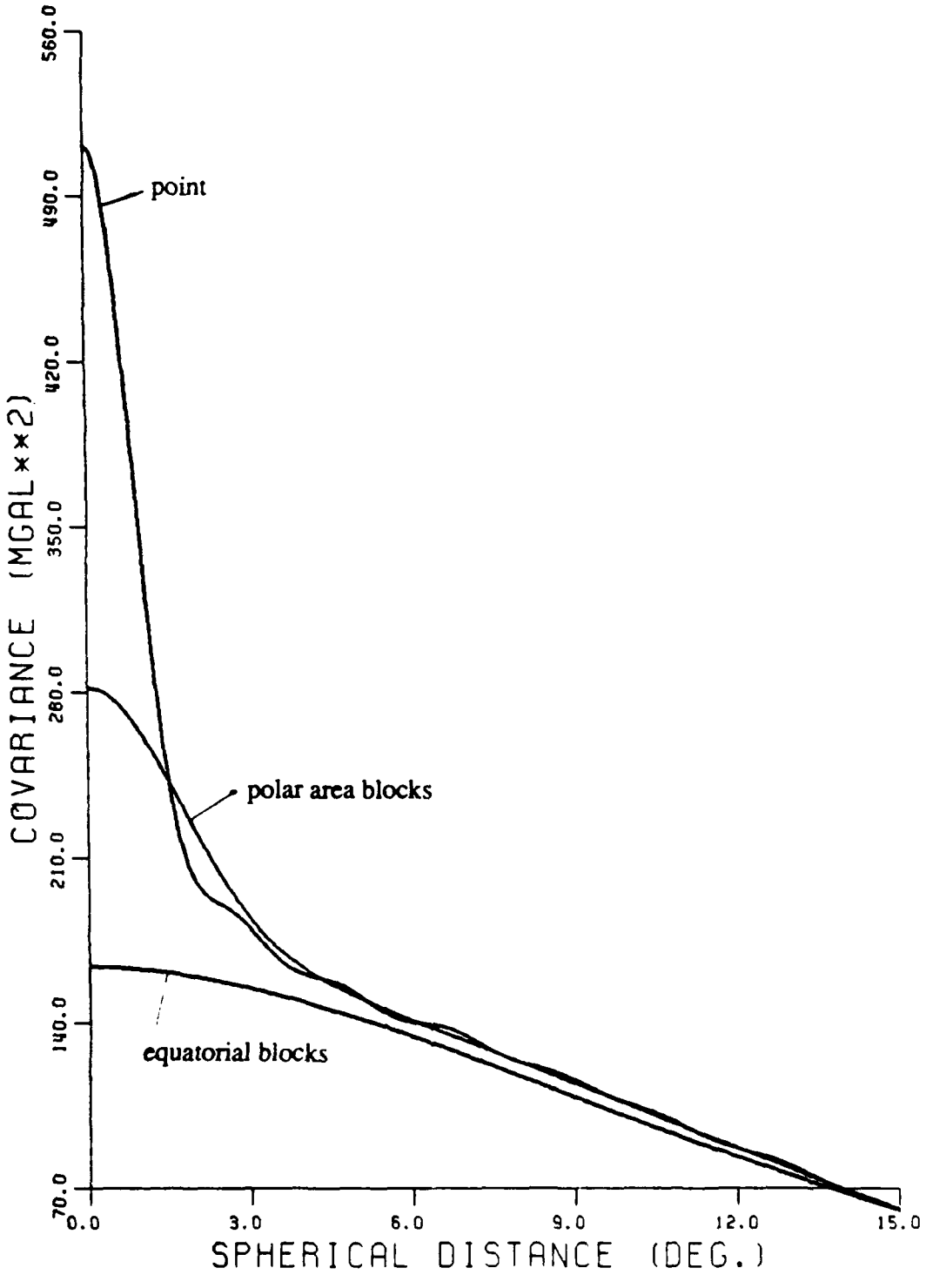

Figure 4. Point and mean anomaly covariance functions, for polar and equatorial blocks for 10° regular grid, computed with Nmax =180 and degree variances implied by the OSU86F field.

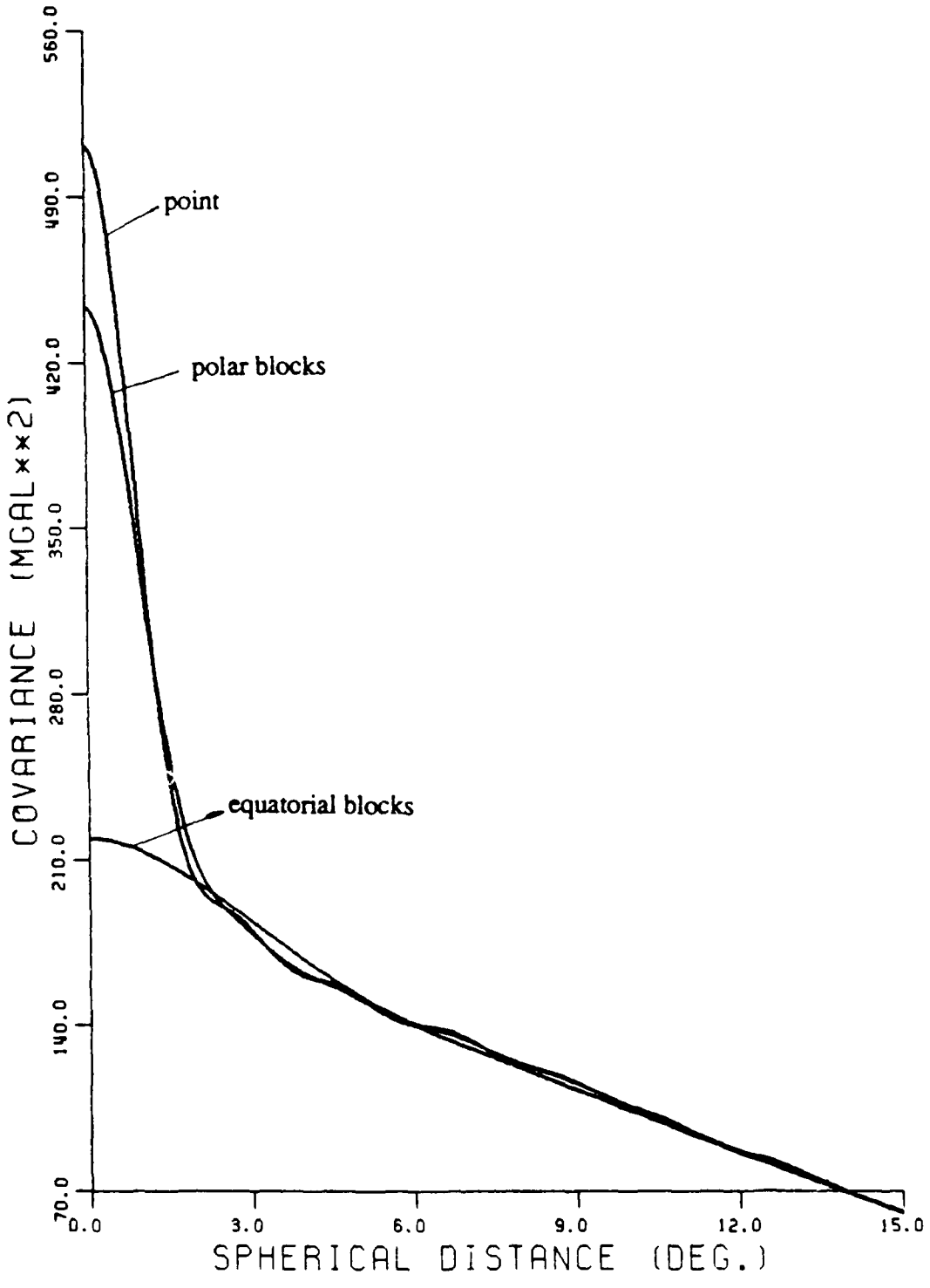

Figure 5. Point and mean anomaly covariance functions, for polar and equatorial blocks for 5° regular grid, computed with Nmax = 180 and degree variances implied by the OSU86F field.

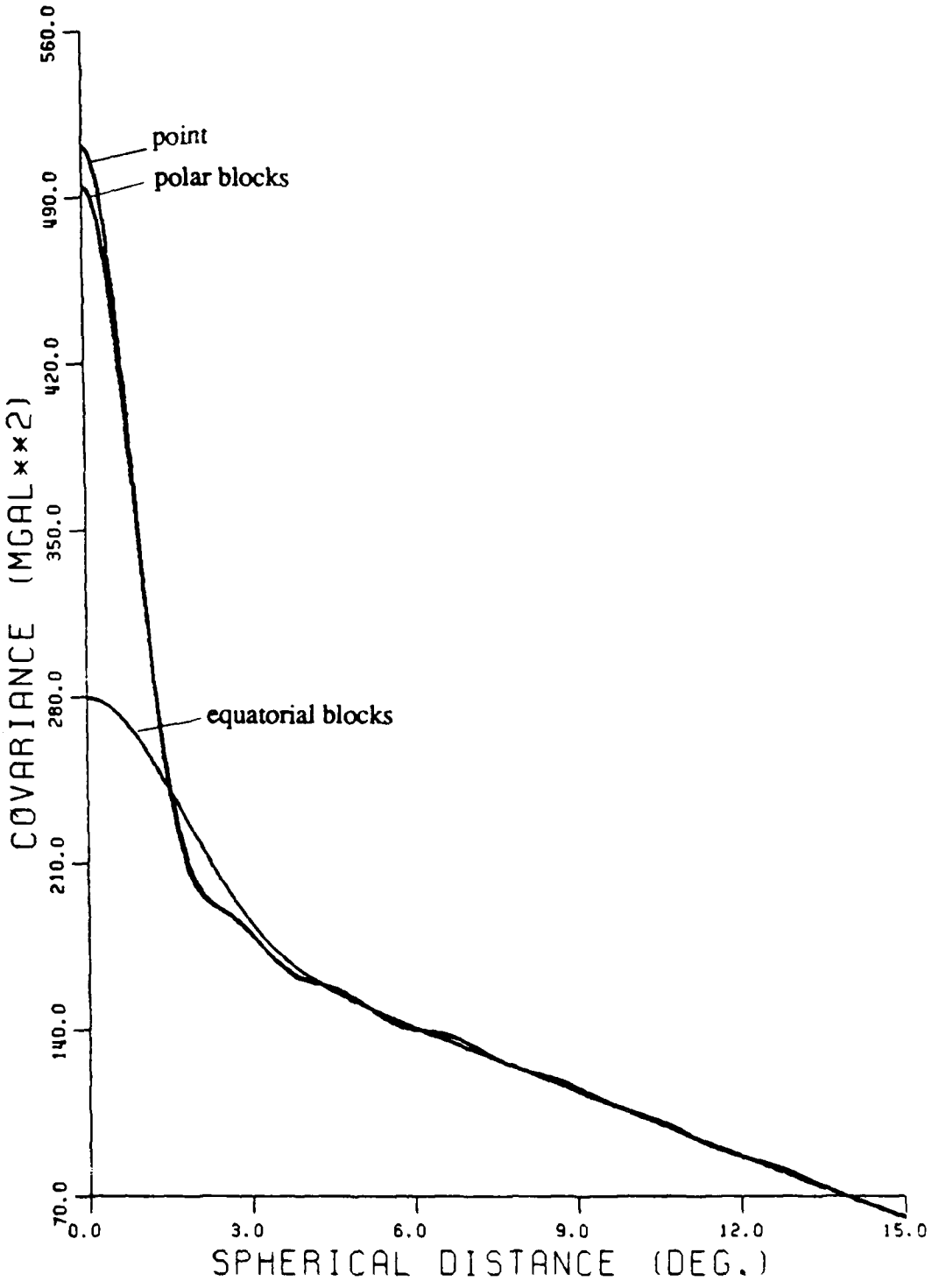

Figure 6. Point and mean anomaly covariance functions for polar and equatorial blocks for 3° regular grid, computed with Nmax = 180 and degree variances implied by the OSU86F field.

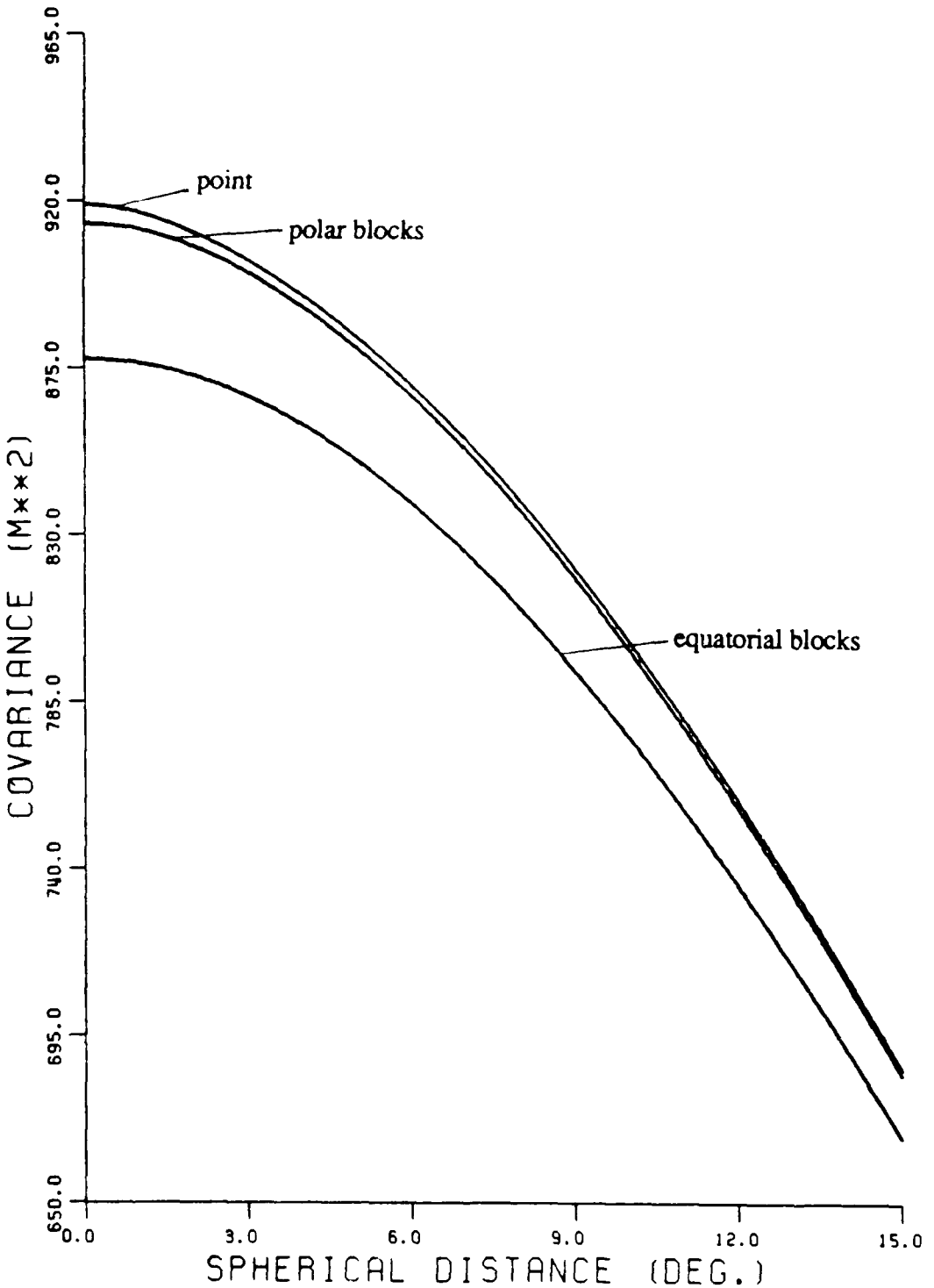

Figure 7. Point and mean undulation covariance functions for polar and equatorial blocks for 10° regular grid, computed with Nmax = 180 and degree variances implied by the OSU86F field.

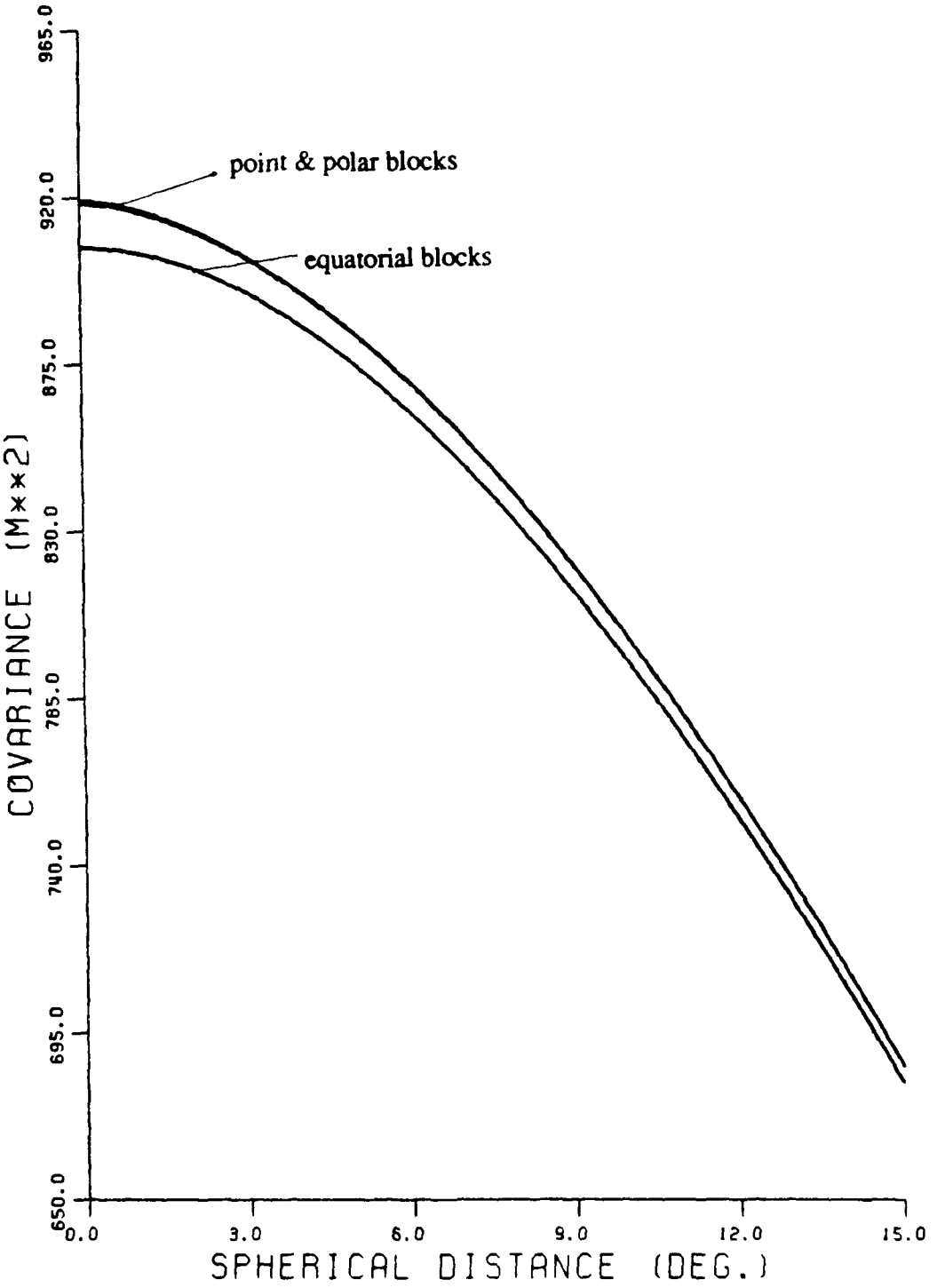

Figure 8. Point and mean undulation covariance functions for polar and equatorial blocks for 5° regular grid, computed with Nmax = 180 and degree variances implied by the OSU86F field.

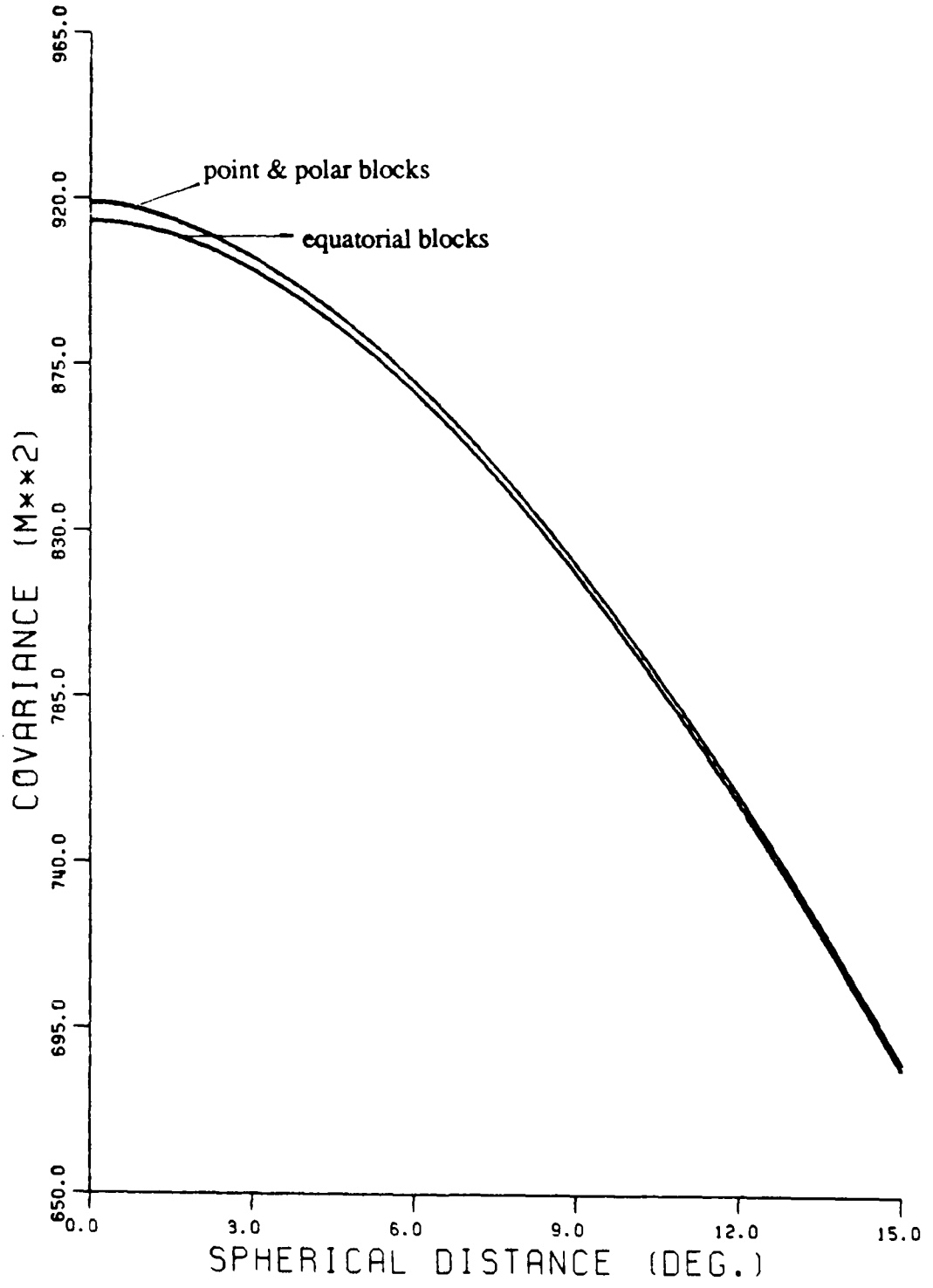

Figure 9. Point and mean undulation covariance functions for polar and equatorial blocks for 3° regular grid, computed with Nmax = 180 and degree variances implied by the OSU86F field.

As stated in the beginning of this section, the data distribution is the second factor that, together with the covariance function, completely determines the matrix C_{tt}; it is discussed next. One related aspect is the number of the observed signals, which should be sufficient to provide a solution. However, the signal should be appropriately sampled, since the data spacing defines the frequency content of the observed signal and therefore the recoverable information. In particular, for a regular grid where $\Delta\varphi = \Delta\lambda$, the global sampling covers a system of Np parallels and Nm meridians, where Nm = 2Np, and the Nyquist frequency is Nq = Np. It is known that it is not possible to estimate a complete set of spherical harmonic potential coefficients to degree and order $n \geq Nq$ (Colombo, 1981, p. 11). When dealing with overdetermined systems, as is generally the case in least-squares collocation, repeated measurements of the same type, result in identical rows of the covariance matrix C_{tt}, and consequently in singularity (in errorless collocation).

All the above arguments point to the fact that it is neither necessary nor appropriate to include large amounts of data, but instead, one should determine the optimal data distribution which could convey the maximum possible information to estimate the gravity field up to degree and order N (: $N < Nq$). Giacaglia and Lundquist (1972) have derived an optimal grid of $(N+1)^2$ sampling points on the sphere, by utilizing $(N+1)^2$ independent sampling functions. At each point, only a single sampling function has a non-zero value and therefore the coefficients of this sampling-function expansion represent the gravity field at the grid points. Also, a one-to-one linear transformation between the above expansion and the spherical harmonic expansion to degree N is derived analytically.

Despite the economy of such grids, the most commonly used grid is the equiangular or regular grid, because it is easily defined and facilitates the data processing. In this type of grid consisting of rows of parallels, each including discrete points, the poles constitute singular points. Hence, they are eliminated form the grid, unless they are individually handled as two discrete points, as demonstrated by Bose et al. (1983). Still the problem is not completely overcome, since the polar areas cause numerical instability in the covariance matrix as it tends to singularity for finer grids. This problem, also reported by Colombo (1979, p. 13), is numerically shown in the next two tables. The condition

numbers computed from the ratio of the largest to the smallest eigenvalue of the covariance matrices, are used for a relative measure of the effect of the polar area data on the numerical stability of the matrix.

The "limited" data sets are defined by neglecting data referring to latitudes larger than ±65° and ±67.5° for 10° and 5° grids respectively.

Table 1. Condition numbers of covariance matrices for 10° regular grid.

Case	global $\overline{\Delta g}$ data set	limited $\overline{\Delta g}$ data set	global $\bar{N}$ data set	limited $\bar{N}$ data set
number of zero eigenvalues	0	0	0	0
condition number	0.3×10^6	0.9×10^3	0.2×10^{10}	0.2×10^6

Table 2. Condition numbers of covariance matrices for 5° regular grid.

Case	global $\overline{\Delta g}$ data set	limited $\overline{\Delta g}$ data set	global $\bar{N}$ data set	limited $\bar{N}$ data set
number of zero eigenvalues	21	0	44	0
condition number	N/A	0.2×10^4	N/A	0.4×10^6

It is seen that the condition of the matrices generally improves when the polar area data are excluded from the 10° global data set as indicated from the decrease of the condition numbers by a factor of 10^3 to 10^4. In the cases concerning the 5° grid the apparent singularity for the global data sets is eliminated when considering the corresponding limited data sets.

Instability and singularity are also caused by decreasing the grid size, whereas the global covariance function cannot distinguish numerically between any two adjacent data

points, thus producing two almost identical rows of the covariance matrix. Within the same reasoning the undulation auto-covariance matrices are ill-conditioned when the corresponding gravity anomaly ones are not. Tables 1 and 2 show smaller condition numbers for the $\overline{\Delta g}$ covariance matrices than the corresponding $\bar{N}$ ones. This is due to the undulation covariance function being even less discriminating, i.e. of low frequency content. Evidence to this end may be also found in the figures presented in this section. Specifically figures 4, 5 and 6 show a large decrease of the covariance values for spherical distances $\psi : 0° \leq \psi \leq 2°$, while the covariances in figures 7, 8 and 9 drop slightly within the same ψ interval. In addition, figures 8 and 9 show that the mean covariance for polar blocks coincides with the point covariance for 5° and 3° regular grids respectively.

3.2 On the regularization of the covariance matrix.

Fundamental definitions and concepts will be exposed below, aiming to provide a concise interpretation of the experiments that will be presented in the next chapter.

When solving a problem in practice, the meaning of a "solution" must be defined as well as the features of the computational algorithm that can be used to obtain a solution.

Consider the equation

$$A\, z(s) = u\,(x) \qquad (3.2\text{-}1)$$

where A is a known continuous operator, z(s) is the unknown function in a space S_1 and u (x) is a known function in a space S_2. Suppose that for some $u = u_1\,(x)$ the function $z_1(s)$ is a solution of equation (3.2-1),

$$A\, z_1\,(s) \equiv u_1\,(x). \qquad (3.2\text{-}2)$$

Generally, values of the function u_1 (x) are measured, and consequently only an approximation u (x) of u_1 (x) is known. The difference between u (x) and u_1 (x) is measured in the metric of the space S_1 as the square root of an inner product ρ_{s1} (u_i, u_j) of the difference function [u (x) - u_1 (x)]. An approximate solution of equation (3.2-1) may then be found, where the error of the approximation is measured in the metric of space S_2 by taking the square root of an inner product ρ_{s2} (z_i, z_j), of the difference function [z (s) - z_1 (s)]. For certain operators A it can be proved (Tikhonov and Arsenin, 1979, p. 4) that for an arbitrarily small difference between u_1 (x) and u_2 (x), the difference between the corresponding solutions z_1 (s) and z_2 (s) can be arbitrary. In such cases the solution is not stable under small changes in the initial data u (x), which brings up the distinction between two groups of problems: well-posed and ill-posed problems. It is of interest here to note that the introduction of this concept was made in the attempt to develop appropriate boundary conditions for differential equations, for example the Dirichlet and analogous conditions for elliptical equations.

The precise mathematical definition of a well-posed problem is given below (ibid., p. 7). Consider equation (3.2-1), where for every element $u \in S_1$ with metric ρ_{s1} (u_1, u_2) there exists a unique solution

$$z = R(u) \tag{3.2-3}$$

in the space S_2 with metric ρ_{s2} (z_1, z_2). The metric is determined by the formulation of the problem. The algorithm for determining the solution z is said to be stable on the spaces (S_1, S_2) if, for every positive number ε, there exists a positive number δ (ε) such that the inequality

$$\rho_{s1}(u_1, u_2) \leq \delta(\varepsilon) \tag{3.2-4}$$

implies

$$\rho_{s2}(z_1, z_2) \leq \varepsilon\,, \tag{3.2-5}$$

where $z_1 = R(u_1)$ and $z_2 = R(u_2)$. The problem of finding the solution z in the space S_2 from the initial data in the space S_1 is said to be well-posed on the pair of metric spaces (S_1, S_2) if the following three conditions are satisfied:

(1) for every element $u \in S_1$ there exists a solution $z \in S_2$;

(2) the solution is unique;

(3) the problem is stable on the spaces (S_1, S_2).

Problems that do not satisfy the above conditions are called ill-posed. In concept, the conditions (1) and (2) verify that the problem at hand is determinable from the mathematical point of view. Condition (3) indicates whether the problem is numerically determinable from the approximate data.

At this point it is clearly understood that the definition of an approximate solution of an ill-posed problem is vague. Still, this is not a sufficient reason to completely avoid any such problem, since there is a large class of problems for which workable solutions are necessary. For example, the inverse operator A^{-1} of the continuous operator A in equation (3.2-1) is not generally continuous on S_1 and, in that case, the solution will not be stable under small changes in u. Procedures may be developed for finding possible solutions by utilizing additional quantitative information, thus leading to a quasi-solution. On the other hand, when qualitative information is available, a procedure called regularization can be used to construct stable approximate solutions.

The essential concept of the regularization method is that of the regularizing operator (ibid., p. 47). An operator $R(u, \alpha)$ depending on a parameter α is called a regularizing operator for equation (3.2-1) if

(1) there exists a positive number δ_1, such that $R(u, \alpha)$ is defined for every $\alpha > 0$ and every $u \in S_1$ for which

$$\rho_{S1}(u, u_T) \leq \delta \leq \delta_1 \qquad (3.2\text{-}6)$$

with u_T being the exact value of u, and

(2) there exists a function $\alpha = \alpha(\delta)$ such that, for every $\varepsilon > 0$, there exists a number $\delta(\varepsilon) \leq \delta_1$ for which the inequality

$$\rho_{S1}(u_T, u_\delta) \leq \delta(\varepsilon), \text{ where } u_\delta \in S_1 \tag{3.2-7}$$

implies

$$\rho_{S2}(z_T, z_\alpha) \leq \varepsilon, \text{ where} \tag{3.2-8}$$

$$z_\alpha = R(u_\delta, \alpha(\delta)). \tag{3.2-9}$$

Thus, a solution z_α, called a regularized solution, can be obtained from $R(u_\delta, \alpha(\delta))$, where α is a numerical parameter called the regularization parameter, by definition consistent with the accuracy δ of the initial data.

Although there is no uniqueness assumption for the regularizing operator, it is critical to devise methods for constructing regularizing operators. Usually the variational method is implemented (ibid., p. 50) where a certain functional, called the smoothing functional is minimized. For example:

$$M^\alpha[z, u] = \rho^2_{s_1}(Az, u) + \alpha \Omega(z), \tag{3.2-10}$$

with $\Omega(z)$ a stabilizing functional. Another useful method makes use of the spectrum of the operator A.

The method outlined in principle above, known in literature as Tikhonov regularization, was implemented by Rummel, et al. (1979). Considering equation (3.2-1) where u and z belong in real Hilbert spaces and A is a continuous linear operator, a minimum norm condition is invoked. In particular:

$$\min\left(\|Az - u_0\|^2_{D^{-1}} + \alpha \|z\|^2_{C_{zz}^{-1}}\right), \qquad \alpha > 0 \tag{3.2-11}$$

where u_0 is the observation vector, D is the à priori covariance matrix for the noise and C_{zz} the à priori covariance matrix of z. Then, the solution is obtained from

$$z_e = \left(A^T D^{-1} A + \alpha C_{zz}^{-1}\right)^{-1} A^T D^{-1} u_0 \tag{3.2-12}$$

or equivalently from

$$z_e = C_{zz} A^T \left(A C_{zz} A^T + \alpha D\right)^{-1} u_0 . \tag{3.2-13}$$

The only difference between the above equation and the least-squares collocation formula (2.2-11) is the regularization parameter α, although in practice it is often implied by scaling the actual error covariance matrix D.

Equation (3.2-13) is recommended by Colombo (1979, p. 15), and it is also implemented in this study, when the grid size is small so as to give rise to unstable covariance matrices. The instability is manifested both in the elements of the inverse matrix and in the estimated signal vector which shows large discrepancy from the true solution. It is important that caution should be exercised in selecting the regularization parameter α, in a way that will stabilize the solution but also minimize the loss of resolution in the initial data, which is expected due to the regularization process. For this reason it is beneficial to interpret the parameter α as a factor varying the weight with which the covariance information C_{zz} influences the solution. The essence of α may be also seen in the frequency domain by analyzing the eigenvalues of the data covariance matrix $C_{uu} = A\, C_{zz}\, A^T$. Again, the fact that the parameter α alters the spectrum of the data covariance shows that it should be chosen compatible with the magnitude of the error in the initial data.

3.3 Computational algorithm and software development

Since it has been a considerable part of this effort to develop workable software for the boundary value problem solutions studied here, it is reasonable to present the sequence of required computations, together with the basic characteristics of the algorithms, the storage schemes and some computer execution times.

Most of the programs were developed and tested on the IBM 3081-D mainframe computer with 32 megabytes of memory, available at The Instruction and Research Computer Center, at The Ohio State University. The detailed computations were done on a CRAY X-MP/48 Supercomputer available at the Pittsburgh Supercomputing Center (PSC), at Carnegie Melon University and the University of Pittsburgh.

Although no special effort was made to improve the source code so as to take full advantage of the vector processing of the CRAY X-MP/48, worthwhile savings in execution time were still realized. It seems very realistic to expect that substantial improvement will be achieved with certain software modifications to enable large scale solutions and the determination of high degree spherical harmonic expansions for the disturbing potential. A crucial factor to this is the continuing upgrading of the CRAY supercomputers. The CRAY X-MP/48 supercomputer at PSC is currently (January, 1989) being replaced by the CRAY Y-MP/832, while a CRAY-3 is scheduled to arrive in October, 1990. A comparison among the three mentioned supercomputers with regard to their features is given in table 3.

Table 3. Supercomputer upgrading at PSC.

Hardware specifications	X-MP/48	Y-MP/832	CRAY-3
Number of processing units	4	8	16
Memory in Megawords	8	32	512
Clock cycle in nsecs	9.5	6	2
Floor space in square feet	112	98	<16
Performance in MFLOPS*	840	2,700	16,000

* MFLOPS "millions of floating-point operations per second", is the overall measure of large-scale computing performance. It indicates the number of floating point additions, multiplications, etc, which the system can do in one second.

Next, the sequence of computations is described briefly. Figure 10 is offered for further illustration of the whole algorithm in a block diagram where each block represents a separate computer program.

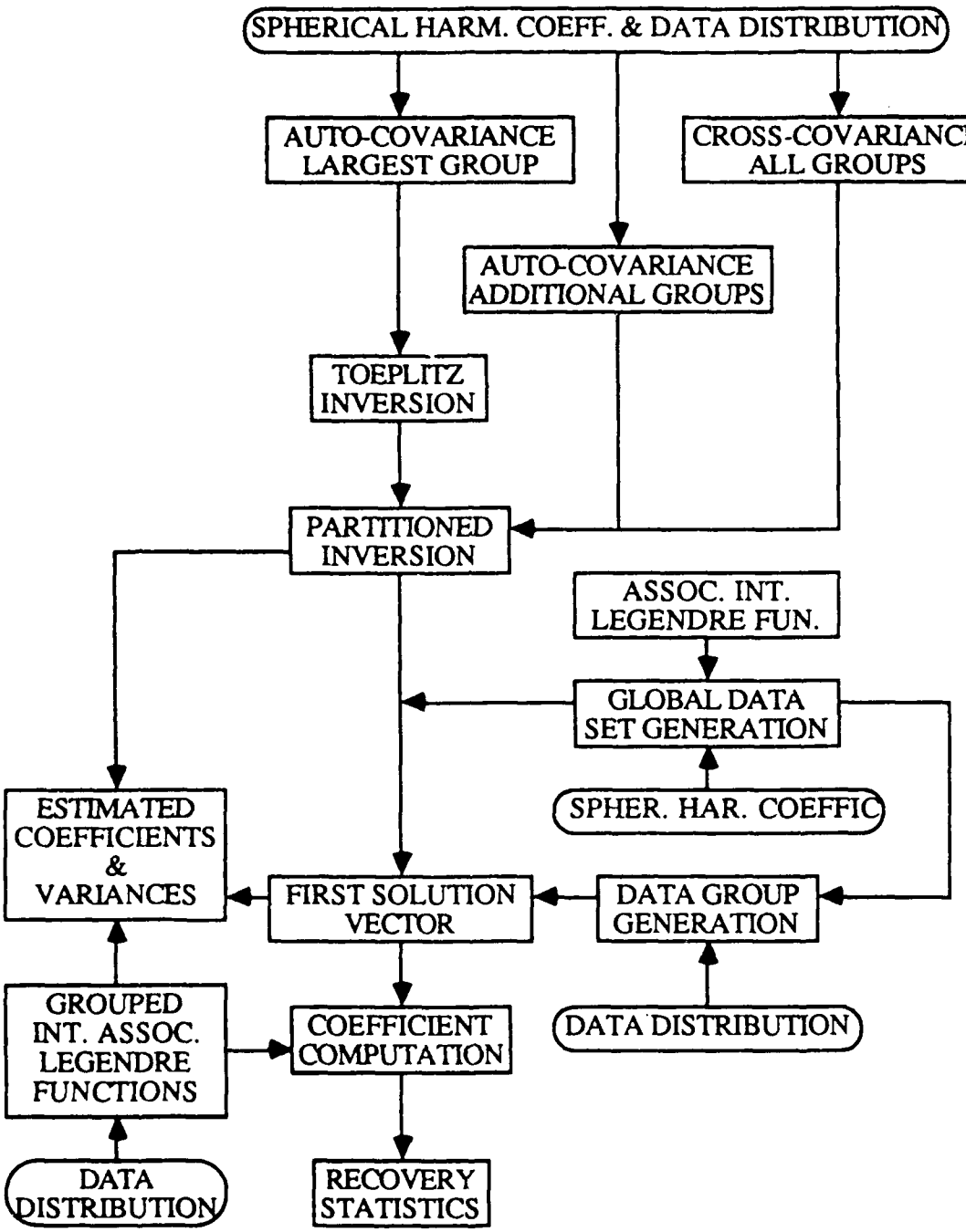

Figure 10. Sequence of computations

In the beginning the covariance matrix is formed in three steps using as input a spherical harmonic potential coefficient set and the data distribution. The latter consists of the number of data groups, and for each group, the grid specification and location, namely: the number of parallels, number of meridians, grid spacing, latitude and longitude of the utmost northwest point, and data type. During the first step the auto-covariance matrix of the largest data set is formed. This matrix is a block-Toeplitz matrix, as described in section 2.3; therefore, only the top block-row elements are computed, and for each block of dimension N_p (N_p is the number of parallels in the group) only $N_p(N_p+1)/2$ elements are formed. A total number of Nm (Nm is the number of meridians) symmetric blocks are formed and stored in a vector array on disk. The elements actually computed are shown in the shaded area of the diagram of figure 11.

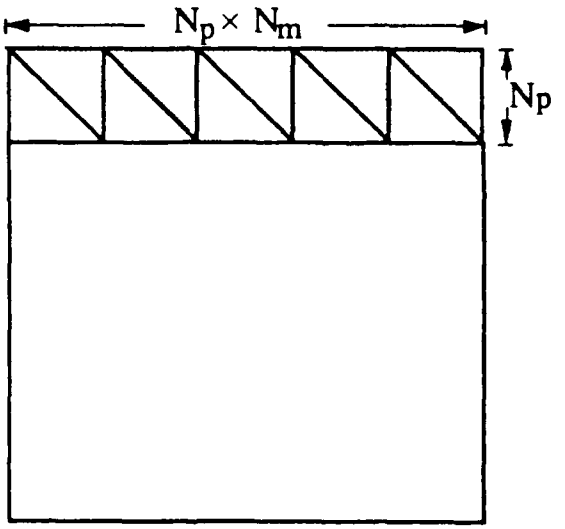

Figure 11. Sufficient elements for the auto-covariance matrix in a single data group.

In the second step, the types of computations performed in the first step are done in a sequential mode, and an auto-covariance matrix is formed for each data group. Then all are stored in one vector on disk. In the last step, the cross-covariances between any two data groups are computed. These covariances are also formed into matrices which are rectangular and therefore do not have the Toeplitz pattern. However, some pattern exists, that may be called "pseudo-Toeplitz", since it possesses a similarity to the Toeplitz one.

This pattern, illustrated in figure 12, allows for the matrix to be fully defined by its first block-row and first block-column, with each block in position (i, j) being repeated at the positions (i+1, j+1), (i+2, j+2) etc.

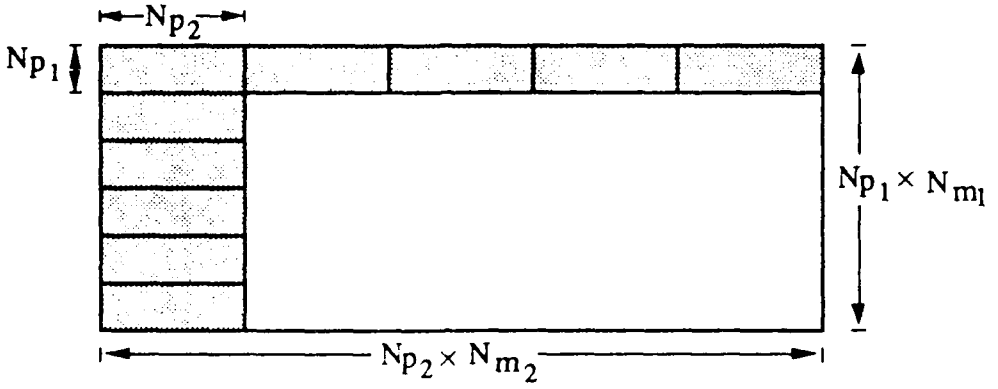

Figure 12. Sufficient elements for the data cross-covariance matrices.

Such structure can offer substantial savings in computer time, but it has not been exploited in this work. After computing the covariances for all possible combinations of data groups, they are stored in a vector on disk.

In the next step of the sequence, the inversion of the covariance matrix takes place. This is again done in two steps, as indicated in the diagram of figure 10. First, the covariance matrix of the largest group is inverted by the Toeplitz algorithm. The equations for this algorithm have been presented in detail in section 2.3. The input consists of the vector containing the auto-covariance matrix elements (shown in figure 11) and the output is obtained in blocks (of dimension N_p x N_p) starting form the bottom block-row. When the core memory is sufficient the elements of the blocks are stored in the matrix in symmetric storage mode. For solutions requiring larger memory the individual blocks are stored on disk as they are computed or they are multiplied directly with the data vector. Execution times for forming the covariance matrices for global data coverage and various grid sizes are presented in table 4, together with the respective Toeplitz inversion times, for both IBM and CRAY compute runs when possible.

Table 4. Time consumed in forming and inverting Toeplitz covariance matrices.

grid size	Number of parallels	Number of meridians	Matrix dimension	IBM-3081-D time in seconds		Cray X-MP/48 time in seconds	
				formation	inversion	formation	inversion
30°	6	12	72	1.0	0.2	0.1	0.1
20°	9	18	162	3.0	1.1	0.3	0.5
15°	12	24	288	7.0	4.4	0.7	1.6
10°	18	36	648	11.0	35.5	2.6	11.1
5°	36	72	2592	-	-	17.2	98.9
4°	40	90	3600	-	-	28.0	338.6

Next, the partitioned inversion is performed in a sequential mode, as illustrated in figure 13. Each time another group of data is added, the most recently computed inverse is used in symmetric storage (e.g. matrix 00) together with the auto-covariance matrix of the next data group (e.g. matrix 11) and the corresponding cross-covariances (e.g. 01). Then, the augmented inverse is computed according to the algorithm given in section 2.3 and stored is symmetric storage where it can be used as input when a new group is considered.

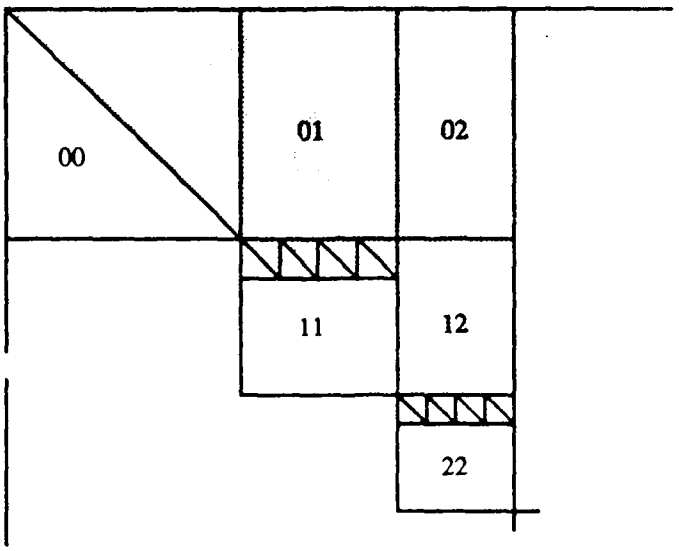

Figure 13. The configuration of the partitioned inversion.

The simulated data is generated using a spherical harmonic potential coefficient set and the integrated associated Legendre functions residing on disk. The Fortran programs

F428AV1 and F431AV2 were used from Prof. R.H. Rapp's program library, Dept. of Geodetic Science and Surveying. Program F428AV1 was used for the associated Legendre function computation utilizing Paul's algorithm (Paul, 1978). A modification of program F431AV2 was used to derive mean gravity anomalies and mean geoid undulations on a sphere. This program was developed by Colombo and it is described in detail by Colombo (1981). The Fast Fourier Transform algorithm implemented in this program generates most efficiently the data values along parallels, creating a global set of values referring to the center of the blocks as far as the computation of the spherical distance, ψ, is concerned. A short program was written to retrieve the appropriate data values given a grid configuration and a particular geographic location by defining the utmost northwest point. The following program was developed to collect all data values in a vector, add random noise, and multiply it with the inverse of the covariance matrix thus obtaining, what is called here, the first solution vector.

After a slight modification, program F428AV1 was used to compute the integrated associated Legendre functions in groups in accordance with the order of the data in the observation vector. These data were stored on disk and used in the program that was designed to compute the covariance matrix between the estimated coefficients and the data, on an element-by-element basis. These elements were multiplied by the appropriate elements of the first solution vector and were summed into two vector arrays; one for the $\bar{C}_{nm}$ and one for the $\bar{S}_{nm}$ coefficients, thus producing the estimated coefficients. Substantial time savings were made possible by using recursive formulae for the computation of cos $m\lambda$ and sin $m\lambda$ required in the equations (2.2-58) to (2.2-61). In particular, the formulae:

$$\sin \eta\alpha = 2 \sin\left((\eta-1)\,\alpha\right) \cos \alpha - \sin\left((\eta-2)\,\alpha\right) \tag{3.3-1}$$

$$\cos \eta\alpha = 2 \cos\left((\eta-1)\,\alpha\right) \cos \alpha - \cos\left((\eta-2)\,\alpha\right) \tag{3.3-2}$$

were used, where only three previously computed sines and three cosines were saved thus completely avoiding any further trigonometric function calculations. Another version of this program takes the inverse of the data covariance matrix as input and

computes the estimated coefficients and their estimated accuracy, using one row of the cross-covariance matrix at a time. In this approach the entire inverse matrix is needed in core, thus increasing the memory requirements, while the computations are overall very time consuming.

Finally, statistics for the recovery of the input potential coefficients are computed using program F159 from Prof. R.H. Rapp's library. Also, additional statistics and differences are computed as discussed in detail in the next chapter.

The software used in the computational scheme described in this section was written by the author, unless credited otherwise. In particular, the source code for forming the various types of auto- and cross-covariance matrices, the block-Toeplitz and sequential inversion routines and the source for the calculation of the potential coefficients and their accuracy constitute the majority of the utilized software and were developed and tested by the author.

CHAPTER IV

NUMERICAL RESULTS AND ANALYSIS

4.1 General experiment strategy

Chapters I and II focus on conveying the role of the overdetermined problem within the general framework of the geodetic boundary value problems, and in presenting the justification for a collocation estimation of the spherical harmonic parameterization of the disturbing potential. The formulation of the methodology is given through the equations of chapter II, while theoretical and practical aspects of the implementation are discussed in chapter III.

This chapter is included for the analysis of the experiments performed with the purpose of evaluating the methodology in terms of both accuracy and overall applicability. The experiments were designed to utilize synthetic data thereby providing a definite control for the evaluation of the results and, at the same time, simplifying the data processing.

Starting with a given spherical harmonic potential coefficient set, in particular OSU86F.HARMIN.TO360 (Rapp and Cruz, 1986b), point and mean gravity anomalies and geoid undulations are computed. Also, the anomaly degree variances implied by the same field are used in the computation of the anomaly and the undulation auto-covariance matrices, as well as the cross-covariances between the potential coefficients and the anomaly and undulation signals. The specific details of the actual calculations are given in section 4.2. A set of potential coefficients is estimated using collocation and the simulated anomaly and undulation data and the necessary covariances. The estimated coefficients are compared against the input coefficients, thus determining their recovery. A number of different quantities are then computed in order to measure the recovery of the coefficients. These quantities are the following:

(1) The correlation between the two coefficient sets per degree n, as computed from the equation:

$$R_n = \frac{Q_n}{\left[\sigma_n^2 \sigma_n^{'2}\right]^{1/2}}, \quad 2 \le n \le Nmax \tag{4.1-1}$$

where

$$Q_n = \sum_{m=0}^{n} \left(C_{nm} C_{nm}^{'} + S_{nm} S_{nm}^{'} \right), \tag{4.1-2}$$

$$\sigma_n^2 = \sum_{m=0}^{n} \left(C_{nm}^2 + S_{nm}^2 \right) \text{ and} \tag{4.1-3}$$

$$\sigma_n^{'2} = \sum_{m=0}^{n} \left(C_{nm}^{'2} + S_{nm}^{'2} \right). \tag{4.1-4}$$

The reference coefficients are denoted by C_{nm} and S_{nm}, while the estimated ones are denoted by $C_{nm}^{'}$ and $S_{nm}^{'}$.

(2) The average correlation between the two coefficient sets is also computed by averaging the correlations from (4.1-1), i.e:

$$R = \frac{\sum_{i=2}^{Nmax} R_i}{(Nmax - 1)}. \tag{4.1-5}$$

(3) The percentage difference (PN) for each degree (n) is computed from the equation:

$$PN_n = \left[\frac{\sum_{m=0}^{n} \left(\Delta C_{nm}^2 + \Delta S_{nm}^2 \right)}{\sum_{m=0}^{n} \left(C_{nm}^2 + S_{nm}^2 \right)} \right]^{1/2} \times 100 \, , \tag{4.1-6}$$

where the difference between the input and the recovered coefficients is:

$$\Delta C_{nm} = C_{nm} - C'_{nm} \text{ and } \Delta S_{nm} = S_{nm} - S'_{nm} \, . \tag{4.1-7}$$

(4) The percentage difference is calculated for the complete coefficient set as an average given by:

$$PS = \frac{\sum_{i=2}^{Nmax} PN_i}{Nmax - 1} \, . \tag{4.1-8}$$

(5) The recovery of the input field is also measured in terms of the difference in the gravimetric quantities. In particular; the root mean square difference in undulation per degree is computed as:

$$UNA_n = R \left[\sum_{m=0}^{n} \left(\Delta C_{nm}^2 + \Delta S_{nm}^2 \right) \right]^{1/2} \, . \tag{4.1-9}$$

and cummulatively to degree Nmax:

$$A = R \left[\sum_{n=2}^{Nmax} \sum_{m=0}^{n} \left(\Delta C_{nm}^2 + \Delta S_{nm}^2 \right) \right]^{1/2} \, . \tag{4.1-10}$$

where R is the earth mean radius.

(6) Similarly the root mean square difference in gravity anomaly is computed from:

$$AAC_n = \gamma(n-1)\left[\sum_{m=0}^{n}\left(\Delta C_{nm}^2 + \Delta S_{nm}^2\right)\right]^{1/2} \qquad (4.1\text{-}11)$$

and cummulatively:

$$TG = \gamma\left[\sum_{n=2}^{Nmax}(n-1)^2\sum_{m=0}^{n}\left(\Delta C_{nm}^2 + \Delta S_{nm}^2\right)\right]^{1/2}. \qquad (4.1\text{-}12)$$

(7) The recovery of the input coefficients is also evaluated with respect to the estimated accuracy ($\tilde{\sigma}$) of each coefficient by calculating the quantities:

$$DNC_{nm} = \frac{C_{nm} - C'_{nm}}{\tilde{\sigma}_{C'_{nm}}} \text{ and} \qquad (4.1\text{-}13)$$

$$DNS_{nm} = \frac{S_{nm} - S'_{nm}}{\tilde{\sigma}_{S'_{nm}}}. \qquad (4.1\text{-}14)$$

(8) Finally, an average value of the above statistics is computed per degree as

$$RMS = \left[\frac{\sum_{m=0}^{n}\left(DNC_{nm}^2 + DNS_{nm}^2\right)}{Ncoef}\right]^{1/2} \qquad (4.1\text{-}15)$$

where Ncoef is the number of coefficients in the degree n.

Within the general construction of the experiments as defined above, there are several inter-related factors that influence the problem and the final recovery of the input coefficients. Since the most critical objective of this study is the combination of different data types, all aspects have been analyzed with regard to the two data types: gravity anomaly and undulation. The specific aspects analyzed and presented in the following sections include: a) the representation of the data as point or mean values, b) the approximation of the appropriate covariance functions and the truncation in the series formulae, c) the error of the data in connection with the regularization procedure and d) the size of the regular grid and the recoverable frequencies of the field.

4.2 Specifications for the data simulation

This section specifies the details of the input in the actual computations that were outlined generally in the previous section.

Boundary values of mean gravity anomalies and geoid heights were computed with program F431AV2 (Colombo, 1981), which in principle implements the equations (2.2-54) and (2.2-55). Modifications were made to compute the data on the surface of a sphere of radius R_E using the equations:

$$\bar{\Delta g}\left(R_E, \theta, \lambda\right) = \frac{\gamma}{\sigma} \sum_{n=2}^{Nmax} (n-1)\left(\frac{R}{R_E}\right)^{n+2} \sum_{m=0}^{n} \left[\bar{C}_{nm} \int_{\sigma} \bar{P}_{nm}(\cos\theta) \cos m\lambda \, d\sigma + \bar{S}_{nm} \int_{\sigma} \bar{P}_{nm}(\cos\theta) \sin m\lambda \, d\sigma \right] \tag{4.2-1}$$

$$\bar{N}\left(R_E, \theta, \lambda\right) = \frac{R}{\sigma} \sum_{n=2}^{Nmax} \left(\frac{R}{R_E}\right)^{n+1} \sum_{m=0}^{n} \left[\bar{C}_{nm} \int_{\sigma} \bar{P}_{nm}(\cos\theta) \cos m\lambda \, d\sigma +

$$\overline{S}_{nm} \int_{\sigma} \overline{P}_{nm}(\cos\theta) \sin m\lambda \, d\sigma \Big] \qquad (4.2\text{-}2)$$

where σ is given from equation (2.2-56) and

$$\gamma = \frac{GM}{R^2} \, . \qquad (4.2\text{-}3)$$

Since the OSU86F spherical harmonic potential coefficients (Rapp and Cruz, 1986b) were used here, the associated scale factor with this particular expansion is also used, which is $R = a_e = 6378136$ m. In addition the GRS80 constants were used, specifically:

$f = 1/298.2572$

$GM = 0.3986005 \times 10^{15}$ m^3/s^2 and

$\omega = 7.292115 \times 10^{-5}$ rad/sec.

The normal field implied by the GRS80 constants is subtracted from the input coefficients by subtracting the zonals of degrees 2, 4 and 6. Then a global set of mean gravity anomalies or undulations is computed. The maximum degree of the expansion (Nmax) and the block size are given as input, although the latter is limited to exact dividers of π, so that the global number of latitude belts is even. Under this scheme there are no blocks crossing the equator, and the data for two latitudinal parallel rows that are symmetric with respect to the equator are calculated simultaneously, by taking advantage of the symmetric and anti-symmetric properties of the integrated Legendre functions. The data calculated for this work refer to blocks of 10°, 5°, 3° and 2° with maximum degree of expansion 18, 36, 60 and 90 respectively.

After the data were generated and stored on disk ordered along the parallels, it was retrieved in a whole or partly and reordered along the meridians, in order to obtain the block-Toeplitz pattern implemented in the covariance matrices. At the same time the

option of adding random error is made available, by utilizing a Gaussian random deviate generator routine from the IMSL software package. First, the subroutine generates a set of uniform pseudo-random numbers in the exclusive range (0, 1) given a seed value. Then, these numbers are transformed to normal (0, 1) deviates using the inverse normal probability distribution function. Finally, normal (0, σ^2) deviates are computed by scaling the generator output by the standard deviation σ.

Consistent with the data simulation is the computation of the auto-covariance and cross-covariance matrices by means of the equations given in section 2.2. The OSU86F potential coefficients were used in equation (2.2-25) to compute the anomaly degree variances c_n after removing the normal zonals of degree 2, 4 and 6 computed from the GRS80 constants. The coefficient scaling factor, R, was used and the value of the ratio s, in equation (2.2-26), was taken as s = 0.999617. Then the radius R_E is defined as

$$R_E^2 = \frac{R^2}{s} \equiv 6379357.8 \text{ m}, \qquad (4.2\text{-}4)$$

which is several kilometers larger than the earth mean radius.

The c_n values as computed refer to a sphere of radius R, but the equations used for the computation of the data covariances (eg. equation (2.2-34)) refer the c_n values, and therefore the covariances, to a sphere of radius R_E by means of the term $(R^2/R_E^2)^{n+2}$ as explained by Rapp (1988).

In case that the radius R in equation (2.2-34) is different than the coefficient scaling factor, the anomaly degree variances computed from these coefficients should be transformed accordingly (Moritz, 1980, p. 181). This is generally done to improve the way the series expression converges by choosing the radius of an imbedded sphere R_B. Then the c_n values are to be multiplied by the term $(R/R_B)^{2n+4}$, which is an option built in the programs for the covariance calculations. However, due to the use of simulated data only, the radius R_E is adjusted instead.

4.3 The effect of the covariance functions on the potential coefficient recovery

The first issue to be addressed is whether it is preferable to use point or mean values as boundary data. Sjoberg (1978) did not examine this in his work, because the available data base at the time consisted of actual area means. On the other hand, Colombo derived the formulae to utilize either point or mean data for harmonic analysis of the disturbing potential on the sphere. He underscored the complexity of this issue but did not provide a definite answer (Colombo, 1979, p. 22). Some intuitive argument was given in support of representing the data as area means; in this case the aliasing is expected to decrease, since the averaging has smoothed out the higher frequencies and only slightly modified the lower ones. No further insight was made available, since in the simulation studies reported by Colombo (1981, p. 33) only area mean data were considered "because area means are preferred for collating information, particularly on a global basis, at present".

Since no conclusive information is available from previous research, it was considered reasonable to undertake a first experiment with point boundary data. For the specific experiment point gravity anomaly data were simulated at a 10° regular grid on the sphere R_E, using Nmax = 18 for the degree of expansion. The auto-covariance matrix was computed by truncating the summation of the point covariance function at 180. Also, the values of 18 and 36 for maximum degree of truncation resulted in singular matrices as seen from the extremely large elements in the calculated inverse and the zero eigenvalues. The reason for the singularity is explained in section 3.1. These computations ended in absolute failure to recover the input potential coefficients. The difference between the input and estimated coefficients was about 100% for most degrees, except for the second degree which was 30%. These differences translate to RMS undulation difference of 40.4 m and RMS anomaly difference of 17.8 mgal.

The legitimate question arises to explain the above outcome, assuming there are no software errors. In order to test the possibility of software errors, the computer program written by Sjoberg (1978), included in Prof. Rapp's program library as program F373, was used. Program F373 estimates by means of collocation the potential coefficients to degree and order 18 and their associated accuracies. A global set of mean gravity

anomalies is given as input, which represent 10° equal area blocks in the system defined by Hajela (1975). The auto-covariance matrix is derived by interpolating the tabulated covariance function, in particular Pellinen's approximation, given by equation (2.2-34), with Nmax = 200. First, the 10° equal area means were substituted by point values on a 10° equiangular grid. Then, the tabulated mean auto-covariance function was replaced by the point auto-covariance function, and finally, the source code was changed to compute the cross-covariances between the estimated potential coefficients and the point data. After each one of these steps, a set of coefficients was estimated. It is clear that such intermediate solutions are theoretically incorrect; nevertheless, they indicate the sensitivity of the results with respect to these three components: the data, the auto-covariance and the cross-covariance matrix. It was evident that the change in the cross-covariance matrix drastically altered the estimated coefficients to the point that no recovery was obtained, thus indicating that it has the strongest influence in the transition from point to mean data.

As a next step, the point data experiments were abandoned and mean data experiments were performed. The first tests were set up in correspondence to the point data test, thus area means of 10° equiangular blocks of gravity anomaly and undulation with maximum degree of expansion 18 were used. The auto and cross-covariance matrices were computed accordingly as explained in section 4.2, with maximum degree of truncation in the auto-covariance function of 180. The results of these two experiments are tabulated in tables 5 and 6 for the $\overline{\Delta g}$ and $\overline{N}$ data respectively. In the same tables the results of two other experiments are shown, where the mean auto-covariance matrices have been substituted by the point ones. Although this configuration is not recommended due to the inconsistencies involved, they are presented here in support of two arguments; first, the strong influence of the cross-covariance matrix when converting from point to mean data, as observed with tests using Sjoberg's software, and second, the distinguishable behavior between the anomaly and undulation data and their covariance functions with regard to the recovery of the input coefficients. In this case the point covariance may be viewed as another approximation of the mean covariance function implemented here.

Note that in the tables presenting the recovery, the term "overall" pertains to the average of the percentage difference (from equation (4.1-8)) and the RMS value for the

undulation difference (from equation (4.1-10)) and the anomaly difference (from equation (4.1-12)). Also, the recovery of the degree 17 is given, since the Nyquist frequency, N_q=18, of the experiments cannot be resolved completely, as explained in section 3.1, p. 60. This fact is manifested by the non-recovery of the N_q frequency zonal, i.e. $C_{18,0}$, while all other order coefficients within this degree are recovered with some accuracy.

Table 5. Recovery for 10° $\overline{\Delta g}$ data, with mean cross-covariance matrices and point and mean auto-covariance matrices with Nmax = 180

Degree	Percent difference		Undulation difference (m)		Anomaly difference (mgals).	
	point	mean	point	mean	point	mean
2	32.61	0.58	5.840	0.103	0.90	0.02
3	11.29	2.20	2.135	0.416	0.66	0.13
4	23.56	1.71	2.273	0.165	1.05	0.08
5	27.11	1.75	2.007	0.130	1.23	0.08
6	36.82	3.76	2.102	0.215	1.62	0.17
12	82.77	18.07	0.938	0.205	1.59	0.35
17	93.49	41.87	0.639	0.286	1.57	0.70
18	92.51	36.25	0.648	0.254	1.69	0.66
overall	60.49	13.79	8.270	0.896	6.53	1.47

Table 6. Recovery for 10° $\bar{N}$ data, with mean cross-covariance matrices and point and mean auto-covariance matrices, with Nmax = 180.

Degree	Percent difference		Undulation difference (m)		Anomaly difference (mgals).	
	point	mean	point	mean	point	mean
2	32.61	58.55	4.150	x	0.64	1.61
3	45.60	363.83	8.640	x	2.66	21.17
4	16.01	24.44	1.546	2.359	0.71	1.09
5	26.82	86.10	1.986	6.375	1.22	3.92
6	18.28	17.78	1.044	1.015	0.80	0.78
12	33.82	9.93	0.383	0.113	0.65	0.19
17	77.08	45.47	0.527	0.311	1.30	0.77
18	69.22	29.25	0.485	0.205	1.27	0.54
overall	37.74	49.21	10.175	70.018	4.62	21.80

It is seen in table 5, that the $\overline{\Delta g}$ set-up gives a recovery of the input field, which is 30% to 40% better for the low degrees (i.e. for n = 2 to 6), than for the higher degrees (i.e. n=16 to 18). As expected, in this case the point auto-covariance approximation is not a desirable one, due to resulting 60% average difference. On the other hand, the undulation data recovery is overall very poor, especially for the low degrees, while the degree 3 is non-recoverable at all. The degrees between 10 and 14 are recovered somewhat better than with the $\overline{\Delta g}$ data. Noticable improvement is seen for the case of the point auto-covariance function, especially for the degree 3. This is in agreement with the discussion in section 3.1, identifying the instability problem arising from the low frequency undulation covariance function.

The other important issue addressed in this section is the one of the appropriate degree of truncation in the auto-covariance functions, which is discussed in principle in section 3.1. Theoretically the summation should be carried out to infinity, with the higher frequencies damped, according to the block size. Colombo's tests (1981, pp. 85-90) have already been summarized in section 3.1. He reported that the approximation used here (equation (2.2-34)) is inadequate for blocks near the poles, as compared to a more rigorous covariance computation by means of numerical quadratures. Such behavior of the covariance function would not be anticipated, since it only depends on the block size and generally improves for finer grids, as is the case near the poles. Also, the covariances computed for this work do not show such discrepancies. Tables 7 and 8 present these covariances between 5° blocks for equatorial and polar rows respectively. These covariance values show similar agreement between the Pellinen approximation and the numerical quadrature computation (columns 1 and 3) for both equatorial and polar rows, which indicates that Colombo's computations for the polar rows with 100% discrepancy (column 2, Table 8) are not reliable. Note that the c_n values used by Colombo were derived from the "2L" model of Jekeli (1978), which probably accounts for the differences between Colombo's and present computations for the equatorial rows (columns 2 and 3, Table 7).

Table 7. Mean auto-covariance comparison of 5° $\overline{\Delta g}$ data, reported by Colombo (1981) and present calculations, Nmax = 180, latitudinal row between 0° and 5° N.

Block No.	Numerical/Colombo	Pellinen/Colombo	Pellinen/Present
1	253.8	251.8	219.3
2	149.5	151.0	152.2
3	93.9	93.9	104.6
4	57.1	57.1	61.4
5	31.7	31.7	29.6
6	13.9	13.9	7.6
12	-18.1	-18.1	-14.1
24	9.1	9.1	10.4
36	-13.7	-13.6	-21.3

Table 8. Mean auto-covariance comparison of 5° $\overline{\Delta g}$ data, reported by Colombo (1981) and present calculations, Nmax = 180, latitudinal row between 80° and 85° N.

Block No.	Numerical/Colombo	Pellinen/Colombo	Pellinen/Present
1	437.2	835.5	361.4
2	318.3	800.1	334.4
3	229.2	709.0	274.3
4	196.4	592.2	220.9
36	58.0	149.4	61.1

In this study the overall recovery was used as the criterion to judge the sufficient degree, Nmax, of the truncation in the summation of the covariance function (equations (2.2-34) to (2.2-36)). Tests for $\overline{\Delta g}$ and $\bar{N}$ were made for Nmax = 360 and a test for Nmax = 3000 was performed for $\bar{N}$ data only, since the $\bar{N}$ type of tests displayed instability with regard to the covariance functions used. The input potential coefficient set being complete to degree 360, the adoption of c_n model was necessary to compute the remaining c_n values to degree 3000. In particular, the Tscherning-Rapp model (1974) was used, defined from:

$$c_n = \frac{A(n-1)}{(n-2)(n+B)} \quad , \qquad n > 2 \tag{4.3-1}$$

where A = 425.28 and B = 24. The recovery obtained for the $\overline{\Delta g}$ data is identical with the one showed in table 5, thus proving the summation of the covariance function to Nmax = 180 satisfactory. Table 9 contains the results for the $\bar{N}$ tests, where the symbol # indicates that the value is the same as the one for Nmax = 360 in the preceeding column.

Table 9. Recovery for 10° $\bar{N}$ data, mean covariance matrices and truncation at Nmax=360 and 3000.

Degree	Percent difference		Undulation difference (m)		Anomaly difference (mgals)	
	360	3000	360	3000	360	3000
2	60.95	60.97	x	#	1.68	#
3	357.09	357.05	x	#	20.78	#
4	24.96	#	2.409	#	1.11	#
5	81.14	81.13	6.230	6.229	3.83	#
6	17.86	#	1.020	#	0.78	#
12	9.95	#	0.113	#	0.19	#
17	45.50	#	0.311	#	0.77	#
18	29.25	#	0.205	#	0.54	#
overall	48.81	#	68.818	68.810	21.41	#

By comparing table 6 with table 9 it may be seen that there is a small improvement going from Nmax = 180 to 360, but there is no difference for Nmax = 3000, which increases tremendously the computation time. In all cases the recovery remains very poor, thus making the small difference completely trivial.

4.4 Data error consideration and regularization effects.

The procedure for incorporating error in the simulated data is presented in section 4.2. According to this algorithm the value of the variance, σ^2, of the white noise $(0, \sigma^2)$ included in the data must be assigned. The appropriate σ is found by means of the accuracy estimates of the input potential coefficients. As explained in section 1.2, the estimated accuracies of the coefficient set OSU86D, described by Rapp and Cruz (1986a), may be used for the OSU86F field to degree 250. Using program F184.JAN26, the error degree variances in gravity anomaly, $m_n^2(\Delta g)$, and undulation m_n^2

(N), are computed from the estimated errors $m_{c_{nm}}$ and $m_{s_{nm}}$ of the coefficients $\bar{C}_{nm}$ and $\bar{S}_{nm}$ respectively:

$$m_n^2(\Delta g) = \gamma^2 (n-1)^2 \left(\frac{R}{R_E}\right)^{2n} \sum_{m=0}^{n} \left(m_{c_{nm}}^2 + m_{s_{nm}}^2\right), \tag{4.4-1}$$

$$m_n^2(N) = R_E^2 \sum_{m=0}^{n} \left(m_{c_{nm}}^2 + m_{s_{nm}}^2\right). \tag{4.4-2}$$

Then, the cumulative estimated error to degree Nmax for these two quantities is given from:

$$\tilde{\sigma}_{\Delta g} = \pm \left[\sum_{n=2}^{Nmax} m_n^2(\Delta g)\right]^{1/2} \quad \text{and} \tag{4.4-3}$$

$$\tilde{\sigma}_N = \pm \left[\sum_{n=2}^{Nmax} m_n^2(N)\right]^{1/2}. \tag{4.4-4}$$

The following table shows the values of both anomaly and undulation standard deviations for Nmax = 18, 36, 60 and 90, which correspond to the expansions estimated in this work.

Table 10. Anomaly and undulation standard deviations to degree Nmax, derived from the estimated accuracy of the OSU86D.

Nmax	18	36	60	90
$\tilde{\sigma}_{\Delta g}$ (mgals)	1.15	2.24	3.20	4.61
$\tilde{\sigma}_N$ (meters)	0.62	0.79	0.85	0.90

When error is included in the simulated observations, the associated variance is taken into account in the error covariance matrix designated by C_{nn} or D in equations (2.2-11) to (2.2-14). In order to maintain the block-Toeplitz structure of the covariance matrix for each data group, the related D matrix is assumed diagonal with the additional assumption of the same error among observations within the same parallel. For the computations described here, the same variances $\tilde{\sigma}^2_{\Delta g}$ and $\tilde{\sigma}^2_N$ were assigned to all gravity anomaly and undulation observations respectively. The individual experiments where data error was included pertain to 18 and 36 degree expansion estimations and they are described below.

The first test utilized point anomaly data, despite the unacceptable results obtained to this point (Section 4.3). The incentive for this was the fundamental difference in truncating the degree of summation in the point and the mean covariance functions. When calculating the mean function, with Nmax = 180, the Pellinen operators smooth out the higher frequencies according to the data block size. However, when calculating the point function with the same Nmax (i.e. 180) for 10° point data (with frequency content to degree 18), additional frequencies in the range 18 to 180 are introduced in the data covariances, while not present in the data. By including error in the data, a positive definite error covariance matrix, D, is added to the data covariance matrix, thus making the matrix inversion possible even for low degree (eg. 18) truncation of the covariance function. Using 10° point Δg data with maximum degree of expansion 18, the same (i.e. 18) maximum degree in the covariance function summation and $\tilde{\sigma}=\pm 1.15$ mgals, the results showed no recovery, as before.

The point data configuration was abandoned once again, and the next tests were made with mean gravity anomaly and mean undulation data computed from an expansion to degree 18. The auto-covariance matrices were computed with input parameters Nmax = 180, $\tilde{\sigma}_{\Delta g} = \pm$ 1.15 mgals and $\tilde{\sigma}_N = \pm$ 0.62m accordingly. Although the adopted values of $\tilde{\sigma}_{\Delta g}$ and $\tilde{\sigma}_N$, as shown in Table 10, pertain to the error associated with point quantities, they are used in the present analysis as rough estimates of the data error in the mean anomaly and mean undulation observations. The results obtained for the potential coefficient recovery are presented in Tables 11 and 12.

Table 11. Recovery for 10° $\overline{\Delta g}$ data with error, mean covariance matrices and Nmax=180.

Degree	Correlation	Percent difference	Undul. diff. (m)	Anomaly diff. (mgals)
2	0.9983	5.95	1.065	0.16
3	0.9990	4.90	0.926	0.28
4	0.9987	5.29	0.511	0.24
5	0.9991	4.37	0.323	0.20
6	0.9994	3.52	0.201	0.15
12	0.9821	24.98	0.283	0.48
17	0.9286	46.39	0.317	0.78
18	0.9391	43.38	0.304	0.79
overall	0.9833	17.86	1.810	1.85

The effect of data error in this case may be seen by comparing the results of tables 5 and 11. The error in the estimated coefficients of second degree increases from 0.58% to 5.95% when data error is included. It is seen that the error increase is smaller for higher degree coefficients, while the coefficients near the Nyquist frequency are recovcered with an error of about 40%. The average error increase to degree 18 is about 30% for using data with error. This figure corresponds to increase of the RMS undulation difference by 102% and increase of the RMS anomaly difference by 26%.

Table 12. Recovery for 10° $\bar{N}$ data with error, mean covariance matrices and Nmax=180.

Degree	Correlation	Percent difference	Undul. diff. (m)	Anomaly diff. (mgals)
2	0.9699	24.42	4.373	0.67
3	0.9743	53.79	x	3.13
4	0.9899	19.65	1.896	0.87
5	0.9722	29.66	2.196	1.35
6	0.9828	18.48	1.055	0.81
12	0.9738	22.80	0.258	0.44
17	0.7074	72.47	0.496	1.22
18	0.7907	63.04	0.442	1.15
overall	0.9345	33.94	11.659	4.69

A drastic improvement is apparent between the results of Table 12 and the corresponding errorless case shown in Table 6, especially for degrees 2 and 3, which amounts to a decrease in RMS undulation difference by 85%. This result provided more evidence of

the instability of the data solutions and the regularization procedure was considered as the most justifiable next step. The fundamental theory of the regularization is briefly described in section 3.2 including formula (3.2-13) which is implemented here. As already mentioned the error covariance matrix, D, is assumed diagonal in all experiments presented here. Therefore, the term αD in equation (3.2-13) may be written as $\alpha\tilde{\sigma}^2 I$, where I is the unit matrix. In all undulation error covariance matrices from this point on, the value $\alpha\tilde{\sigma}^2=9m^2$ is used. For the case of 10° $\bar{N}$ data, the corresponding error suggested in Table 10 is $\tilde{\sigma}_N = \pm 0.62m$, thus defining the value of α to be about 23. Tables 13 and 14 contain the results for the potential coefficient recovery, obtained from two experiments with 10° $\bar{N}$ data and regularized auto-covariance matrices by a factor $\alpha \cong 23$. In the first experiment the noise $(0, \tilde{\sigma}_N^2)$ is included in the simulated data (table 13), while in the second one (table 14), errorless data are used.

Table 13. Recovery for 10° $\bar{N}$ data with error, mean covariance matrices with Nmax=180 and regularization of $\alpha \cong 23$.

Degree	Correlation	Percent difference	Undul. diff. (m)	Anomaly diff. (mgals)
2	0.9795	20.18	3.614	0.56
3	0.9820	45.11	8.535	2.63
4	0.9941	14.79	1.427	0.66
5	0.9784	24.50	1.814	1.12
6	0.9925	12.34	0.704	0.54
12	0.9809	35.44	0.402	0.68
17	0.7293	80.41	0.550	1.35
18	0.8735	76.81	0.538	1.41
overall	0.9549	35.73	9.744	4.41

The comparison of Table 13 to Table 12 shows improvement in the recovery of the low degree coefficients, but poorer recovery of the coefficients of the second half of the estimated spectrum. Thus, the average percent difference changes from 34% to 36% when regularization is applied. On the other hand, the RMS undulation difference is decreased by 16% and the RMS anomaly difference is decreased by 6%.

Table 14. Recovery for $10°\bar{N}$ errorless data, mean covariance matrices with Nmax=180 and variance $\alpha\tilde{\sigma}^2_{\bar{N}}=9m^2$

Degree	Correlation	Percent difference	Undul. diff. (m)	Anomaly diff. (mgals)
2	0.9758	21.91	3.925	0.60
3	0.9835	42.87	8.112	2.49
4	0.9930	16.15	1.559	0.72
5	0.9807	23.85	1.766	1.09
6	0.9898	14.29	0.816	0.63
12	0.9934	32.50	0.368	0.62
17	0.7687	80.13	0.548	1.35
18	0.9258	73.95	0.518	1.35
overall	0.9632	35.44	9.517	4.32

The overall improvement in the recovery when neglecting the error in the simulated data, while already including the regularized error covariance matrix is generally small, of the order of 3%. However, a comparison on a per-degree basis of the numbers shown in Tables 13 and 14 shows that the improvement of the overall recovery does not mean improvement in individual degree recovery.

Before presenting the tests for various regularization parameter values, the tests including data error in 36 degree expansion estimation are presented. Specifically, mean anomaly and mean undulation data referring to 5° blocks were derived with maximum degree 36. Both, anomaly and undulation, auto-covariance matrices were singular due to decreased data spacing. To enable the inversion of the covariance matrix the value of 3 $mgals^2$ was added to the diagonal elements in the case of $\overline{\Delta g}$ data, and the value of $9m^2$ in the case of $\overline{N}$ data. Then, the noise added to the $\overline{\Delta g}$ simulated observations is distributed as $(0, 1.73^2)$ and the noise added to the $\overline{N}$ simulated observations is destributed as $(0, 0.79^2)$, which implies a regularization factor of $a \cong 14$. In the following, Tables 15 and 16 show the results of the $\overline{\Delta g}$ data tests with data error and without data error respectively. However, the same error covariance matrix is included in both cases.

Table 15. Recovery for 5° $\overline{\Delta g}$ data with error, mean covariance matrices with Nmax=180 and variance $\alpha\tilde{\sigma}_{\Delta g}{}^2$ = 3 mgals^2.

Degree	Correlation	Percent difference	Undul. diff. (m)	Anomaly diff. (mgals)
2	0.9998	3.05	0.547	0.08
3	0.9998	2.33	0.441	0.14
4	0.9995	3.24	0.313	0.14
5	0.9994	3.58	0.265	0.16
6	0.9995	3.65	0.209	0.16
12	0.9933	12.67	0.144	0.24
18	0.9874	17.28	0.121	0.32
24	0.9652	33.38	0.130	0.46
36	0.9087	50.91	0.152	0.82
overall	0.9786	21.26	1.107	2.47

Table 16. Recovery for 5° $\overline{\Delta g}$ errorless data, mean covariance matrices with Nmax=180 and variance $\alpha\tilde{\sigma}_{\Delta g}{}^2$ = 3 mgals^2.

Degree	Correlation	Percent difference	Undul. diff. (m)	Anomaly diff. (mgals)
2	1.0000	0.32	0.057	0.01
3	1.0000	0.51	0.097	0.03
4	1.0000	0.43	0.041	0.02
5	1.0000	0.57	0.042	0.03
6	1.0000	1.09	0.062	0.05
12	0.9996	6.33	0.072	0.12
18	0.9975	10.92	0.076	0.20
24	0.9939	24.44	0.095	0.34
36	0.9434	47.61	0.142	0.77
overall	0.9929	16.96	0.542	2.10

Including data error increased the error of the estimated coefficients, as is seen by comparing the results of Tables 15 and 16. Especially, the recovery of the low degrees is mostly affected, for example the error of estimating the second degree coefficients increased from 0.32% to 3.05%. In the overall sense, the average error to degree 36 increased by 25%, while the RMS undulation difference increased by 104% when error is included, thus reflecting the large impact on the low degree coefficient recovery. However, the increase in RMS anomaly difference is about 18%. It may be pointed out that the effect of the data error is generally smaller than the same effect for the 10° $\overline{\Delta g}$ data, presented earlier in this section. The corresponding results for 5° $\overline{N}$ data with and without error are presented in Tables 17 and 18 respectively.

Table 17. Recovery for 5° $\overline{N}$ data with error, mean covariance matrices with Nmax=180 and variance $\alpha\sigma_N^2$=9 m^2

Degree	Correlation	Percent difference	Undul. diff. (m)	Anomaly diff. (mgals)
2	0.9847	17.51	3.137	0.48
3	0.9912	24.86	4.703	1.45
4	0.9948	12.49	1.206	0.56
5	0.9934	11.90	0.881	0.54
6	0.9956	9.36	0.535	0.41
12	0.9967	11.21	0.127	0.22
18	0.9895	30.85	0.216	0.57
24	0.9175	71.33	0.278	0.98
36	0.7475	89.05	0.267	1.43
overall	0.9346	44.52	6.034	5.37

Table 18. Recovery for 5° $\overline{N}$ errorless data, mean covariance matrices with Nmax=180 and variance $\alpha\sigma_N^2$=9 m^2.

Degree	Correlation	Percent difference	Undul. diff. (m)	Anomaly diff. (mgals)
2	0.9874	15.87	2.842	0.44
3	0.9906	23.55	4.455	1.37
4	0.9957	11.48	1.108	0.51
5	0.9936	11.69	0.866	0.53
6	0.9963	8.60	0.491	0.38
12	0.9995	8.44	0.096	0.16
18	0.9965	29.21	0.205	0.54
24	0.9761	67.92	0.264	0.93
36	0.8999	88.34	0.264	1.42
overall	0.9710	43.37	5.652	5.28

Table 18 shows better recovery for errorless data as compared to Table 17. In particular, the error of the second degree coefficients increases by 10%, while the average error to degree 36 increases by 3%. Note that the large influence on the low degree recovery observed in the $\overline{\Delta g}$ tests is not observed here, due to the large regularization factors. The RMS undulation difference increased by 7% while the RMS anomaly difference increased by 2%. These figures show an error influence of the same order of magnitude as the 10° $\overline{N}$ tests, presented in Tables 13 and 14.

Finally seven regularized solutions for $\bar{N}$ errorless data are presented for various regularization factors. Since generally the solutions improve for the lower degrees but deteriorate for the higher frequencies, they are compared with each other in terms of overall recovery to various degrees, in particular 4, 9 and 18. These statistics are given in Tables 19 and 20, together with the recovery measures for degree 2. Note, that for the computation of the covariance matrices the covariance function was truncated at Nmax=360. According to the tests presented in section 4.3, the results would be identical if the value of Nmax = 180 were used instead.

Table 19. RMS undulation differences (in meters) for 10° $\bar{N}$ errorless data and mean covariance matrices (Nmax = 360) from various regularized solutions. Variance = $\alpha\, \tilde{\sigma}^2_N$.

variance (m^2)	n = 2	n = 2 to 4	n = 2 to 9	n = 2 to 18
4	4.124	10.887	11.172	11.222
9	3.962	9.358	9.634	9.724
20	3.582	7.741	7.982	8.174
50	2.951	6.025	6.268	6.669
100	2.344	4.734	5.119	5.776
300	1.413	2.980	4.375	5.425
600	1.031	2.285	4.982	6.05

Table 20. RMS anomaly differences (in mgals) for 10° $\bar{N}$ errorless data and mean covariance matrices (Nmax = 360) from various regularized solutions. Variance = $\alpha\, \tilde{\sigma}^2_N$.

variance (m^2)	n = 2	n = 2 to 4	n = 2 to 9	n = 2 to 18
4	0.63	3.21	3.71	4.37
9	0.61	2.73	3.22	4.30
20	0.55	2.23	2.69	4.54
50	0.45	1.72	2.28	5.04
100	0.36	1.34	2.33	5.58
300	0.22	0.86	3.36	6.70
600	0.16	0.73	4.39	7.51

The results in Tables 19 and 20 show a continuing improvement in the recovery of degree 2 for increasing variance values. In fact, the RMS undulation difference is

decreased by 75% between variance = $\alpha\,\tilde{\sigma}_N^2 = 4$ and variance = $\alpha\,\tilde{\sigma}_N^2 = 600$. However, the recovery of the higher degrees of the estimated expansion deteriorates when the variances increases. This is seen more clearly by observing the overall RMS anomaly difference which increases for larger variances. Such results are to be anticipated in applying a regularization procedure, especially for large regularization factors as in the presented experiments where the value of α varies from 10 to 1.5×10^3.

4.5 Recovery in relation to the grid size.

The sets of spherical harmonic potential coefficients estimated from various grid size data are analyzed in this section. All solutions are regularized except for the one obtained from 10° mean anomaly data to degree 18. The same value was added to the diagonal of the auto-covariance matrix for each data type, regardless of the block size. In particular, the value of 3 mgals^2 was used to regularize the $\overline{\Delta g}$ solutions which, according to the standard deviations given in table 10, would actually correspond to underscaling the variance of the data. To the contrary, the results shown in tables 19 and 20 suggest large regularization factors in the case of $\bar{N}$ data. The value of 9m^2 was used in all the solutions with $\bar{N}$ data, which corresponds to regularization parameters, α, in the range from 10 to 23.

The data, consisting of $\overline{\Delta g}$ and $\bar{N}$ values, were computed on regular grids of size 10°, 5°, 3° and 2° with maximum degrees of expansion of 18, 36, 60 and 90 respectively. The auto-covariance matrices were derived with the mean covariance function summed to Nmax = 180. Among the recovery statistics, the percent difference and the correlation per degree are shown in figures 14 to 17 and figures 18 to 21 for all four solutions derived from $\overline{\Delta g}$ data. Similarly, the results obtained from $\bar{N}$ data are shown in figures 22 to 29.

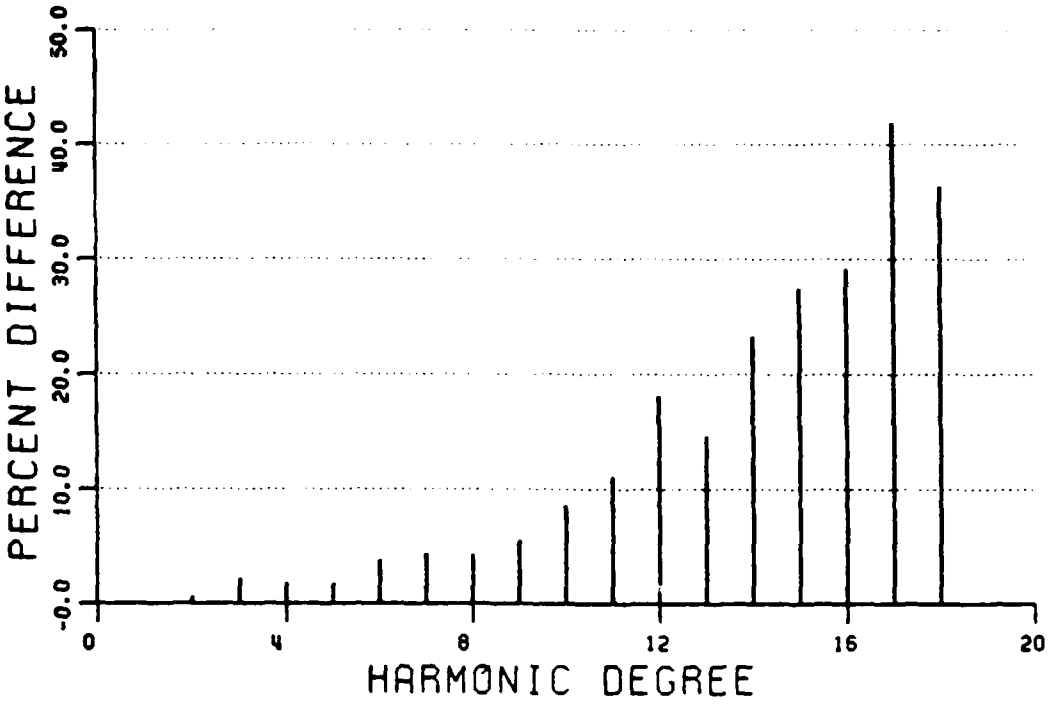

Figure 14. Percent difference per degree between the input coefficients and the coefficients recovered from 10° $\overline{\Delta g}$ errorless data to degree 18.

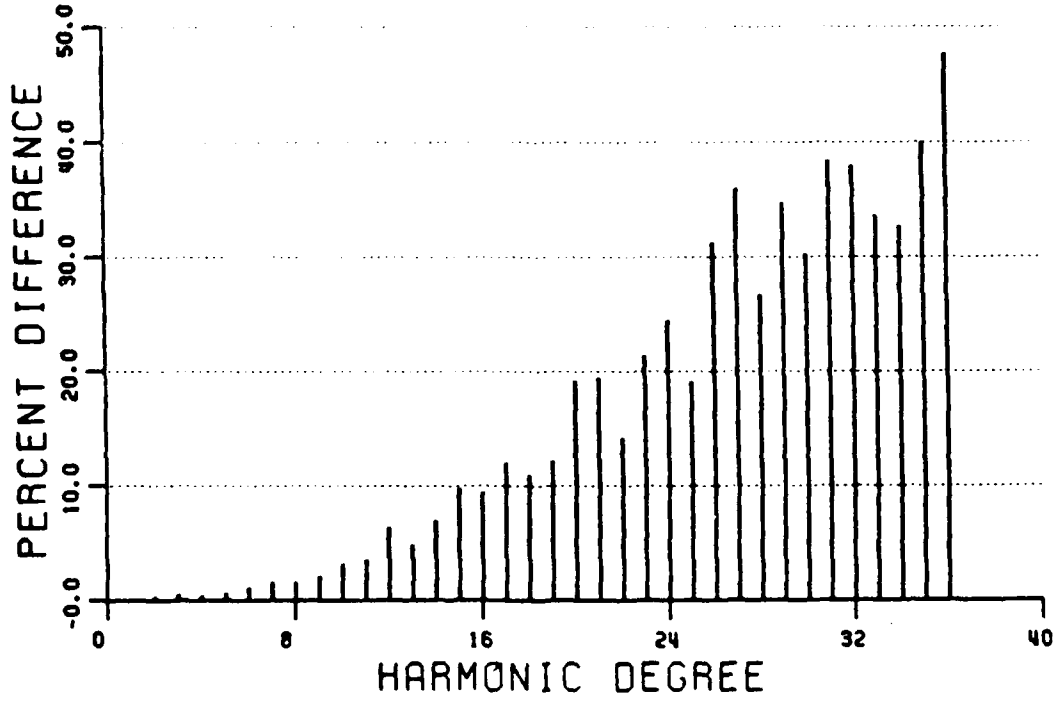

Figure 15. Percent difference per degree between the input coefficients and the coefficients recovered from 5° $\overline{\Delta g}$ errorless data to degree 36.

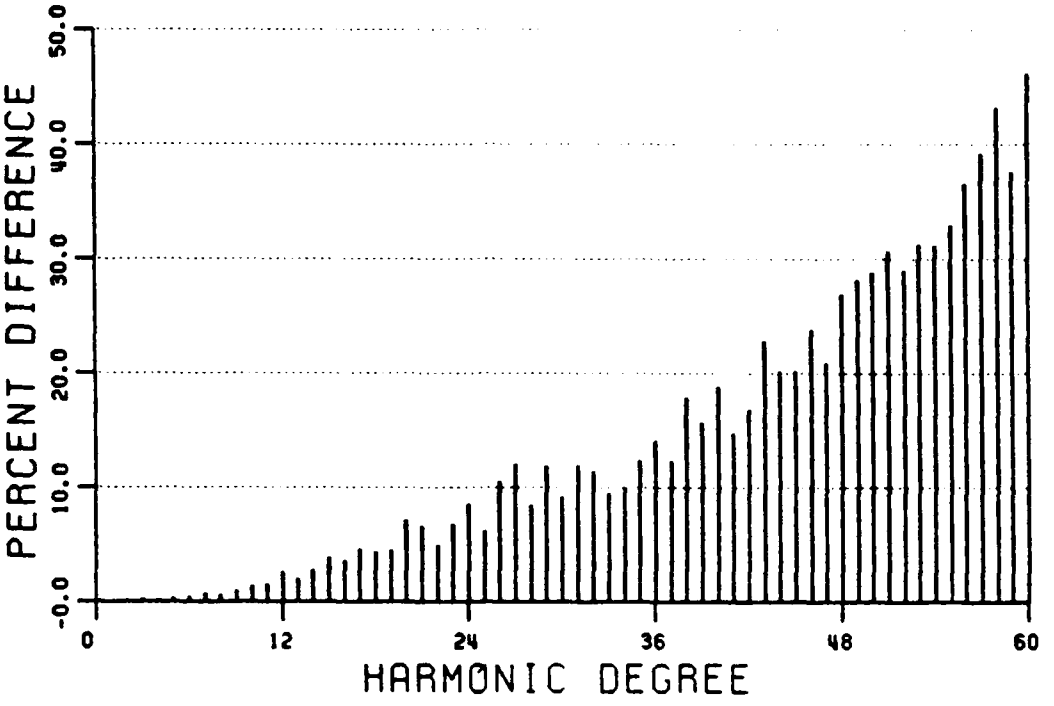

Figure 16. Percent difference per degree between the input coefficients and the coefficients recovered from 3° $\overline{\Delta g}$ errorless data to degree 60.

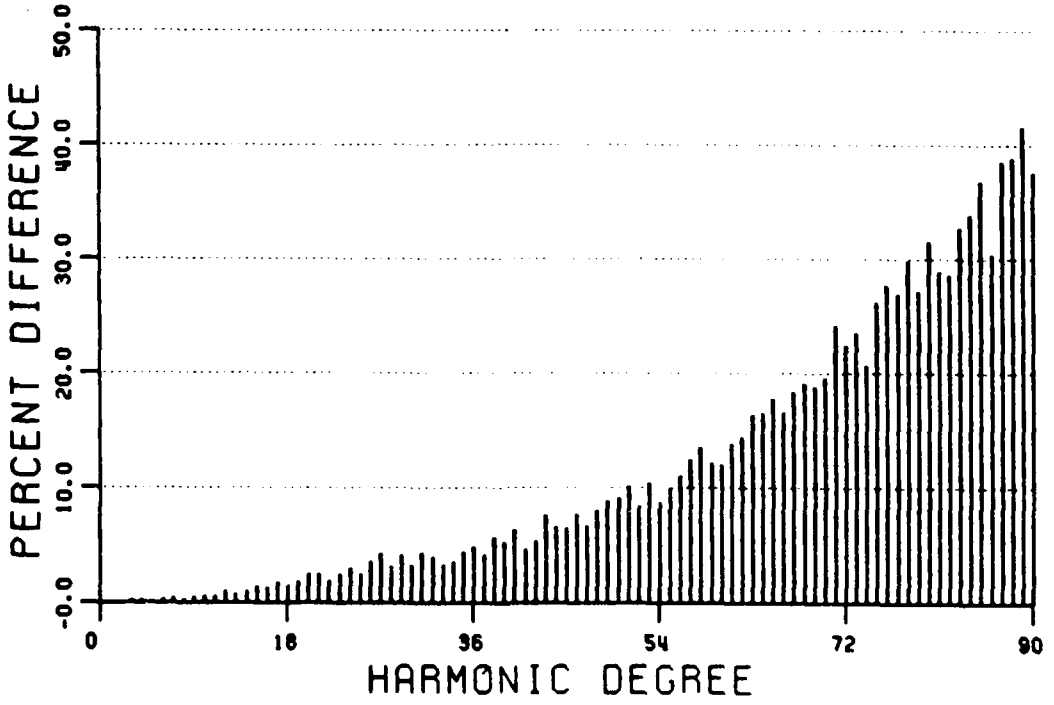

Figure 17. Percent difference per degree between the input coefficients and the coefficients recovered from 2° $\overline{\Delta g}$ errorless data to degree 90.

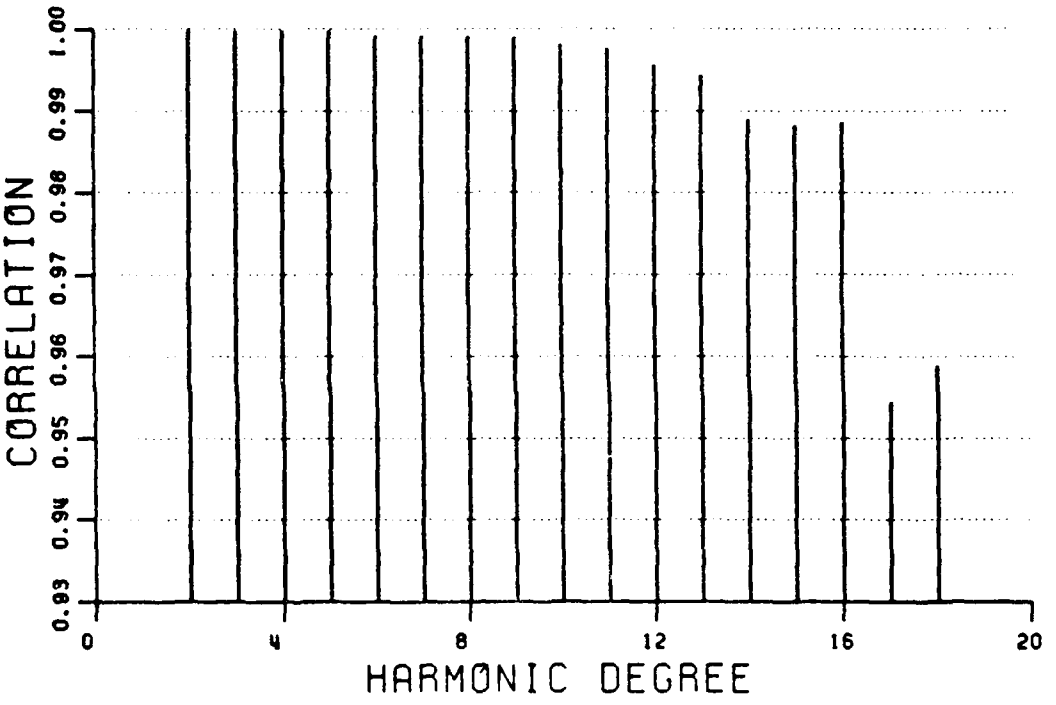

Figure 18. Correlation per degree between the input coefficients and the coefficients recovered from 10° $\overline{\Delta g}$ errorless data to degree 18.

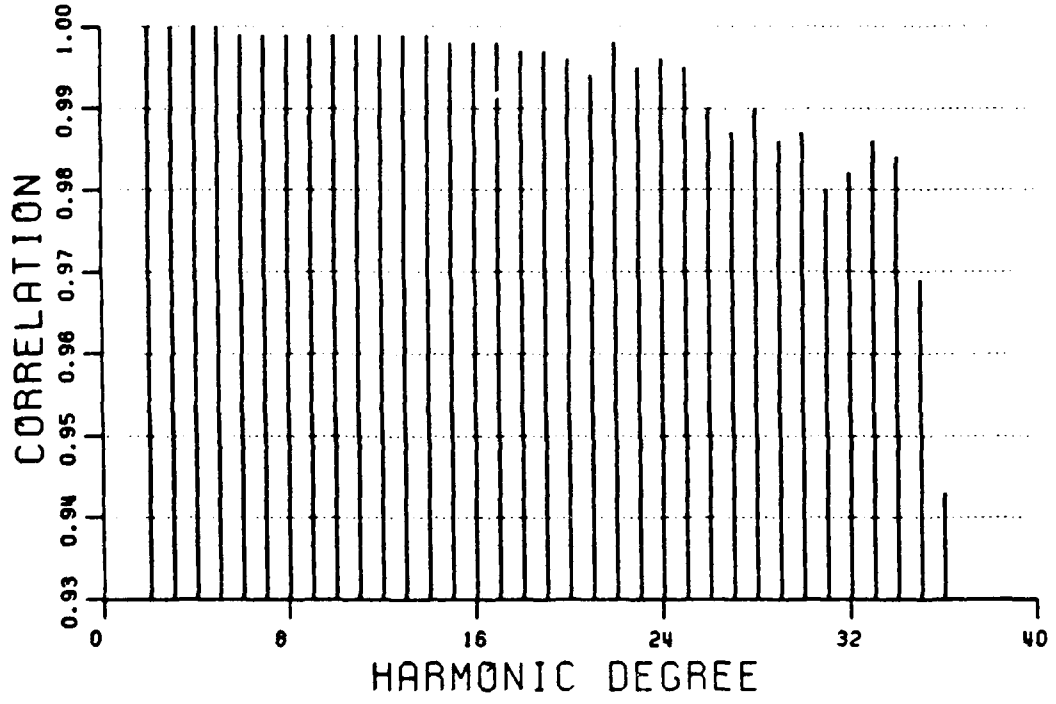

Figure 19. Correlation per degree between the input coefficients and the coefficients recovered from 5° $\overline{\Delta g}$ errorless data to degree 36.

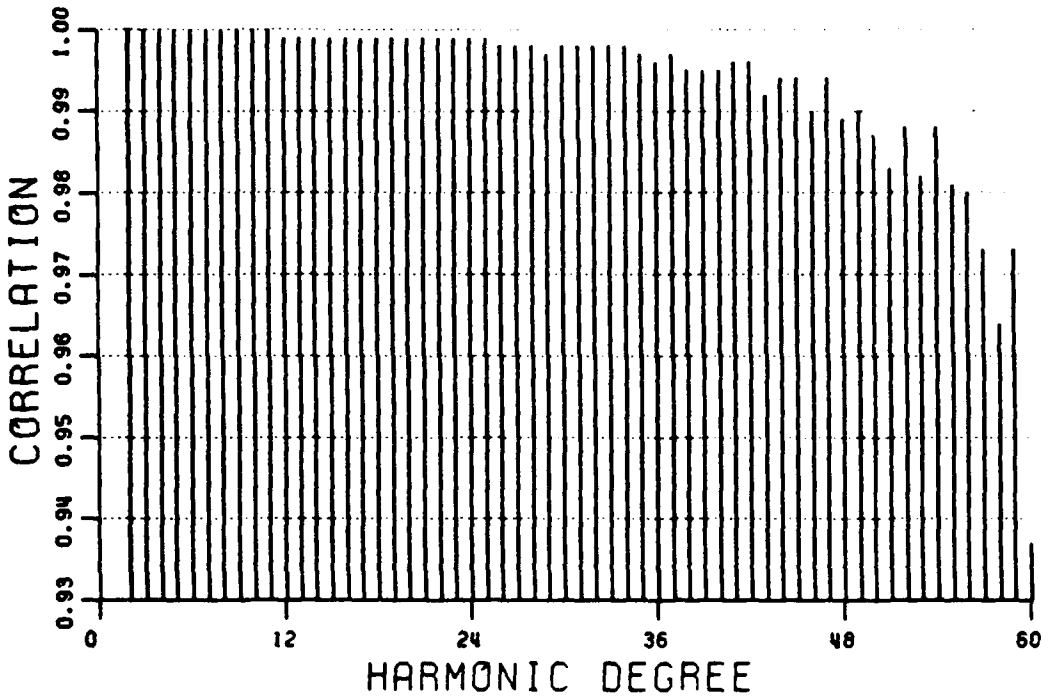

Figure 20. Correlation per degree between the input coefficients and the coefficients recovered from 3° $\overline{\Delta g}$ errorless data to degree 60.

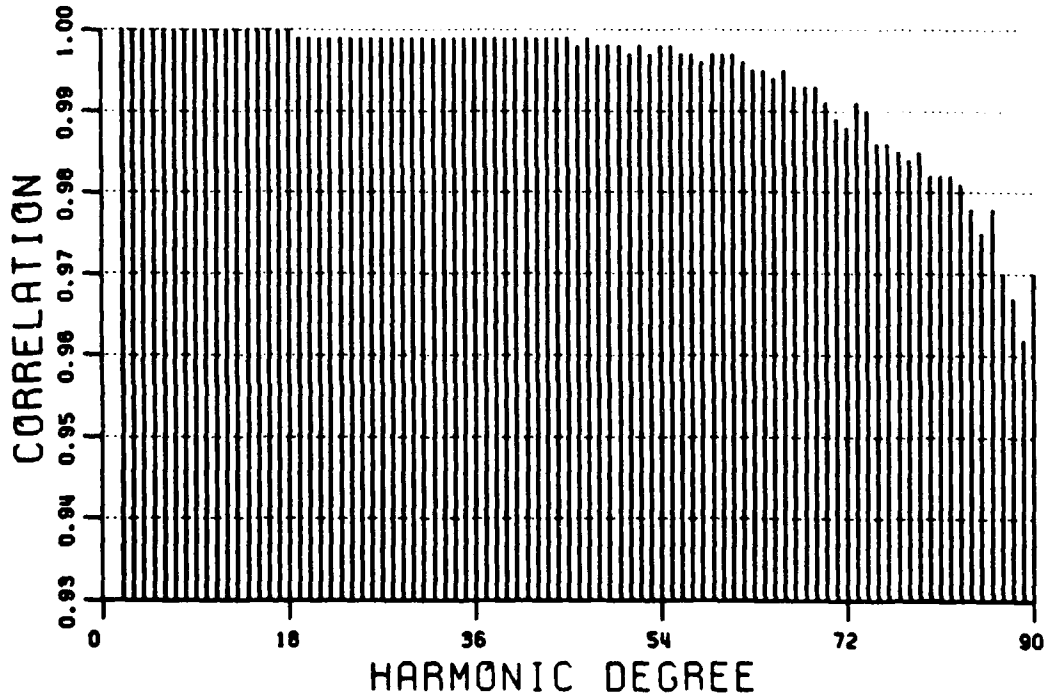

Figure 21. Correlation per degree between the input coefficients and the coefficients recovered from 2° $\overline{\Delta g}$ errorless data to degree 90.

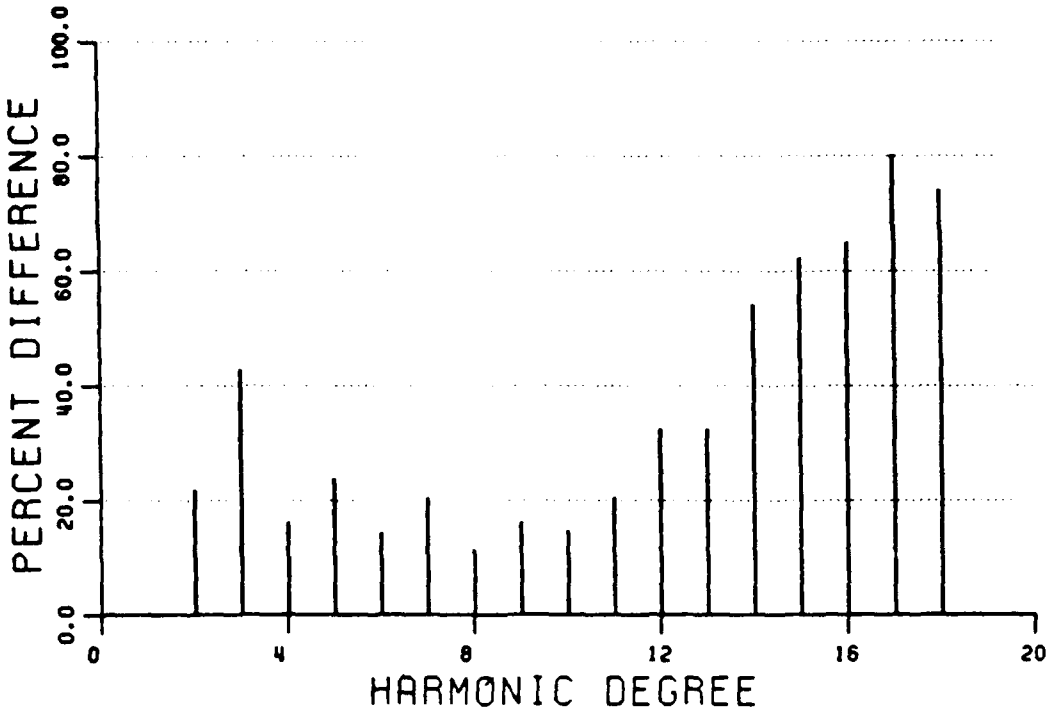

Figure 22. Percent difference per degree between the input coefficients and the coefficients recovered from 10° $\bar{N}$ errorless data to degree 18.

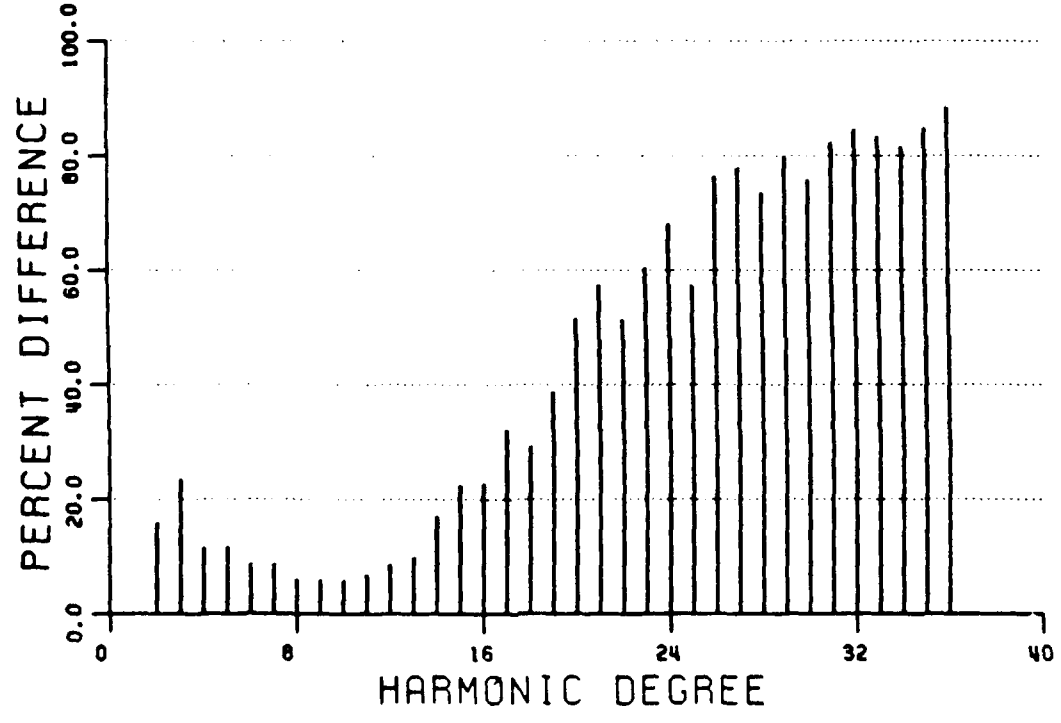

Figure 23. Percent difference per degree between the input coefficients and the coefficients recovered from 5° $\bar{N}$ errorless data to degree 36.

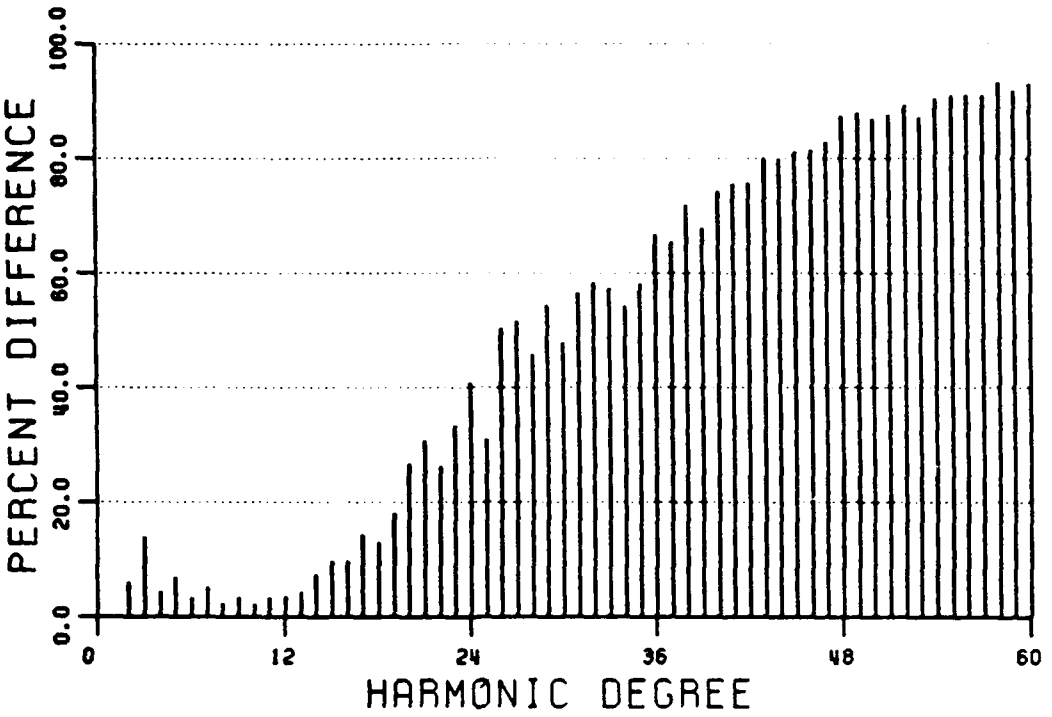

Figure 24. Percent difference per degree between the input coefficients and the coefficients recovered from 3° $\bar{N}$ errorless data to degree 60.

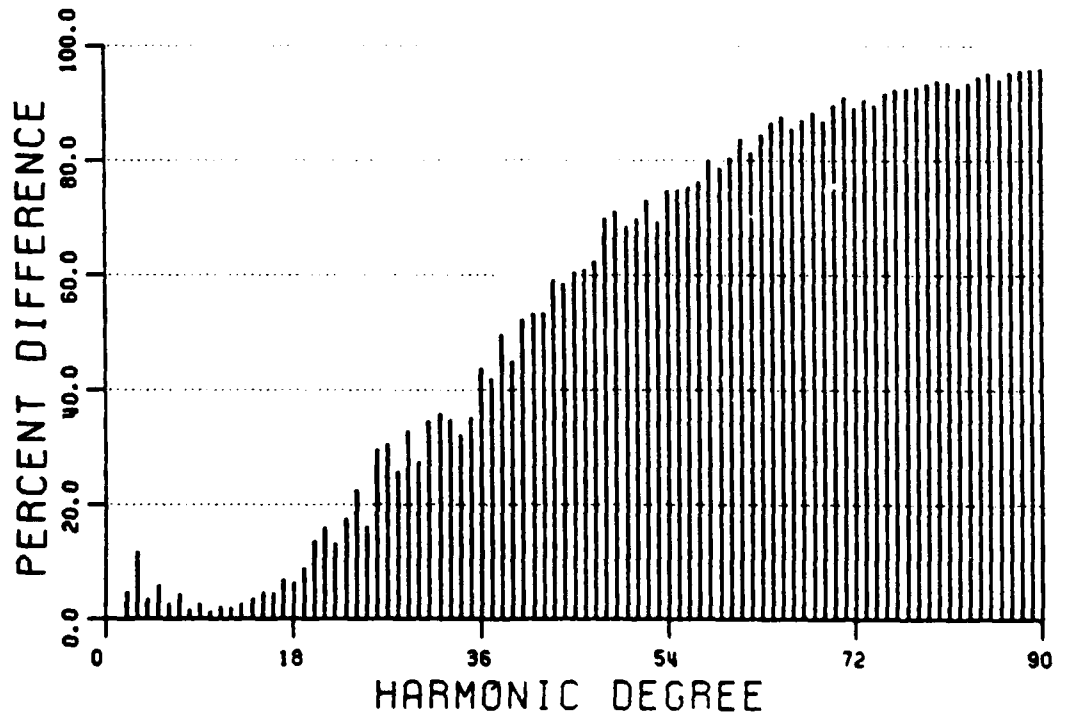

Figure 25. Percent difference per degree between the input coefficients and the coefficients recovered from 2° $\bar{N}$ errorless data to degree 90.

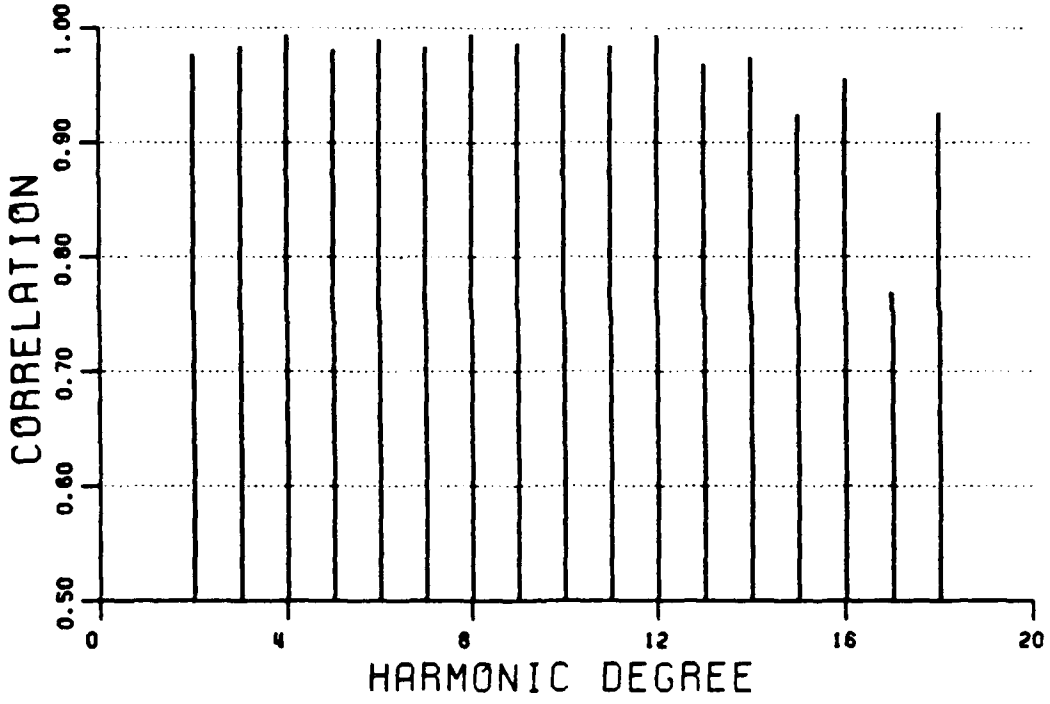

Figure 26. Correlation per degree between the input coefficients and the coefficients recovered from 10° $\bar{N}$ errorless data to degree 18.

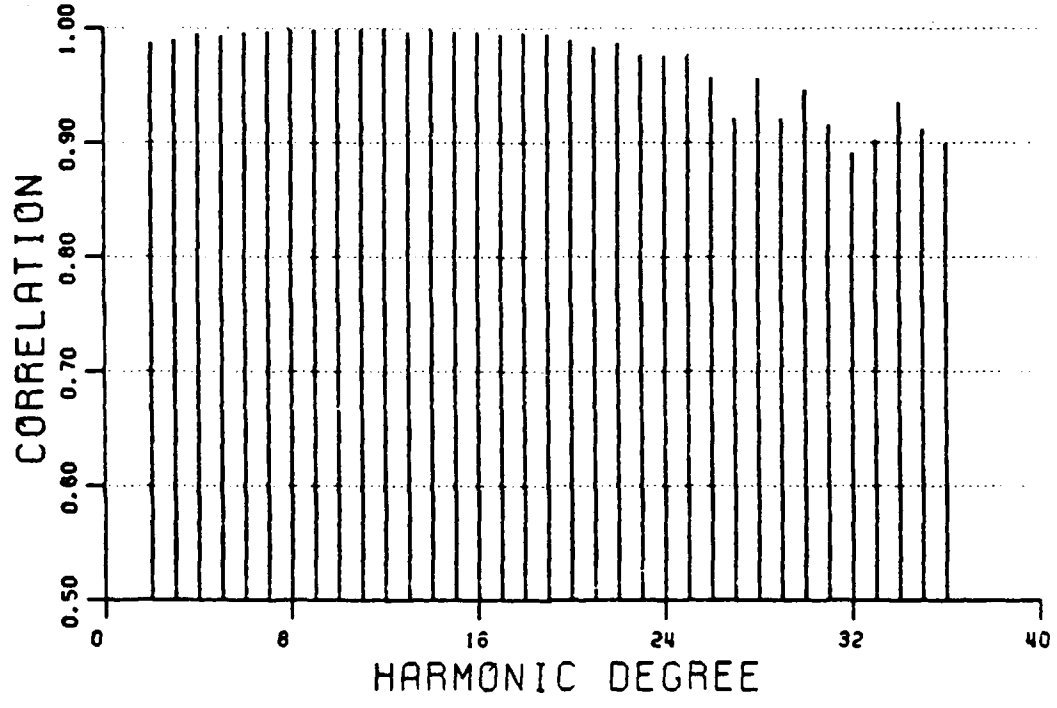

Figure 27. Correlation per degree between the input coefficients and the coefficients recovered from 5° $\bar{N}$ errorless data to degree 36.

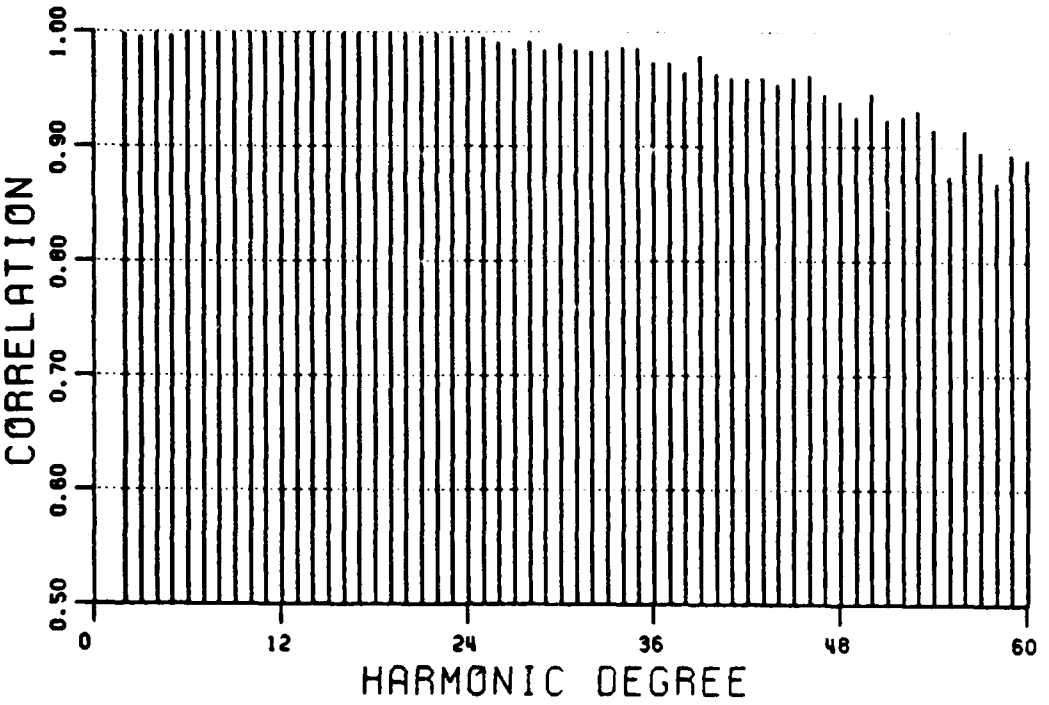

Figure 28. Correlation per degree between the input coefficients and the coefficients recovered from 3° $\bar{N}$ errorless data to degree 60.

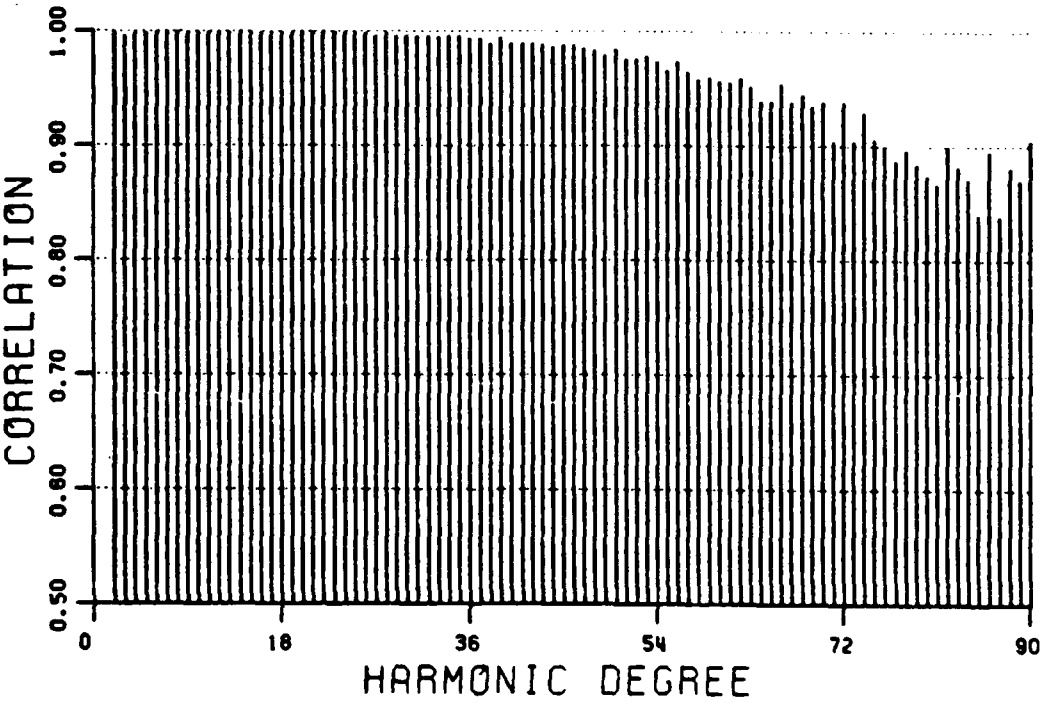

Figure 29. Correlation per degree between the input coefficients and the coefficients recovered from 2° $\bar{N}$ errorless data to degree 90.

Several observations may be made from examining figures 14 to 29: (1) the lower degrees in any estimated set of coefficients are recovered better than the higher degrees within the same expansion, (2) the recovery of the input coefficients improves with decreasing grid size for both data types and (3) the recovery obtained from the $\overline{\Delta g}$ data is better than the one obtained from $\overline{N}$ data.

Average recovery statistics are presented to degrees 18, 36, 60 and 90. These include average correlation, average percent difference, RMS undulation difference and RMS anomaly difference as defined in section 4.1. Tables 21 to 24 contain these statistics for the $\overline{\Delta g}$ solutions, and tables 25 to 28 the corresponding results for the $\overline{N}$ solutions.

Table 21. Average correlation to various degrees, Nmax, between the input coefficients and the coefficients recovered from $\overline{\Delta g}$ errorless data given on various grids.

block size / Nmax	10°	5°	3°	2°
18	0.9918	0.9994	0.9999	1.0000
36		0.9929	0.9993	0.9999
60			0.9939	0.9994
90				0.9947

Table 22. Average percent difference to various degrees, Nmax, between the input coefficients and the coefficients recovered from $\overline{\Delta g}$ errorless data given on various grids.

block size / Nmax	10°	5°	3°	2°
18	13.79	4.40	1.77	0.73
36		16.96	5.60	2.06
60			14.26	4.63
90				11.82

Table 23. RMS undulation difference (in meters) to various degrees, Nmax, between the input coefficients and the coefficients recovered from Δg errorless data on various grids.

block size / Nmax	10°	5°	3°	2°
18	0.896	0.277	0.121	0.071
36		0.542	0.192	0.089
60			0.355	0.129
90				0.235

Table 24. RMS anomaly difference (in mgals) to various degrees, Nmax, between the input coefficients and the coefficients recovered from Δg errorless data on various grids.

block size / Nmax	10°	5°	3°	2°
18	1.47	0.47	0.19	0.08
36		2.10	0.67	0.24
60			2.42	0.76
90				2.48

Table 25. Average correlation to various degrees, Nmax, between the input coefficients and the coefficients recovered from $\bar{N}$ errorless data given on various grids.

block size / Nmax	10°	5°	3°	2°
18	0.9632	0.9963	0.9991	0.9994
36		0.9710	0.9946	0.9985
60			0.9702	0.9910
90				0.9630

Table 26. Average percent difference to various degrees, Nmax, between the input coefficients and the coefficients recovered from $\bar{N}$ errorless data given on various grids.

block size / Nmax	10°	5°	3°	2°
18	35.44	14.46	6.62	4.18
36		43.37	26.28	15.47
60			49.53	35.59
90				54.20

Table 27. RMS undulation difference (in meters) to various degrees, Nmax, between the input coefficients and the coefficients recovered from $\bar{N}$ errorless data given on various grids.

block size / Nmax	10°	5°	3°	2°
18	9.517	5.533	2.940	2.450
36		5.652	3.028	2.486
60			3.171	2.590
90				2.683

Table 28. RMS anomaly difference (in mgals) to various degrees, Nmax, between the input coefficients and the coefficients recovered from $\bar{N}$ errorless data given on various grids.

block size / Nmax	10°	5°	3°	2°
18	4.32	2.03	1.06	0.83
36		5.28	3.35	2.06
60			7.63	5.77
90				9.83

The general trend indicated by the numbers in tables 21 to 28 may be pointed out. First, for both data types, there is an improvement in the recovery of the potential

coefficients with denser data. For example, the improvement in average percent difference up to degree 18 is 87% and in RMS undulation difference is 86%, when decreasing from 10° to 3° blocks of $\overline{\Delta g}$ data. The corresponding figures for $\bar{N}$ data are 81% and 70%. In decreasing from 10° to 2° blocks these numbers improve to 95% and 92% for the $\overline{\Delta g}$ data and, 88% and 75% for the $\bar{N}$ data.

It is also apparent that superior results are obtained using $\overline{\Delta g}$ data than when using $\bar{N}$ data. From the statistics in the preceeding paragraph the improvement with decrease in grid size is also superior for the $\overline{\Delta g}$ data. Consider the percent difference between the recovered and the input coefficients shown in tables 22 and 26 for $\overline{\Delta g}$ and $\bar{N}$ data respectively. The differences between columns 4 of these two tables are 3.45, 13.41, 30.96 and 54.20 for corresponding Nmax values of 18, 36, 60 and 90. Thus, the difference in the recovery statistics between the two data types increases with degree, especially for degrees larger than 36, as the two last differences indicate. Also, figures 28 and 29 show that the percent differences for $\bar{N}$ data are more than 40% for degrees higher than 36.

In addition to the coefficients their accuracy is estimated by means of the equation (2.2-14) for the expansions to degrees 18 and 36. Due to the large size of the auto-covariance matrices for the case of 3° and 2° mean data (actually 7,200 and 16,200 observations respectively) as well as due to the time consuming computation required, the accuracy estimates of these expansions have not been computed.

Negative variances were computed for certain coefficients which generally suggest that the covariances used are not optimal in the sense of representing the true covariances. In particular, the variances estimated from 10° $\overline{\Delta g}$ data for the coefficients $\bar{C}_{30}$, $\bar{C}_{31}$ and $\bar{S}_{31}$ are -1.8×10^{-14}, -6.9×10^{-15} and -6.9×10^{-15} respectively. These values are practically zero, since the internal representation of the double-precision numbers retains 15 significant digits. No negative variances were calculated in estimating the 36 degree field from the 5° $\overline{\Delta g}$ data. However, several negative variances were calculated from the $\bar{N}$ data, especially for the low degrees, which indicate inadequacy of the covariance function used for the undulation data. Tables 29 and 30 show the particular coefficients

with negative estimated variances as well as the extremes of these variance values. The symbol "#" means the same variance with the one of the $\bar{C}_{nm}$ coefficient.

Table 29. Extreme values of negative variances and all related coefficients, derived from 10° $\bar{N}$ errorless data.

	Order		Largest Variance		Smallest Variance	
Degree	$\bar{C}_{nm}$	$\bar{S}_{nm}$	$\bar{C}_{nm}$	$\bar{S}_{nm}$	$\bar{C}_{nm}$	$\bar{S}_{nm}$
2	0 to 2	1, 2	-0.9×10^{-11}	-0.3×10^{-12}	-0.3×10^{-13}	-0.3×10^{-13}
3	0 to 3	1 to 3	-0.1×10^{-10}	-0.3×10^{-11}	-0.3×10^{-14}	-0.3×10^{-14}
4	0 to 4	1 to 4	-0.2×10^{-12}	-0.5×10^{-13}	-0.3×10^{-17}	-0.3×10^{-17}
5	0 to 4	1 to 4	-0.9×10^{-13}	-0.2×10^{-13}	-0.3×10^{-15}	-0.3×10^{-15}
6	0 to 5	1 to 5	-0.1×10^{-13}	-0.6×10^{-14}	-0.1×10^{-15}	-0.1×10^{-15}
7	0 to 6	1 to 6	-0.3×10^{-14}	-0.3×10^{-14}	-0.9×10^{-16}	-0.9×10^{-16}
8	1to3, 5to7	1to3,5to7	-0.2×10^{-15}	-0.2×10^{-15}	-0.2×10^{-16}	-0.2×10^{-16}
9	2,3,6,7,8	2,3,6,7,8	-0.4×10^{-15}	-0.4×10^{-15}	-0.1×10^{-16}	-0.1×10^{-16}
10	2,6,7	2,6,7	-0.2×10^{-15}	-0.2×10^{-15}	-0.2×10^{-16}	-0.2×10^{-16}

Table 30. Extreme values of negative variances and all related coefficients derived from 5° $\bar{N}$ errorless data.

	Order		Largest Variance		Smallest Variance	
Degree	$\bar{C}_{nm}$	$\bar{S}_{nm}$	$\bar{C}_{nm}$	$\bar{S}_{nm}$	$\bar{C}_{nm}$	$\bar{S}_{nm}$
2	0 to 2	1, 2	-1.9×10^{-13}	#	-1.6×10^{-15}	#
3	0 to 2	1, 2	-3.3×10^{-13}	#	-9.1×10^{-14}	#
4	1, 2	1, 2	-2.9×10^{-14}	#	-1.3×10^{-15}	#
5	1, 2	1, 2	-1.1×10^{-14}	#	-7.2×10^{-16}	#
6	1, 2	1, 2	-4.6×10^{-15}	#	-3.1×10^{-16}	#
7	1, 2	1, 2	-2.3×10^{-15}	#	-1.7×10^{-16}	#
8	1	1	-2.7×10^{-16}	#	N/A	N/A
9	1	1	-9.4×10^{-17}	#	N/A	N/A

The last recovery statistics, i.e. the differences between the recovered and the input coefficients, were computed and normalized by the estimated standard deviations of the particular coefficients (see equations (4.1-13) and (4.1-14)). Then the RMS value of the

normalized differences was computed for each degree (from equation (4.1-15)) and was plotted together with the extremes of the absolute values of the normalized differences within the particular degree. These plots are presented for the variances of the coefficients derived from 10° and 5° $\overline{\Delta g}$ data in figures 30 and 31. Also, figures 32 and 33 show these results derived from 10° and 5° $\bar{N}$ data. Note that the negative variances have been set to zero and the corresponding coefficient differences have not been included in the RMS computation.

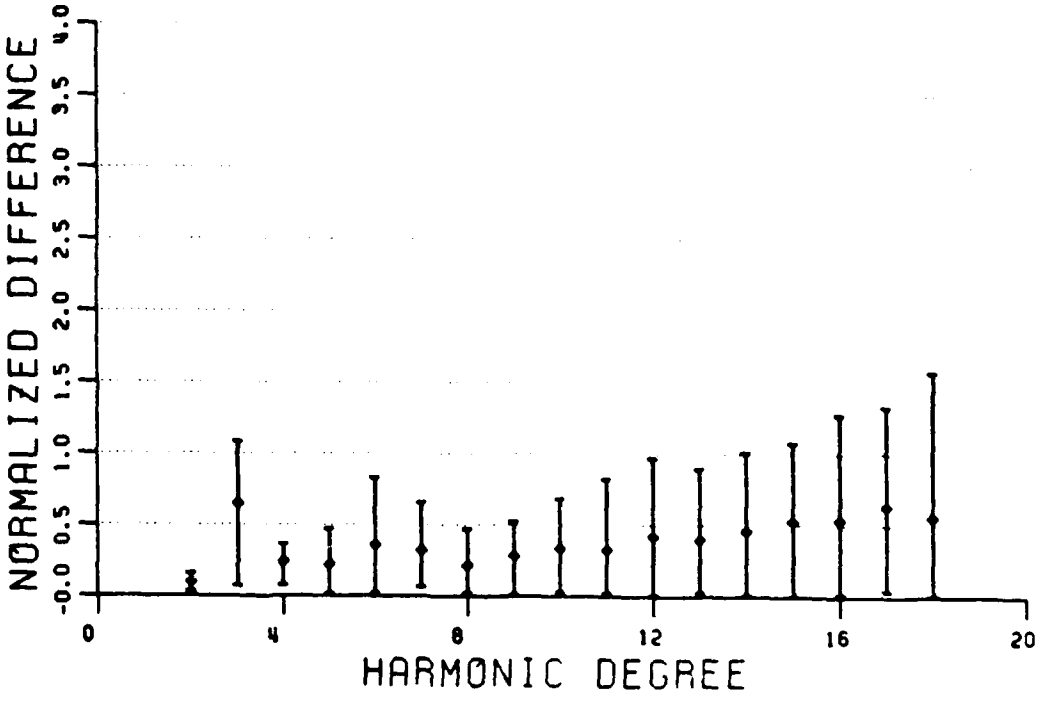

Figure 30. RMS and extreme absolute values of the normalized differences between the input and the recovered coefficients from 10° $\overline{\Delta g}$ errorless data.

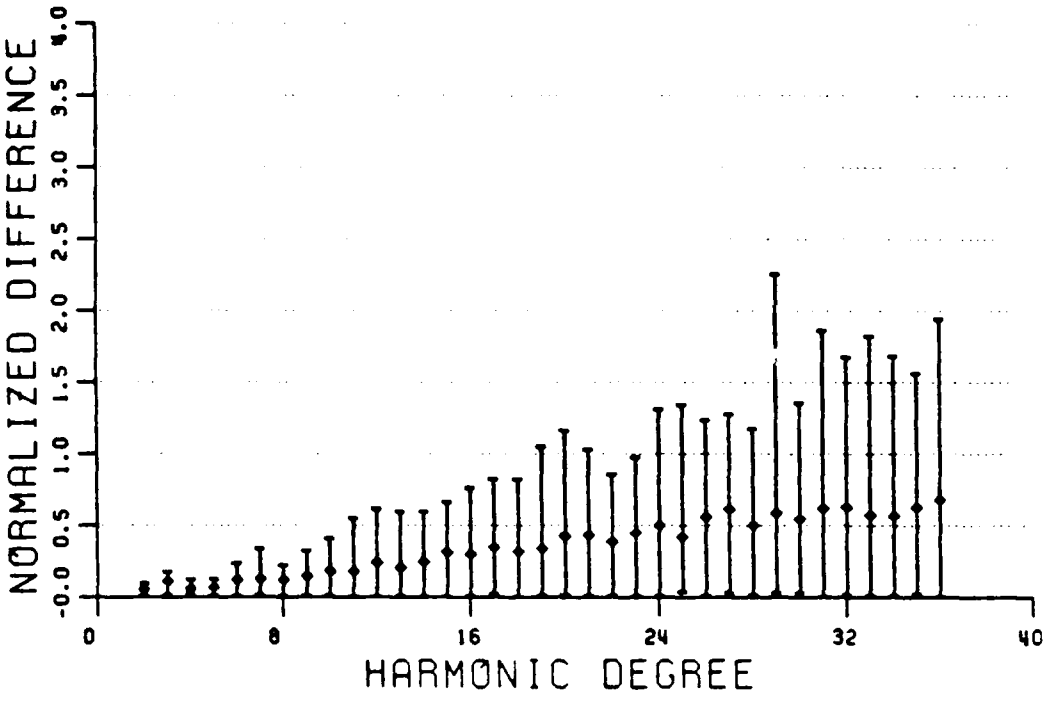

Figure 31. RMS and extreme absolute values of the normalized differences between the input and the recovered coefficients from 5° $\bar{\Delta g}$ errorless data.

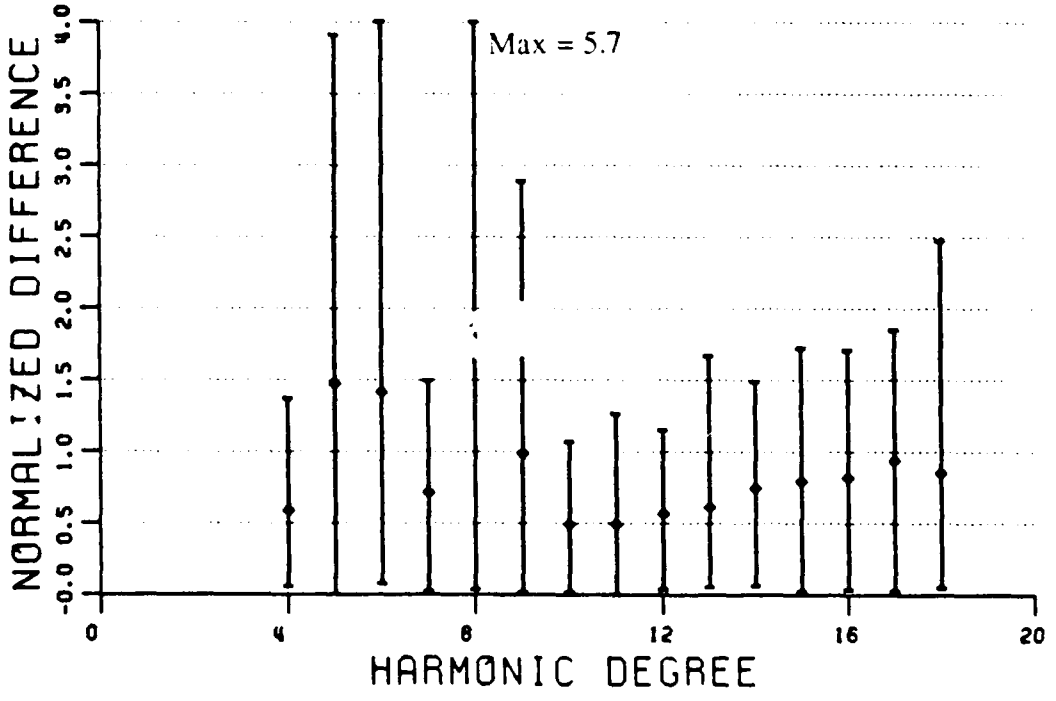

Figure 32. RMS and extreme absolute values of the normalized differences between the input and the recovered coefficients from 10° $\bar{N}$ errorless data.

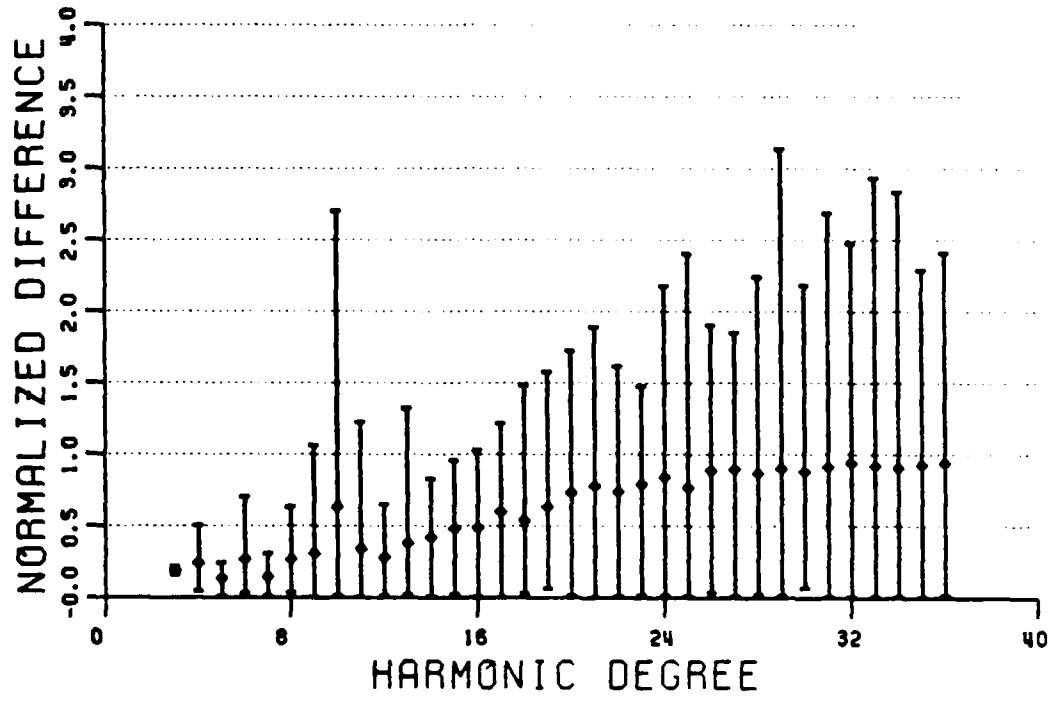

Figure 33. RMS and extreme absolute values of the normalized differences between the input and the recovered coefficients from 5° $\bar{N}$ errorless data.

From figures 30 and 31 it is seen that the RMS values are generally centered between the extremes for each degree, and also they increase with increasing degree. The RMS values as well as the ranges of the normalized differences are decreased for the degrees up to 18 when using the 5° $\overline{\Delta g}$ data instead of 10° $\overline{\Delta g}$ data. However, the other end of the spectrum (i.e. for $24 \leq n \leq 36$) shows increased values compared to the differences for $12 \leq n \leq 18$ in figure 30.

Figures 32 and 33 do not indicate as clear as figures 30 and 31 the trend of increasing value with increasing degree, although the RMS values tend to stabilize for the second half of the predicted specurum. Also, the differences referring to the predicted coefficients from the $\bar{N}$ data are generally larger than the corresponding ones predicted from the $\overline{\Delta g}$ data. Finally, it is clear that the RMS values of the normalized differences are smaller than one, i.e. the overall differences of the predicted coefficients from the reference ones are within the accuracy of the prediction. There are only three exceptions, as it can be seen in figure 32, specifically, values between 1.5 and 2.0 for n = 5, 6 and 8.

Similar graphs have been produced for the experiments where data noise was included, which were discussed in section 4.4. Since the solutions presented in this section are regularized (i.e. with the error covariance matrix effectively added to the signal covariance matrix), the estimated accuracy of the predicted signals remains identical to the errorless data case, as it is clearly seen from equation (2.2-14). However, the estimated coefficients themselves are affected by the data error, thus changing the values of the normalized differences. The coefficient error normalized by the corresponding estimated accuracy is shown per degree in Figures 34 and 35 for 5° $\overline{\Delta g}$ and $\bar{N}$ noisy data respectively.

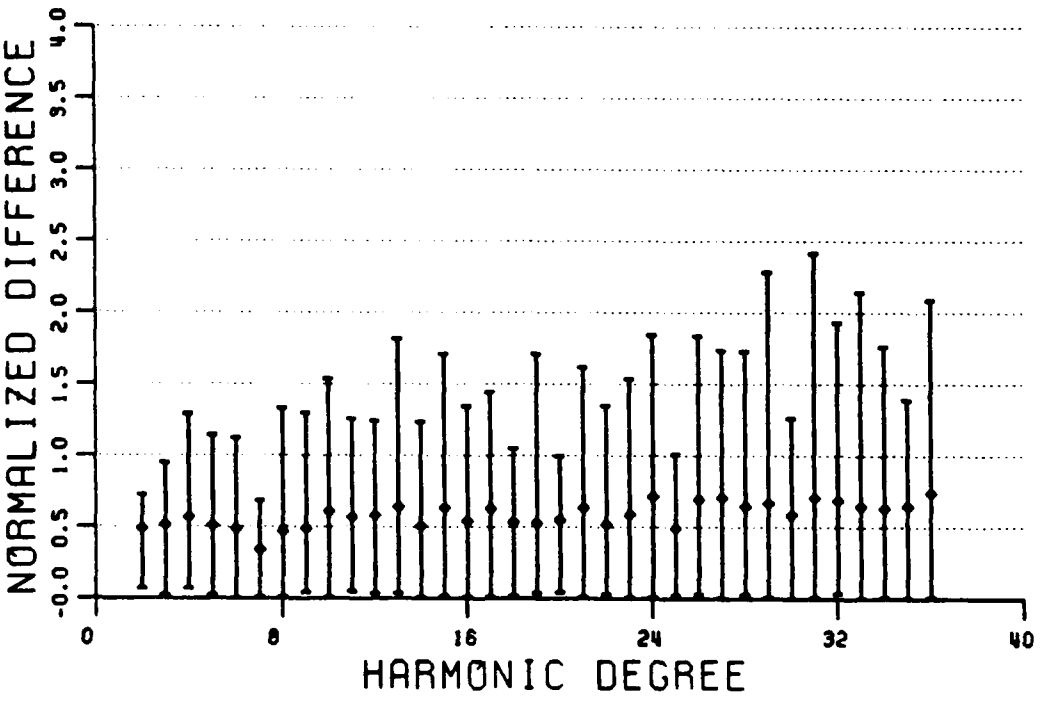

Figure 34. RMS and extreme absolute values of the normalized differences between the input and the recovered coefficients from 5° $\overline{\Delta g}$ data with noise.

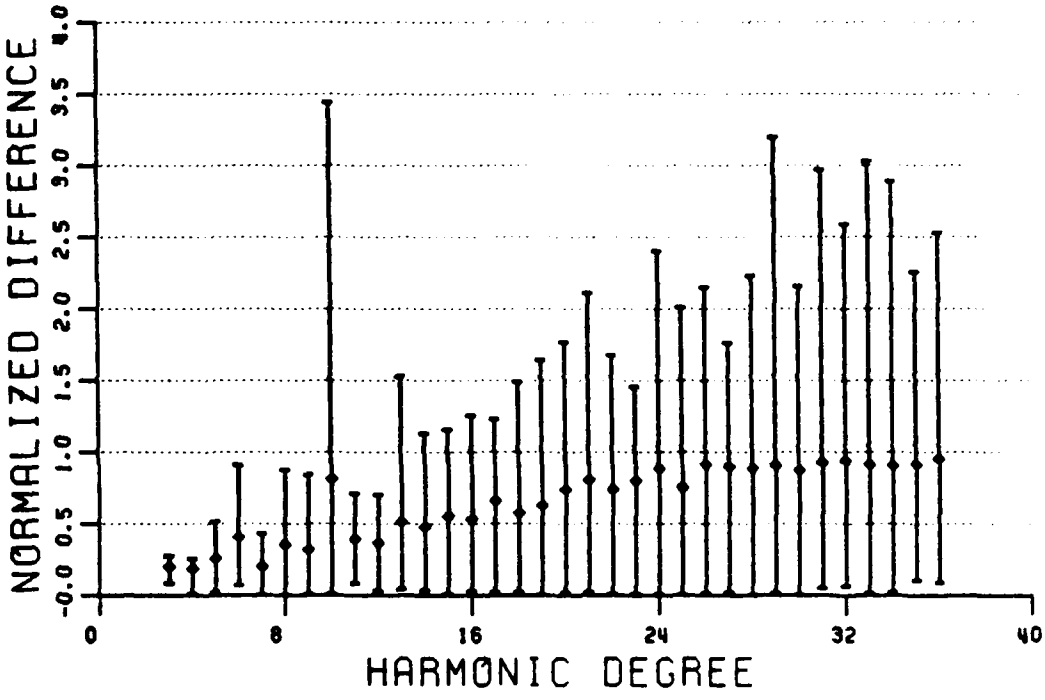

Figure 35. RMS and extreme absolute values of the normalized differences between the input and the recovered coefficients from 5° $\bar{N}$ data with noise.

By comparing Figure 34 to Figure 31 it is seen that only the first half of the predicted spectrum is affected by the data noise, thus bringing the normalized differences to the same order of magnitude for all degrees, about 0.5. Such effect is not observed for the $\bar{N}$ data. The comparison of Figure 35 to Figure 33 shows only slight changes in the low degrees. For the other degrees there are only small changes in the extreme values, while the RMS values are unaffected.

4.6 Solutions combining data types.

So far, all the computations were made in order to analyze the behavior of the two data types individually in estimating spherical harmonic coefficients with collocation. This section presents experiments made with combined data types, namely mean gravity anomalies and mean undulations.

Two different tests were made to estimate potential coefficients to degree 18 and 36, using mean data given on 10° and 5° regular grids, respectively. The 10° data were derived from the OSU86F expansion to maximum degree 18, and the 5° data were derived from the same expansion to degree 36. The auto-covariance matrices were computed by summing the covariance function to Nmax = 180. The value of $9m^2$ was added to the diagonal elements of the undulation auto-covariance matrices and the value of 3 $mgals^3$ was added to the anomaly covariance matrix of 5° block data only, in order to perform experiments comparable to the ones presented in section 4.5.

Five data groups were included in each experiment. The first group is a global $\overline{\Delta g}$ data set, as used in the experiments presented previously in section 4.5. The other four data groups contain $\bar{N}$ data and cover the following geographic areas:

(1) $-10° \text{ S} \le \varphi \le 40° \text{ N}$ and $140° \text{ E} \le \lambda \le 240° \text{ E}$, which includes 5 rows of parallels and 10 zones of meridians on a 10° regular grid,

(2) $0° \le \varphi \le 60° \text{ N}$ and $300° \text{ E} \le \lambda \le 350° \text{ E}$, which includes 6 rows of parallels and 5 zones of meridians,

(3) $-70° \text{ S} \le \varphi \le -30° \text{ S}$ and $0° \le \lambda \le 120° \text{ E}$, which includes 4 rows of parallels and 12 zones of meridians, and

(4) $-60° \text{ S} \le \varphi \le -10° \text{ S}$ and $180° \text{ E} \le \lambda \le 290° \text{ E}$, which includes 5 rows of parallels and 11 zones of meridians.

The data location is also shown on the map of figure 35.

When estimating potential coefficients to degree 18 from 10° grid data, the number of observations contained in each group above is 50, 30, 48 and 55, for a total of 183 undulation observations. There are 648 anomaly observations, which constitute 78% of the 831 total observations. In the case of 5° grid, the number of data is exactly doubled by densifying the coverage at the same geographic locations.

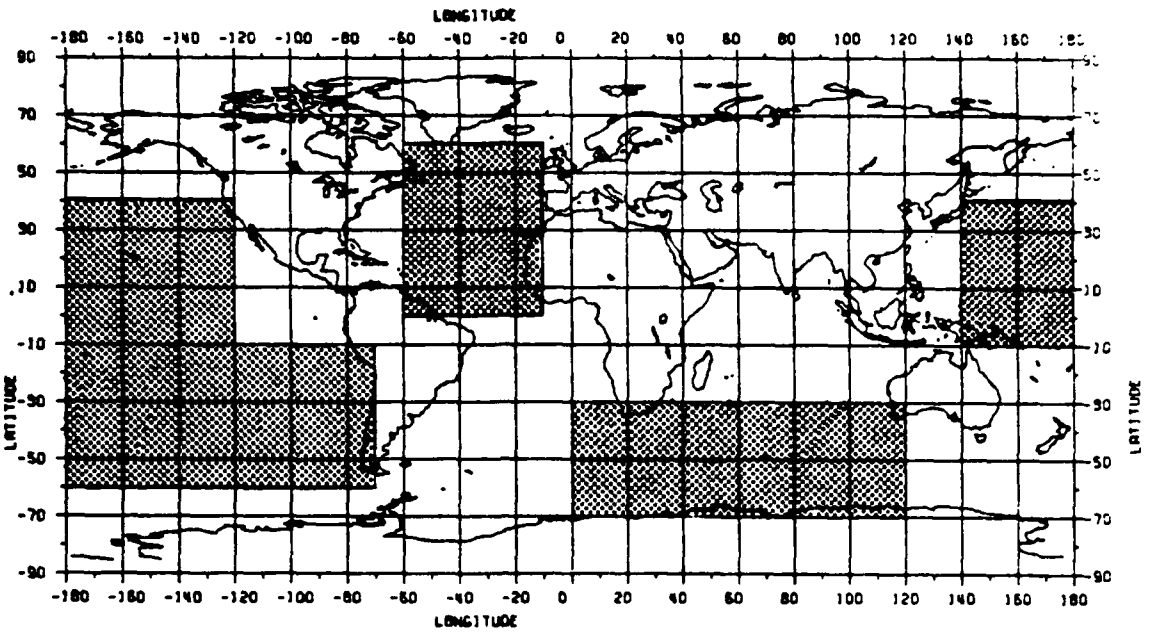

Figure 36. Undulation data coverage for the combination solutions.

Using the above data configuration, the coefficients were estimated by employing the sequential type of algorithm which was described in section 3.3. The statistics of the recovery of the reference potential coefficients resulting from these tests are presented in the following figures and tables. Figures 37 and 38 show the percent differences per degree for the recovery obtained from 10° and 5° data respectively, while figures 39 and 40 show the correlation per degree between the input coefficients and the ones obtained from these tests.

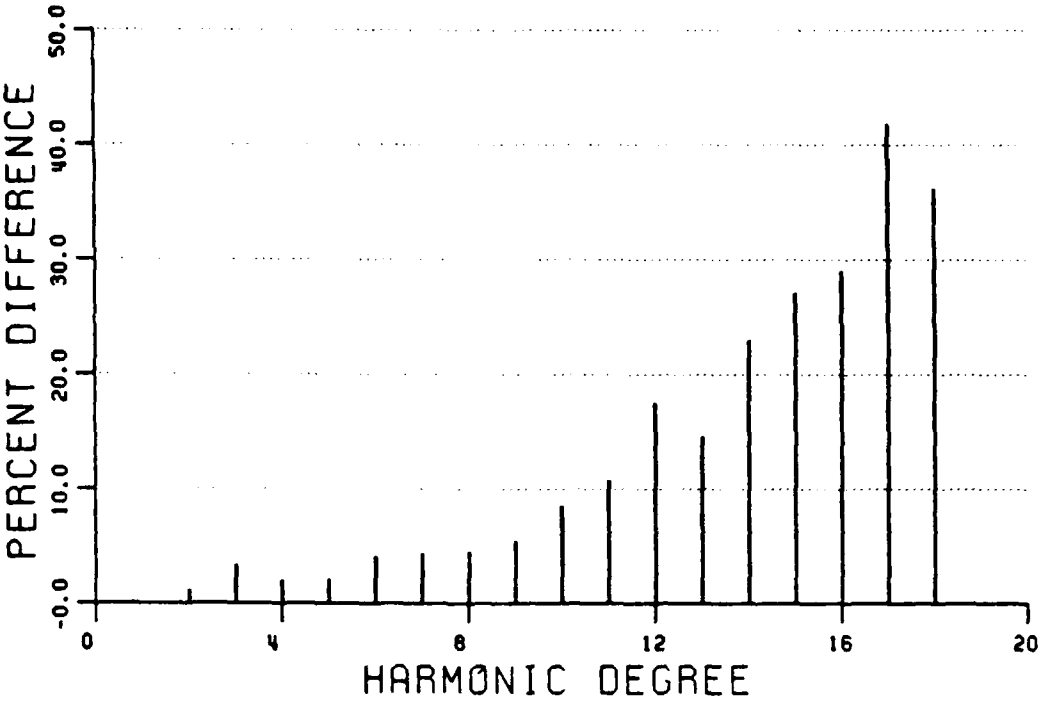

Figure 37. Percent difference per degree between the input coefficients and the coefficients recovered from 10° $\bar{\Delta g}$ and $\bar{N}$ combined errorless data to degree 18.

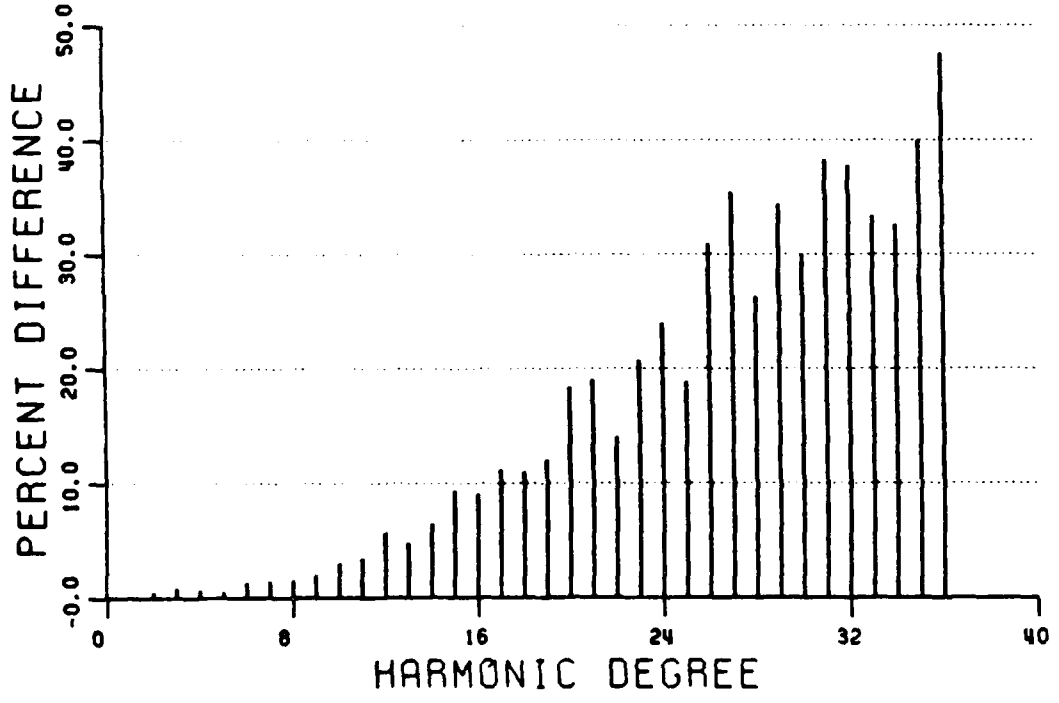

Figure 38. Percent difference per degree between the input coefficients and the coefficients recovered from 5° $\bar{\Delta g}$ and $\bar{N}$ combined errorless data to degree 36.

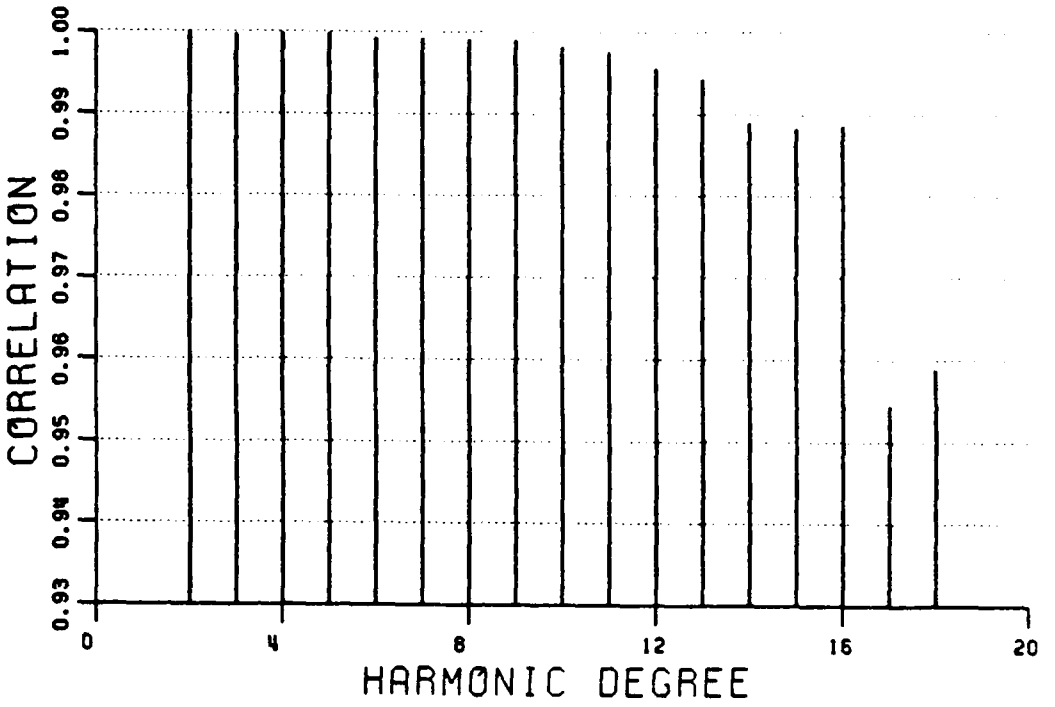

Figure 39. Correlation per degree between the input coefficients and the coefficients recovered from 10° $\overline{\Delta g}$ and $\bar{N}$ combined errorless data to degree 18.

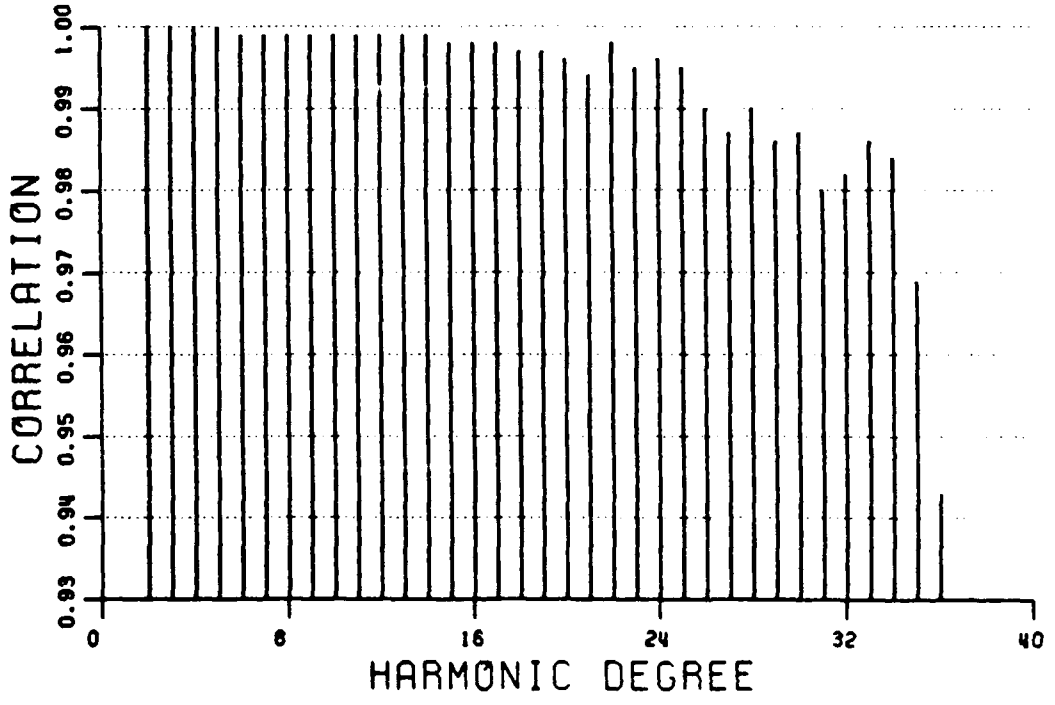

Figure 40. Correlation per degree between the input coefficients and the coefficients recovered from 5° $\overline{\Delta g}$ and $\bar{N}$ combined errorless data to degree 36.

Figures 37 and 38 show the same general trend as figures 14 and 15 respectively, which reflect recovery from $\overline{\Delta g}$ data alone. A more detailed comparison indicates that for degrees: $2 \leq n \leq 6$ the percent differences in the combination solution increase about 1%, and for degrees: $11 \leq n \leq 15$ decrease by 1%, while they are the same for the remaining degrees. This may be interpreted as the influence of the incorporation of the $\bar{N}$ data on the $\overline{\Delta g}$ obtained solution. Figures 39 and 40 compare in a similar way to figures 18 and 19.

Specific values of the computed statistics for selected degrees are presented in table 31 for the 18 degree solution and table 32 for the 36 degree solution. The overall recovery to degrees 18 and 36 is given in table 33.

Table 31. Recovery statistics for 10° $\overline{\Delta g}$ and $\bar{N}$ combined errorless data.

Degree	Correlation	Percent difference	Undul. diff. (m)	Anomaly diff. (mgals)
2	1.0000	1.18	0.212	0.03
3	0.9997	3.34	0.631	0.19
4	0.9998	2.02	0.195	0.09
5	0.9998	2.06	0.153	0.09
6	0.9992	4.09	0.234	0.18
12	0.9956	17.51	0.198	0.34
18	0.9588	36.17	0.253	0.66

Table 32. Recovery statistics for 5° $\overline{\Delta g}$ and $\bar{N}$ combined errorless data.

Degree	Correlation	Percent difference	Undul. diff. (m)	Anomaly diff. (mgals)
2	1.0000	0.52	0.094	0.01
3	1.0000	0.84	0.160	0.05
4	1.0000	0.69	0.067	0.03
5	1.0000	0.51	0.038	0.02
6	0.9999	1.30	0.074	0.06
12	0.9996	5.64	0.064	0.11
18	0.9974	10.96	0.077	0.20
36	0.9435	47.47	0.142	0.76

Table 33. Overall recovery to degree Nmax obtained from $\overline{\Delta g}$ and $\bar{N}$ combined errorless data given on 10° and 5° regular grids.

Nmax	Grid size	Average Correlation	Average % diff.	RMS undulation diff. (m)	RMS anomaly diff. (mgals)
18	10°	0.9918	13.84	1.039	1.47
18	5°	0.9995	4.27	0.312	0.45
36	5°	0.9929	16.73	0.557	2.08

By comparing the second row in table 33 with the corresponding statistics in tables 21 to 24 it is evident that all statistics are slightly better, except for the RMS undulation difference, which is increased by 3.5 cm.

Finally, the estimated accuracy of the predicted coefficients was computed. Several negative variances were found for the case of 10° data solution, in particular for degrees 2 to 5 and various orders, as shown in table 34. A single negative value was computed for the $\bar{C}_{30}$ coefficient estimated from 5° data, which was of the magnitude -4.7×10^{-15}.

Table 34. Extreme values of negative variances and all related coefficients derived from 10° $\overline{\Delta g}$ and $\bar{N}$ combined errorless data

	Order		Largest Variance		Smallest Variance	
Degree	$\bar{C}_{nm}$	$\bar{S}_{nm}$	$\bar{C}_{nm}$	$\bar{S}_{nm}$	$\bar{C}_{nm}$	$\bar{S}_{nm}$
2	0, 2	2	-0.2×10^{-13}	-0.5×10^{-14}	-0.6×10^{-14}	N/A
3	0 to 3	1 to 3	-0.1×10^{-13}	-0.5×10^{-14}	-0.1×10^{-13}	-0.3×10^{-14}
4	3	3	-0.5×10^{-15}	-0.3×10^{-15}	N/A	N/A
5	4	4	-1.0×10^{-16}	-0.8×10^{-16}	N/A	N/A

In addition, the estimated standard deviations are used to normalize the difference of the respective estimated coefficients from the reference ones, excluding the coefficients given in table 34. The range of the absolute values of the normalized differences as well as the RMS value for each degree is shown in figures 41 and 42.

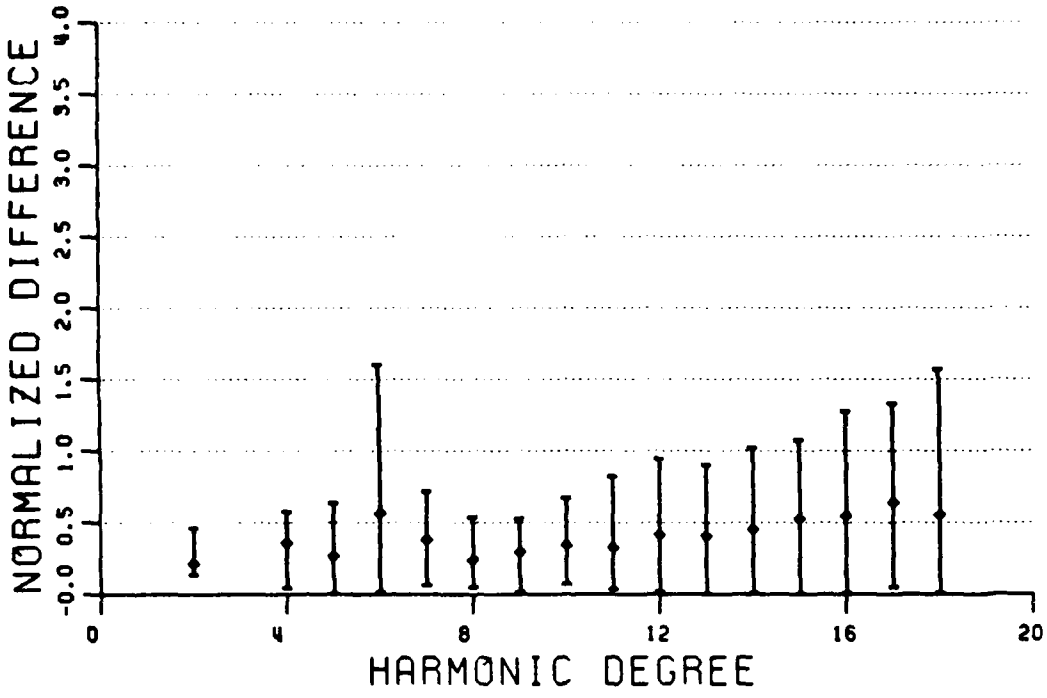

Figure 41. RMS and extreme absolute values of the normalized differences between the input and the recovered coefficients from 10° $\overline{\Delta g}$ and $\overline{N}$ combined errorless data.

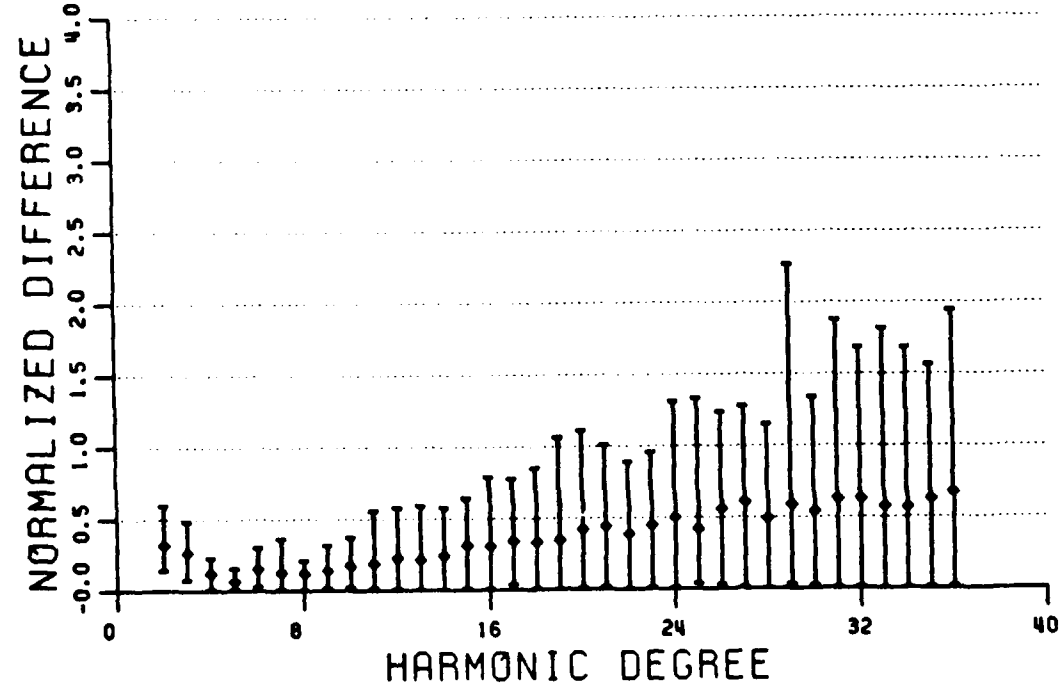

Figure 42. RMS and extreme absolute values of the normalized differences between the input and the recovered coefficients from 5° $\overline{\Delta g}$ and $\overline{N}$ combined errorless data.

The comparison of figures 41 and 42 with figures 30 and 31 shows larger RMS values and larger extremes for the first half of the predicted spectrum in the combination solutions, while the second half seems unaffected. On the other hand the comparison of these figures with figures 32 and 33 shows the same general trend for the low degrees, but with the extreme values supressed when combining data types.

CHAPTER V

CONCLUSIONS

Numerical solutions to the overdetermined geodetic boundary value problem have been derived using the method of least-squares collocation. The boundary value problem is defined by the Laplacian for the disturbing potential and the boundary conditions of the first and third (or mixed) type holding on overlapping parts of the spherical boundary of radius R_E. The solutions are expressed in terms of solid spherical harmonics, thus sets of coefficients are obtained to the degree defined by the Nyquist frequency of the boundary data. The boundary data are mean values referring to equiangular blocks on the sphere R_E and they have been simulated using the OSU86F potential coefficient set. In particular, mean gravity anomaly and mean undulation data were computed on regular grids of 10° and 5° using expansions to degree 18 and 36 respectively. The equations applied to estimate the coefficients and their accuracies are given in section 2.2, as well as the equations used to compute the data covariances and the cross-covariance between the estimated coefficients and the data. Specifically, for the computation of the data covariances equations (2.2-34) to (2.2-36) are used, where the anomaly degree variances are computed from the OSU86F coefficients and the summation is carried out to Nmax = 180. As a consequence of the implemented isotropic and homogeneous covariance functions, the auto-covariance matrix of data given on a regular grid (defined by a number of parallels and meridians) is identified as a block-Toeplitz matrix. Substantial savings in computing effort are realized in forming and inverting such matrices. An algorithm is implemented to exploit this pattern for the largest data group, while additional groups are included in a sequential algorithm as described in section 3.3. Since only simulated data are analyzed, the error of the solution is determined by means of the recovery of the reference field. The errors of the estimated solutions to degree 18 and 36 increase with degree, ranging from 0.5% to maximum of 10% for the first half of the estimated spectrum and reach 40% near the Nyquist frequency.

To consider the influence of the two data types, a number of solutions were carried out based exclusively on gravity anomaly data or undulation data. By comparing the combination solutions with the corresponding one-data-type solutions, the former can be

viewed as a weighted average of the latter. This averaging is done in an optimal way under the least-squares collocation minimum principle, and the combination solutions ultimately depend on the relative amounts of data as well as their distribution. In the case that data error is included, it also affects the combination in a relative sense: the more accurate data has greater influence on the combined solution. Similar effects happen due to the regularization process. When large regularization factors are used, the data error is effectively increased and the weight it carries on the solution is decreased. The solutions presented in this work are obtained with a factor of 10 for scaling the undulation variances. The anomaly variances are not scaled, thus the final result is influenced more by the anomaly data, as discussed in section 4.6.

Since the result of data combination may be predicted based on solutions from anomaly data and solutions from undulation data, several parameters of the system can be analyzed with respect to the individual data types. This does not only simplify the computations, but also provides a better insight into the behavior of the different data, and some guidelines towards optimizing their combination.

Given the analytical form of a covariance function, the two fundamental properties of positive definiteness and symmetry are required in order for it to represent a true covariance function, and also in principle, a reproducing kernel in the Hilbert space where the collocation solution is derived. For the functions implemented in this study the positive definiteness is assured when the power spectrum, defined by the degree variances k_n, is positive for all n. As it is discussed in detail in section 3.1, truncation of the covariance function summation at finite degree n results, theoretically in singular covariance matrices. Numerical tests, presented in section 4.3, have shown that truncation at Nmax = 180 is sufficient for data given on a 10° regular grid. Note that this condition holds for point and mean covariance functions. The issue of using point vs mean data has been addressed in section 4.3. However, meaningful solutions were derived when using area mean values only. Point data on a 10° regular grid completely failed to recover the input coefficients. Other than with regard to the covariance matrix singularity, the value of Nmax was tested with regard to the recovery of the input coefficients. The results shown in tables 5, 6 and 9 prove that the value of Nmax = 180 is sufficient, since there is no noticeable change for Nmax = 360 and 3000.

After studying corresponding solutions obtained separately from global anomaly and undulation data sets, several statements may be made about the existing differences and similarities. First, the undulation point covariance function used is generally a low frequency function with correlation length of about 22°, whereas the correlation length for the anomaly point function is about 2°, as is seen in figures 3 and 2. These correlation lengths increase for mean covariance functions, especially with decreasing grid size as shown in figures 4 to 9. As a result of the implemented global covariance function characteristics, ill-conditioning appears in the auto-covariance matrices, which introduces instabilities in the solutions. This type of effect occurs in both types of covariance matrices, although more acutely in the undulation one, as a result of using data in polar areas of an equiangular grid, where the blocksize decreases when approaching the poles. For data given on a regular grid of size equal or smaller than 5°, singularity occurs in the covariance matrix of both data types, as is indicated by their condition numbers given in tables 1 and 2.

The singularity can be handled by adding the error covariance matrix, $D = \sigma^2 I$, to the signal covariance matrix. In this case error may be included in the simulated observations, in the manner explained in section 4.1, by adding pseudo-random numbers distributed as Gaussian $(0, \sigma^2)$. The effect of the data error is tested for mean data referring to 10° and 5° equiangular blocks and it is discussed in section 4.4. When using 10° $\overline{\Delta g}$ noisy data, the average error of the estimated coefficients to degree 18 increased by 30%, as opposed to the errorless data. Especially, the error of the lower degrees is mostly affected, as the results of Table 11 indicate. However, the results obtained from 10° $\bar{N}$ noisy data are not comparable (Table 12). In this case, a regularization method is recommended, where the variance of each observation is scaled by a factor $\alpha>1$. Specifically, the variance of $\alpha\tilde{\sigma}^2_{\bar{N}} = 9m^2$ was added to the diagonal elements of the $\bar{N}$ signal covariance matrix. Then, the recovery of the input coefficients was tested for noisy as well as errorless simulated observations. Tables 13 and 14 show 3% increase of the average error to degree 18, due to observation noise. The same increase was observed in the average error to degree 36, derived from 5° $\bar{N}$ noisy data (Tables 17 and 18). The value of 3 $mgals^2$ was used for the variance of 5° $\overline{\Delta g}$ data and was added to the $\overline{\Delta g}$ signal covariance matrix. When including the equivalent noise in the observations the average error to degree 36 increased by 25%, as the results in Tables 15 and 16 indicate.

Tests made using undulation signals on a 10° regular grid, showed that the error of the estimated low degree coefficients decreases with increasing regularization factors, as presented in tables 19 and 20. Specifically, the coefficients of degree 2 are estimated with an RMS error of 6% for $\alpha \cong 1.5 \times 10^3$, while for $\alpha \cong 10$, this error is about 30%. However, it is known that the regularization effectively decreases the data resolution, i.e. increases the data error, thus the error in the estimated higher degrees increases rapidly with the factor α. The errors corresponding to the two previous α values are 99% and 80% near the Nyquist frequency. An indication of the implemented undulation covariance function being problematic, i.e. not approximating well the true covariance, are the unrealistic error estimates obtained by the least-squares collocation formula; in this case, negative variances are calculated for coefficients of degrees 2 to 10. These values are practically zero and are given in tables 29 and 30. The data densification by decreasing the grid size has a positive influence on the results. The improvement is well manifested for both data types, and it is discussed in the comparative analysis of section 4.5, by analyzing the overall recovery statistics given in tables 21 to 28. For example, the average percent difference to degree 18 is reduced by 95% for the anomaly solutions and 80% for the undulation solutions, going from 10° to 2° blocksize. Further improvement is expected when approaching the limit of continuous data. Finally the recovery ability of the two data types is compared. The anomaly data, of all block sizes, produce coefficients with error less than 1% for the low degrees, approaching a maximum of 10% for coefficients of degree half the Nyquist frequency and reaching 40% near degrees of the Nyquist frequency. The error definitely increases with increasing degree. On the other hand, the undulation data recover the 2nd and 3rd degree coefficients with an error of 10% - 20%. Then the error decreases to about 5% for coefficients to degree 10 and afterwards it continues to increase reaching 90% near the Nyquist frequency. Specific numbers are presented and discussed in section 4.5.

As expected, the solutions require considerable computer time, even in a CRAY supercomputer. High degree solutions for a global data set, although time consuming, are manageable under the Toeplitz covariance matrix scheme. However, the time requirements increase rapidly when the sequential algorithm is implemented in adding groups of data. In particular, for the experiments performed, the time required for the estimation of the 36 degree expansion using a global data set is about 2 minutes, while the

combination solution to degree 36 with 4 additional data groups requires about 60 minutes. Other than the required computer time, the need in storage is another limiting factor. For example, the 90 degree expansion involves 16,200 observations and the associated covariance matrix. There is no need for storing this matrix, unless the error estimates are computed. In this case, the matrix can only be stored on tape by writing parts of it at a time.

To end this discussion, several recommendations are made for future improvement.
(1) The undulation global covariance function must be studied; an improvement should be made, which will affect the solution in a way similar to the regularization procedure, thus improving the prediction of the low degree coefficients.
(2) For further improvement of the low degrees, a satellite-derived field should be included. This can be done easily in including these potential coefficients as an additional data group in the sequential algorithm, which is simplified considering that the errors of the satellite coefficients are not correlated with the other data errors.
(3) Programming effort should be dedicated in order to take advantage of the pseudo-Toeplitz pattern (section 3.3) in forming the cross-covariances between any two data groups, as well as utilizing these matrices in the partitioned inversion scheme. Also, fully vectorized software should be used to take advantage of the continually improving supercomputer capabilities. Considering that the CRAY Y-MP/832, currently in operation at PSC, is at least 3 times faster and has 4 times larger memory than the CRAY X-MP/48 used in this work, combination solutions to degree 90 are feasible. Depending on the improvement that can be achieved by implementing the suggestions made here and on the impact that fully vectorized software will have, high degree solutions to degree 180 may be possible. However, when judging the required time of the methodology of this study in comparison with other methods utilizing one data-type, the effort required for the data type conversion should be considered.

REFERENCES

Bjerhammar, Arne, A Stochastic Approach to the Mixed Boundary Value Problem in Physical Geodesy, Geodesy in Transition, K.P. Schwarz and G. Lachapelle, eds., pp. 25-42, University of Calgary, Alberta, Canada, (1983).

Bose, S.C., G.E. Thobe, J.T. Kouba and R.E. Mortensen, Optimal Global Gravity Field Estimation, Proceedings of the IAG symposia, IUGG XVIII General Assembly, Hamburg, Federal Republic of Germany, (1983).

Colombo, Oscar L., Optimal estimation from data regularly sampled on a sphere with applications in geodesy, Report No. 291, Dept. of Geodetic Science and Surveying, The Ohio State University, AFGL-TR-79-0227, ADA 083034, (1979).

Colombo, Oscar L., Numerical methods for Harmonic Analysis on the Sphere, Report No. 310, Dept. of Geodetic Science and Surveying, The Ohio State University, AFGL-TR-81-0038, ADA 104178, (1981).

Dermanis, Athanasios, Probabilistic and deterministic aspects of linear estimation in geodesy, Report No. 244, Dept. of Geodetic Science and Surveying, The Ohio State University, NASA Grant No. NGR 36-008-204, (1976).

Eren, Kamil, Spectral analysis of GEOS-3 Altimeter data and frequency domain collocation, Report No. 297, Dept. of Geodetic Science and Surveying, The Ohio State University, NASA Grant No. NSG 5275, (1980).

Faddeeva, V.N., Computational methods of linear algebra, Dover Publications, Inc., New York, (1959).

Giacaglia, G.E.O. and C.A. Lundguist, Sampling Functions for Geophysics, Smithsonian Astrophysical Observatory, Special Report 344, Cambridge Massachusetts, (1972).

Hajela, D. P., Equal area blocks for the representation of the global mean gravity anomaly field, Report No. 224, Dept. of Geodetic Science, The Ohio State University, NASA Grant No. NGR 36-008-161, (1975).

Hein, Gunter W., Integrated Geodesy: State-of-the-art 1986 Reference Text, Lecture Notes, Fourth International Summer School in the Mountains, Admont, Austria, (1986).

Heiskanen, Weikko A. and Helmut Moritz, Physical Geodesy, W.H. Freeman and Company, San Francisco, (1967).

Holota, P., The Altimetry-Gravimetry Boundary Value Problem, Presented at the International Scientific Conference of sec. 6 Intercosmos, Albena, (1980).

Jekeli, C., An Investigation of Two Models for the Degree Variances of Global Covariance Functions, Report No. 275, Dept. of Geodetic Science, The Ohio State University, AFGL-TR-78-0235, ADA 063196 (1978).

Katsambalos, Kostas E., The Effect of the Smoothing Operator on Potential Coefficient Determinations, Report No. 287, Dept. of Geodetic Science and Surveying, The Ohio State University, NASA Grant No. 36-008-161, (1979).

Krarup, Torben, A contribution to the mathematical foundation of physical geodesy, Publication No. 44, Danish Geodetic Institute, Copenhagen, Denmark, (1969).

Kutikov, L.M., The structure of matrices which are the inverse of the correlation matrices of random vector processes, USSR Computational Mathematics and Mathematical Physics, Vol. 7, No. 4., (1967).

Meissl, Peter, A study of covariance functions related to the earth's disturbing potential, Report No. 151, Dept. of Geodetic Science, The Ohio State University, AFCRL-TR-71-0240, AD 728688, (1971).

Molodenskii, M.S., V.F. Eremeev and M.I. Yurkina, Methods for study of the External Gravitational Field and Figure of the Earth, Transl. from Russian (1960), Israel Program for Scientific Translations, Jerusalem, (1962).

Moritz, Helmut, Covariance functions in least-squares collocation, Report No. 240, Dept. of Geodetic Science and Surveying, The Ohio State University, AFGL-TR-76-0165, ADA 030302, (1976).

Moritz, H., Advanced Physical Geodesy, Herbert Wichmann Verlag, Karlsruche, West Germany, (1980).

Paul, M.K., Recurrence relations for integrals of Associated Legendre functions, Bulletin Geodesique, Vol. 52, No. 3, pp. 177-190, (1978).

Rapp, R.H., The Earth's Gravity Field to degree and order 180 using SEASAT altimeter data, terrestrial Gravity Data, and other data, Report No. 322, Dept. of Geodetic Science and Surveying, The Ohio State University, AFGL-TR-82-0019, ADA 113098, (1981).

Rapp, R.H., Global Geopotential Solutions, in Mathematical and Numerical Techniques in Physical Geodesy, Lecture Notes in Earth Sciences, edited by H. Sunkel, Springer-Verlag, Berlin, Heidelberg, (1986).

Rapp, R.H., Gravitational Potential Coefficient Models-Developments and Comparison, Proceedings of the IAG Symposium, XIX General Assembly, Vancouver, (1987).

Rapp, R.H., Unpublished partial lecture notes for Advanced Gravimetric Geodesy, GS871, Dept. of Geodetic Science and Surveying, The Ohio State University, (1988).

Rapp, R.H. and J.Y. Cruz, The Representation of the Earth's Gravitational Potential in a Spherical Harmonic Expansion to Degree 250, Report No. 372, Dept. of Geodetic Science and Surveying, The Ohio State University, AFGL-TR-86-0191, ADA 176479, (1986a).

Rapp, R.H. and J.Y. Cruz, Spherical Harmonic Expansions of the Earth's Gravitational Potential to Degree 360 Using 30' Mean Anomalies, Report No. 376, Dept. of Geodetic Science and Surveying, The Ohio State University, NASA Grant No. NGR 36-008-161, (1986b).

Rummel, R., K.P. Schwarz and M. Gerstl, Least squares collocation and regularization, Bulletin Géodésique, Vol. 53, No. 4, pp. 343-361, (1979).

Sacerdote, F. and F. Sansò, Overdetermined boundary value problems in physical geodesy, manuscripta geodaetica, Volume 10, No. 3, pp. 195-207, (1985).

Sacerdote, F. and F. Sansò, New developments of boundary value problems in physical geodesy, in Proceedings of the International Association of Geodesy, Symposia Tome II, IUGG XIX General Assembly, Canada, (1987).

Sansò, Fernando, A Discussion on the Altimetry-Gravimetry Problems, in Geodesy in Transition, K.P. Schwarz and G. Lachapelle, eds., pp. 71-107, University of Calgary, Alberta, Canada, (1983).

Sansò, Fernando, Recent Advances in the Theory of the Geodetic Boundary Value Problem, in Reviews of Geophysics and Space Physics, Vol. 19, No. 3, pp. 437-449), Advances in Geodesy, edited by E.W. Grafarend and R.H. Rapp, (1984).

Sansò, F., Private Communication, (1986).

Sansò, F., The Wiener Integral and the Overdetermined Boundary Value Problems of Physical Geodesy, manuscripta geodaetica, Vol. 13, No. 2, pp. 75-98, (1988).

Sjoberg, Lars, Potential coefficient determinations from 10° terrestrial gravity data by means of collocation, Report No. 274, Dept. of Geodetic Science and Surveying, The Ohio State University, AFGL-TR-78-0241, ADA 063198, (1978).

Tikhonov, A.N. and V.Y. Arsenin, Solutions of ill-posed problems, John Wiley and Sons, New York, (1979).

Tscherning, C.C. and R.H. Rapp, Closed covariance expressions for gravity anomalies, geoid undulations, and deflections of the vertical implied by anomaly degree variance models, Report No. 208, Dept. of Geodetic Science and Surveying, The Ohio State University, AFGL-TR-74-0231, AD786417, (1974).

Tyrtyshnikov, E.E., On the solution of systems with matrices of Toeplitz type, in Cooperative Development of Mathematical Software, Vol. 2, ed. J. R. Bunch, University of California, San Diego, (1980).

Wenzel, Hans-Georg, "Hochauflosend Kugelfunktionsmodelle fur das Gravitationspotential der Erde." Wissenschaftliche Arbeiten der fachrichtung Vermessungswesen der Universitat Hannover, Nr. 137, (1985).